Extreme Extratropical Cyclones in The North Atlantic and Arctic Oceans
- Numerical Analysis of Coastal Impacts and Future Threats -

北大西洋と北極海の極端な温帯低気圧による沿岸災害
-沿岸への影響と将来変化の数値解析-

February 2020

Martin MAELL
マエル マーティン

Extreme Extratropical Cyclones in The North Atlantic and Arctic Oceans
- Numerical Analysis of Coastal Impacts and Future Threats -

北大西洋と北極海の極端な温帯低気圧による沿岸災害
-沿岸への影響と将来変化の数値解析-

February 2020

Waseda University

Graduate School of Creative Science and Engineering

Department of Civil and Environmental Engineering,

Research on Coastal Engineering and Management

Martin MAELL

マエル マーティン

Abstract

In order to estimate the possible changes and impacts of future extreme extratropical cyclones (ETCs), a pseudo climate modelling study framework is developed for North Atlantic (NAO) and Arctic Ocean (AO) regions. Three historical storms originating from the Atlantic Ocean, one from the Black Sea and one from the Arctic Ocean area are studied using multi-model approach considering IPCC AR5 emission scenarios RCP4.5 and RCP8.5 for mid and late 21st century. The study combines and makes use of base and secondary modules of established numerical models: Weather Research and Forecasting model (WRF and Polar optimized WRF), Finite Volume Community Ocean Model (FVCOM with SWAVE module), and Simulating Waves Nearshore (SWAN) model. The future simulation considered changes in atmospheric air temperature (AAT), sea surface temperature (SST) and relative humidity (RH), on the basis of 14 CMIP5 general circulation models (GCM) ensemble for years 2050 and 2090 in Arctic and North Atlantic Ocean regions, respectively. The results under applied methodology suggest no notable changes in minimum atmospheric pressure fields. Under most extreme storms, southward extension of strong wind fields occurred for extreme NAO storms under 2090 RCP8.5 scenarios (most notably for ETC "Gudrun"). This extension of strong wind fields translated into future increase in hydrodynamic results at the Baltic Sea study areas – larger distribution of high wave fields and storm surge changes at Pärnu city (~16-20% increase). Under RCP4.5 scenarios some intensity increase could be expected as well, however considerably less pronounced. Westerly approaching ETCs will bring more precipitation to the Baltic Sea area in the (warmer) future. In case of a southerly cyclone (2008 Snow Storm), the results are more mixed. For AO the future results were inconclusive, under weak synoptic flows the future scenarios tend not to follow, and are either under- or overestimated over simulation period (strong storm fields are captured with higher accuracy). In the future Arctic, the storm response to atmospheric changes is uncertain, however during periods of sea ice fee seasons, can expect increased wave energy distribution in the central and coastal regions of AO, which would make socio-economic activities in the area increasingly difficult. Coastal disaster and adaptation measures a in the considered study area communities likely need to follow different approaches for a sustainable future. In Tuktoyaktuk (AO) hard measures would be more effective, whereas soft and smart solutions seem more feasible for Pärnu (NAO). The study results indicate more energized atmospheric and sea state response during future ETCs (at least for truly extreme events). To increase the level of confidence of future storm responses, further studies in the field are recommended.

Acknowledgements

First and foremost, I would like to give my utmost gratitude to Prof. Tomoya Shibayama, my academic supervisor throughout the doctoral program. It is because of his kindness, wisdom and optimistic nudging I got to pursue my scientific aspirations in the higher degree. Through the many years under his supporting wing I have grown in nearly every aspect of my life. The largest and perhaps a cumulative impact of those years are manifested in this dissertation.

I would like to thank all the other people who have assisted in bringing this work into fruition. Lot of gratitude goes to Dr. Nakamura, with whom I have had countless of hours well spent on stimulating discussions about various aspects of modelling and climate change. Deeply grateful for all his discussions and shared efforts during various projects undertaken. Also, would like to thank Dr. Tomoyuki Takabatake and Prof. Esteban for their interesting and motivating discussions over the past years. Further, would like to extend my uttermost gratitude to all the student members in the Shibayama Lab who have been an integral part during the past years! Deep gratitude goes to Dr. Ülo Suursaar, my Estonian master's degree supervisor. Thanks to his kind and patient directions I learned a great deal about coastal processes in Estonian waters and the Baltic Sea. Thank you for all the insightful discussions and supporting my academic progress!

I would like to extend a deep gratitude to all the members I worked with in the Waseda University Academic Writing Center. During my 1-year stay there, I met many incredible people who taught me a great deal about academic writing and tutoring. Without doubt this experience has been one of the more rewarding ones.

I would also like to extend my sincere gratitude to all the member of Japanese Embassy in Estonia and Monbukagakusho (MEXT). Without their support and funding the whole study process in Japan would have been near impossible. Therefore, I truly appreciate the opportunity given, and I thank everyone involved in making that happen.

Lastly, and perhaps in many ways most importantly – my dear family and friends back in Estonia. Everyone has been supportive beyond belief. Especially would like to mention my mother Janika Olup, and grandmother Aino Soots, your visits and constant support have helped to keep part of home always close by. I love you all, and this work is dedicated to you!

TABLE OF CONTENTS

1 Introduction

1.1 Background info

Contemporary climate change has already caused cascading changes and adverse effects in Earth System and, according to modern scientific opinion expressed e.g. in the latest IPCC's (Intergovernmental Panel on Climate Change) Fifth Assessment Report (AR5), will most likely cause even more in the future. Consequently, the study of future climate change related risks is of crucial importance in order to help societies cope with the impacts (Hill 2012). According to many researchers, climate variability and uncertainty has grown over the last fifty years (e.g. Stainforth et al. 2005) and extreme weather events are becoming more intense (Emanuel 2005; Matulla et al. 2008). However, the discussion on changes in storminess is still full of uncertainties. There is no overall agreement on whether the frequency and intensity of storms has increased or will increase in the future: compared to the sample size, the natural variability of storms is large (Trenberth 2005); geophysical data series are frequently plagued by inhomogeneities (Van Gelder et al. 2008); increasing storm-related economic losses do not only reflect the trend in a geophysical phenomenon but also the growth of population and infrastructure in the coastal zones (Webersik et al. 2010). It is increasingly possible that at least tropical cyclones will get stronger as a result of further climate warming (Knutson & Tuleya 2004; Mei & Xie 2016). However, the discussion on changes in storminess is still full of controversies. There is no overall agreement on whether the frequency and intensity of mid- and high latitude storms has increased or will increase in the future.

In Europe, much of the high-impact weather events are associated with extratropical cyclones (ETCs; e.g. Feser et al. 2014). In addition to impacts as windstorms, ETC-s have caused heavy precipitation and storm surges in many coastal areas, including the Baltic Sea (Averkiev and Klevannyy 2010; Wolski et al. 2014). Coastal zones are highly vulnerable to changes in Earth climate system, firstly, due to anticipated mean sea level rise, and secondly, regarding changes in storm activity. Concurrent impacts are inundation of low-lying urban areas, coastal erosion, damage to infrastructure or even loss of life (Emanuel 2005). The activity of ETCs is a dominant feature anywhere in the mid-latitudes during the period from autumn to spring (Mizuta 2012); any change in this activity due to global warming would have a marked influence on socio-economic and ecological systems, as well as the daily lives of many people (Hoegh-Guldberg and Bruno 2010).

Arctic Ocean and the rapid changes in its system has gained increasing international attention from researcher, policy-makers and local inhabitants over the past decades. Historically, measurements and data from the Arctic have been extremely low. With the advent of satellite age an increasing number of workable data has been made available to better understand the Arctic system and changes within. For instance, the annual Arctic sea ice extent has decreased around 0.45 – 0.51 million km^2/decade over the period of 1979-2012. For sea ice minimum during the summer period the decrease has been at around 0.73 to 1.07 million km^2/decade (IPCC, 2013). According to Hartmann et al. (2013) the satellite data shows particularly significant losses of Arctic sea ice at the end of annual melt season in September, when the sea ice extent is at its minimum. The ongoing Arctic amplification (positive feedback loop) has an extremely wide range of global and local implications. The latter has already caused negative impacts to coastal communities along the Arctic coastline. The decreasing annual sea ice extent leaves much of the coastal water open for potential high wave attacks for a longer period of time (Stopa et al. 2017). In return, exposing the low-lying and soft coastline to rapid erosion. The hamlet of Tuktoyaktuk in Northern Canada is one of such settlements that has experienced these rapid changes first hand. Over the period of 21st century it is very likely that the Arctic sea ice will continue to decrease (IPCC, 2013), and recent studies have even suggested that by 2050 there is a risk for ice-free summer (Screen & Deser 2019). These ongoing changes further increase the annual wave energy flux in the region (Wang et al. 2015), and the Arctic settlements along the southern Beaufort Sea (such as Tuktoyaktuk) face many challenges to keep their cultural heritage and homes from the advancing sea.

Most climate related research in the Arctic region mainly focus at more general atmospheric and coastal changes through historical records or climate models (e.g. Semedo et al. 2014). On the other hand, single extreme storm event and their local impact studies are rare and not discussed in detail. A notable exception is The Great Arctic Cyclone of 2012, which has received more in-depth research (e.g. Khon et al. 2014), however those studies investigated more the cyclogenesis processes and its impact to sea ice changes through wind and wave fields. Whereas in Northern Europe there are historically many high intensity storm cases, which have prompted hindcast studies into these individual storms. However, there are still very few studies made on individual extreme storm cases under future climate conditions. In terms of climate adaptation, it is increasingly important to further our scientific knowledge on the future storms and their potential implications to our society.

1.2 Rationale and objectives

If the storms would retain their strength throughout the 21st century, mild storm surges still become severe and severe ones turn to catastrophic. Storm pathways may also change in time (e.g. Sepp et al. 2005; Pinto et al. 2007). In Northern Europe, it is necessary to understand if the ETCs become stronger under the rising temperatures in the Baltic Sea region; will floods become more dangerous due to global sea level rise, higher storm surges or as a combination of both? In Arctic the same questions apply to an extent, however more importantly it is necessary to understand how the wave climate will change under warmer climate (new thermal conditions and ice-free Arctic Ocean).

The aim of the study is to determine and analyse the possible changes of future cyclones (under RCP4.5 and RCP8.5 scenarios) in Northern Europe and Arctic basin and the subsequent potential implications to coastal communities in those areas for years 2100 and 2050, respectively. Most notable and recent extreme storm event are chosen and numerical methodology is developed that fits for the study areas. For Europe, the study considers four seasonally different winter storms (tracks and thermal conditions), mainly due to the potential socio-economic impact consideration these storms have in that area (wind and surge damage). Whereas Arctic, in contrast, is scarcely populated and the current economic significance in the area is low. Furthermore, since the Arctic as a study area is challenging for numerical studies (mainly due to data availability), the current research mainly aims to establish a working methodology for past storm hindcasting and future simulation through a single case study. Additionally, since the main coastal concerns in the Arctic come from the accelerated erosion processes, the study focus is mostly placed on surge-wave-ice fields.

The main contribution of the study lies in providing an appropriate method for mid- and high latitude storm studies in the Northern Europe and Arctic, respectively. The secondary contribution lies in the added value for scientific communities through future study results. More precisely, the results of this research should provide some additional perspective in regards to climate change effects on extratropical cyclones, and thereby decrease a level of uncertainty which revolves around these storm systems in the future.

2 Literature Review

2.1 Definition of storms

In different section of Earth, various storm types are more dominant. The main storm systems, going from the equator to the poles are the tropical cyclones, extratropical cyclones and polar lows. The concurrent socio-economic impacts these storms usually cause, also decrease respectively. The spatial and temporal occurrence of cyclones also exhibit notable differences. The TCs develop near the tropics over warm ocean water and propagate towards west-northwest. The ETCs on the other hand develop in the mid-latitudes and usually tend to propagate towards east-northeast in the North Atlantic Ocean. The polar lows however, develop above the Arctic circle and their directional movement can vary greatly. In this section the general characteristics of ETCs in the Northern Europe and Arctic are discussed.

2.1.1 European windstorms

In Europe the most impactful (potential damage) are the extratropical cyclones, which are synoptic-scale low pressure systems (~1000 km) that grow from unstable frontal waves (Eady 1949, Shapiro & Keyser 1990). These storm systems need a strongly baroclinic atmosphere and strong north-south temperature gradient to grow. During the winter period (October – March) these conditions are met in the region of North Atlantic Ocean, allowing ETCs to form through cyclogenesis. Usually the storms travel eastwards towards Europe. The storm path tends to curve northwards (Hoskins & Hodges 2002), and therefore Iceland and northern European countries (e.g. the Ireland, Faroe Islands, UK, and Scandinavia) are frequently hit. However, occasionally the storms can travel further southwards, for example when the jet stream is in a more southerly position (e.g. Liberato et al. 2013), affecting countries such as Portugal, Spain, and France. Figure 1 shows the conceptual model of windstorms in the North Atlantic (Hewson & Neu 2015).

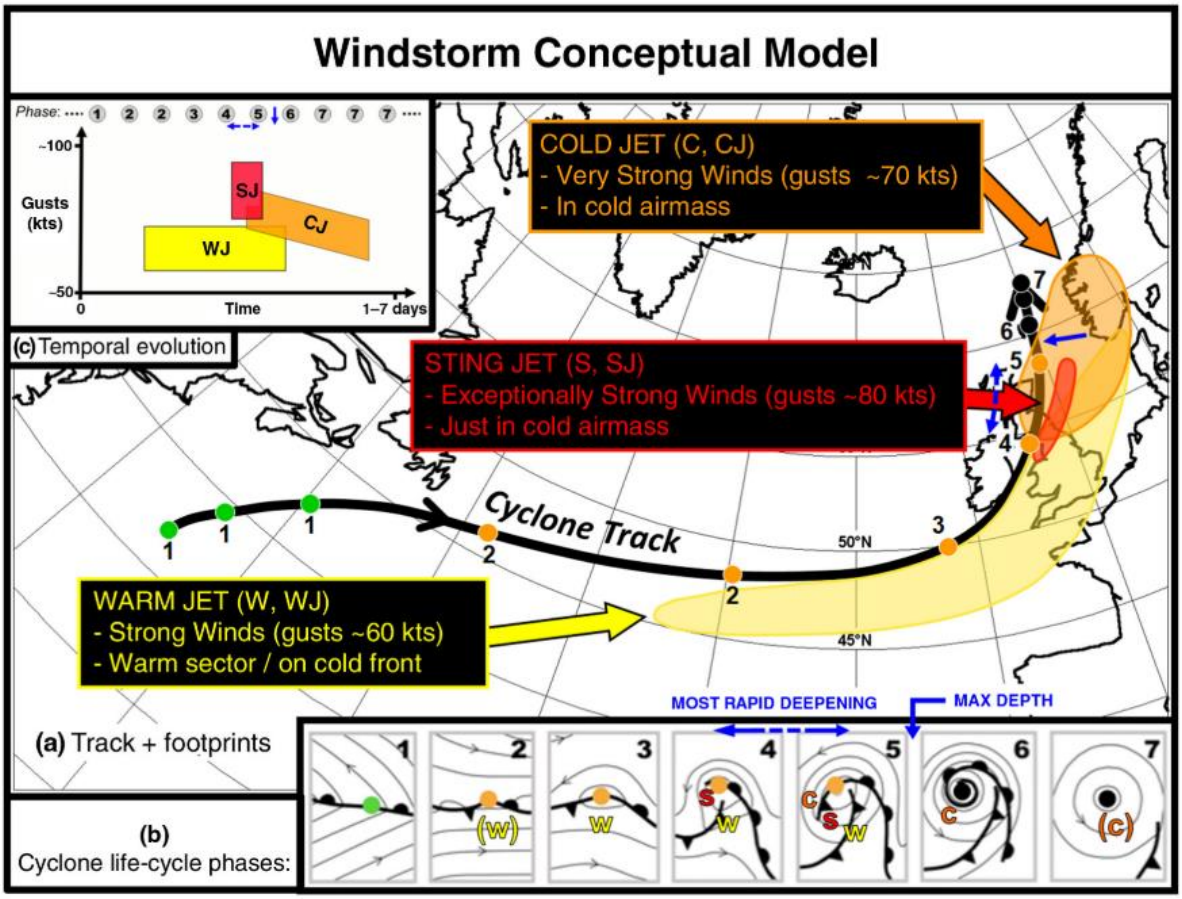

Figure 1. Conceptual model of an extra-tropical cyclonic windstorm. Panel (a) shows the cyclone track (black), with spots denoting positions equally separated in time, and numbered according to the cyclone life-cycle phases in panel (b). Figure after Hewson & Neu (2015).

2.1.2 Arctic cyclones

The storm climatology in the Arctic basin has a wider range of weather systems and it is often difficult to classify the type of atmospheric low pressure system. As in Europe, in the Arctic also extratropical cyclones can form, as was the case with the Great Arctic Cyclone of 2012 in August (Fig. 2) which was the strongest summer cyclone in record and 13th strongest overall since the beginning of the satellite measurements (Simmonds & Rudeva 2012, Zhang et al. 2013). Cyclones during the winter months are usually stronger than the summertime ones since the conditions for cyclogenesis process that allows ETCs to form are met – the meeting of the Arctic's colder fronts and the equatorial area's warmer fronts – are at their respective peaks (Kirkpatrick 2018).

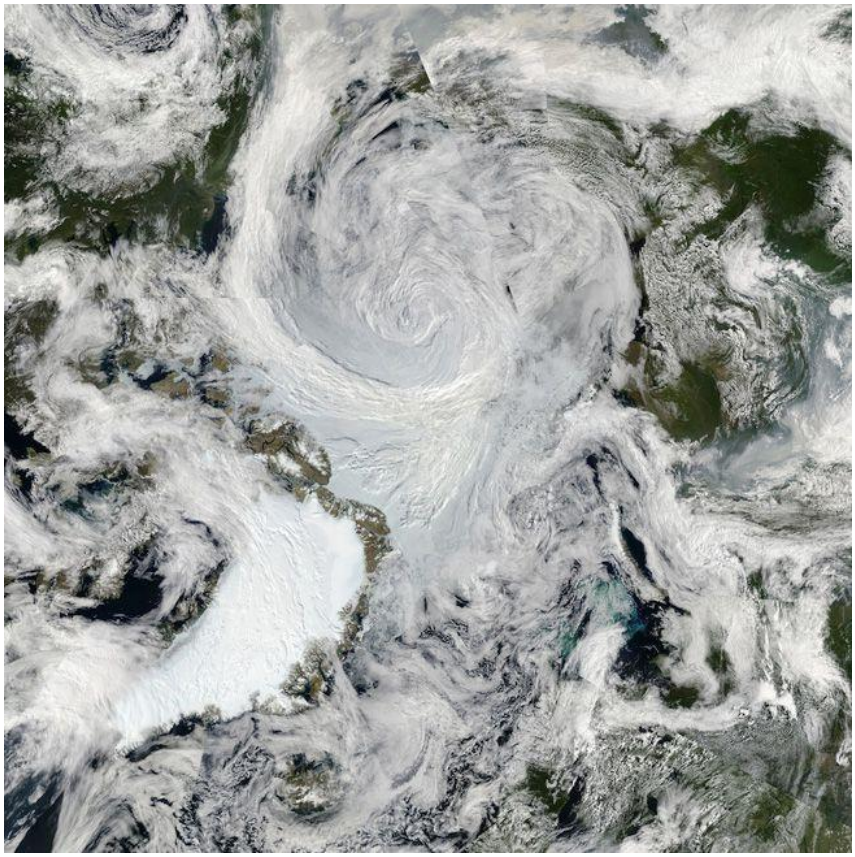

Figure 2. Satellite imagery of The Great Arctic Cyclone of 2012 on August 6. The cyclone started in Siberia and settled between Alaska and the North Pole (Source: NASA).

Another weather system type in the Arctic are the polar lows. These systems usually have a horizontal length scale of less than 1,000 km and exist for no more than a couple of days. The polar lows mostly occur during the winter season in the Arctic, while during the summer period the disturbances are very few. In contrast to ETCs, the active polar lows have a horizontal length scale of around 400-600 km. However, sometimes convective systems can have smaller vortices embedded within them. Polar lows are part of a polar mesocyclones, these are a broad category of disturbances that include many minor vortices (observed from satellite data in the polar region; Harold et al. 1999). The definition of a polar low is that its surface wind speed of gale force should be 17 m/s or more. These system cause some of the worst weather conditions in Arctic coastal and island locations. Observations have indicated that they can have wind speeds as high as 33 m/s (Turner & Bracegirdle 2006). There are various types of polar lows and even hybrid systems. In the Arctic, 7 categories have been identified by Rasmussen and Turner (2003).

2.2 Observations and trends of ETCs

The impacts of storms are always strongly dependent on storm track in relation to coastline configuration, bathymetry and other factors (Tasnim et al. 2015). For instance, a truly remarkable storm making its landfall on straight and sparsely populated coast may have a smaller impact than the one which happens to hit a heavily indented, low-lying and densely populated coastal areas. Thus, the physical intensity of a storm does not necessarily coincide with the severity of the event in terms of environmental or societal impact. Extreme sea levels can sometimes occur due to a favourable combination of factors, though within their normal range of variability. If the individual factors are statistically independent, the probability of the "perfect storm" or the most devastating storm surge can be so low, that it has not occurred yet within the measured history, although in principle it can happen at any time. For instance, in spite of the incredible damage hurricane Sandy caused in late October 2012, recent modelling studies demonstrated that Sandy's storm surge was not the worst-case scenario for the New York area (Forbes et al. 2014). The same was in principle noticed for the cyclone Gudrun in the Baltic Sea in 2005 (Suursaar et al. 2006). Moreover, as a result of climate change and global sea level rise, the probability of one or more constituents for a perfect storm may be gradually changing for worse.

In the Baltic Sea region, which is the main study area for the current study, the increase in storminess has been observed over the last 50 years (e.g. Gregow et al. 2012), however not over the longer, 100-150 years period (e.g. Weisse et al. 2009; BACC 2015). Those observed changes are largely related to the northward shift and eastward extension of the storm tracks (Ulbrich et al. 2009; Zappa et al. 2013b), which also means that time-varying and different, even contrasting, tendencies above Southern and Northern Europe are possible. Cyclones affecting the Baltic Sea may propagate along several distinct tracks.

In the Beaufort Sea region (and in Arctic in general), no long-term observations are available and the few longer data timeseries that do exist are more than often plagued with uncertainties and long gaps in measurement recordings (e.g. Manson & Solomon 2007). However, over the past decades various satellite products in conjunction with available in-situ measurements (Hudak & Young 2002, Francis et al. 2011, Wood et al. 2013) and numerical models (Thomson & Roger 2014, Wang et al. 2015) have been used to study trends in storm climatology in the Arctic. In terms of long-term variability, Hudak & Young (2002) studied NCEP reanalysis dataset from 1970-1995 (June-November months

exclusively) and found that on average 14 storms entered Beaufort Sea area per storm season (overall, 58% of the storms were Arctic, 27% Pacific and 15% Irregular). Although no distinct trend was found over the 25-year period. In contrast, Zhang and Walsh (2004) extended the earlier study periods to 55 years (1948-2002) and found that during the second half of the 20th century that the number and intensity of cyclones entering the Arctic from the midlatitudes had increased. Similar time period study was conducted by Hakkinen et al. (2008), by looking at changed in wind stress and ice drift. The results identified a new trend where surface wind stresses have increased over the 56 year period and that sea ice movement and storm activity are connected via cause-and-effect relationship. Furthermore, recently more studies have emerged that investigate not just changes in climatology but also changes in wave climate. A study by Stopa et al. (2016) conducted a wave hindcast study with 1992-2014 NCEP CFSR wind forcing and for verification used wave altimetry data. The study results confirm that with the sea ice further decreasing, the swells are becoming more prevalent as the effective fetch increases as the sea ice minimum decreases. Similar results were presented by Wang et al. (2013), where the 1970-2013 Arctic sea state changes were studied with the Environment Canada's Beaufort Wind and Wave Reanalysis data.

2.3 Future projection of ETCs

Future change in storminess has been extensively studied in recent decades using various approaches and modelling tools. One possible way is to project future climatological changes in relation to various greenhouse gas concentration trajectories (Representative Concentration Pathways or RCPs) using general (global) circulation models (GCMs) and subsequent downscaling models. Although yielding a vast amount of statistics and secondary projections on basic climatological variables such as sea surface temperature (SST), air temperature and humidity on various heights, precipitation, and sometimes also wind speeds, individual events can be hardly separated and investigated from such projections. Kimura and Kitoh (2007) and Sato et al. (2007) introduced a dynamical downscaling method which uses both present re-analysis data and the monthly mean value difference between present climate and future climate for creating new boundary conditions. In addition, Kawase et al. (2009) further developed this idea and proposed a pseudo-climate simulation. Further on, the idea of nesting a past notable event into hypothetical future with altered boundary conditions was e.g. used by Oh and Moon (2013), and Vecchi et al. (2013). Using a set of atmospheric and ocean

models, the Advanced Research Weather Research and Forecast Model (ARW-WRF) and the Finite Volume Community Ocean Model (FVCOM), Tasnim et al. (2015) simulated the historic cyclone Nargis (2008) under the future climate conditions (i.e. in 2100). They found that the cyclone would be stronger and the storm surge in the Bay of Bengal much higher. Using a similar approach but more advanced methodology, Nakamura et al. (2016) studied the storm and surge parameters of super-typhoon Haiyan (2013). The tsunami-like, approximately 6 m high surge at Tacloban, Philippines, was the most devastating one in the region's history. Yet the storm surge got about 1-2 m higher when only the SST rise was considered and roughly 0.5 m higher when a wider set of meteorological parameters were used for describing the future change. Although the degree of uncertainties for such calculations was fairly large (e.g. Nakamura et al. 2016), they mostly seemed to confirm that tropical cyclones could indeed get stronger under warming future climates. However, this kind of methodology deals with a specific event and it cannot indicate how the frequency of storm events generally would change.

Future Recent climatic changes in Northern Europe have been faster than the global ones, especially when considering atmospheric temperatures of winter months (Rutgersson et al. 2015). Climate changes in Europe are well studied and there are also several climate modelling projects based on different future greenhouse gas emission scenarios (e.g. projects CMIP5, EURO-CORDEX; Jacob et al. 2012) enabling an ensemble approach. Still, future projections regarding winds and extra-tropical cyclones (ETCs) are generally less elaborated and not as reliable as those of temperatures and precipitation (Christensen et al. 2015). Recently, there have been pan-European studies on storm surge frequency (Vousdoukas et al. 2016; Groenemeijer et al. 2016), which have provided some new insight into the topic.

Currently, an increase in storm track intensity above the Baltic Sea region is generally assumed (Gregow et al. 2012). Those observed and anticipated changes are mainly related to the northward shift and eastward extension of the storm tracks (Ulbrich et al. 2009; Zappa et al. 2013a). However, possible future changes in parameters of individual ETCs have been less studied so far and the results are more controversial (Feser et al. 2015). Even in case if the ETCs would not significantly increase in the future, the storm-related marine risks will still do, as the global sea level rise and its acceleration aggravates the threat (Hogarth 2014). According to the latest IPCC's assessment report from 2014 (AR5), global mean sea level (GMSL) has risen by 0.19 m over the period of 1901–2010; it is very likely that the mean rate increased to 3.2 mm yr^{-1} between 1993 and 2010. For the period of 2081–2100, compared to

1986–2005, and following the IPCC's Representative Concentration Pathways (RCP's), the GMSL is likely to be 0.32 to 0.63 m for RCP4.5, and 0.45 to 0.82 m for RCP8.5. By 2100, this yields a mean rise rate of 5 to 10 mm yr^{-1}.

Future projection studies in the Arctic are still at their early stages when it comes to studying changes in storm frequencies and intensities. Currently most of the research for the future looks at changes from the perspective of diminishing yearly sea ice extent (e.g. Thomson & Roger 2014), and less so under energized climate state. Most projection studies however also utilize the CMIP5 experiment output in order to estimate changes in climatological shifts by looking at long period GCM simulation results (e.g. Zappa et al. 2013b). Similar approach has also been applied for the Arctic Ocean studies. For instance, Dobrynin et al. (2012) looked at change in global wind wave climate by forcing the WAM wave model with wind from Earth system model (EC-Earth) over the 250 year period. Their results suggested increase in wind speed and subsequent wave heights in the Arctic (under both RCP4.5 and RCP8.5 scenarios). Similar research was conducted by Khon et al. (2014), however they used the WAVEWATCH-III model and forced by winds and sea ice concentrations from the HIRHAM regional model with the SRES-A1B scenario. Their study was Arctic specific (not global) and the results suggested regional significant wave height (and its extremes) intensification in the 21st century over different inner areas. Although in some regions of the Arctic Ocean opposite trends was noted (Atlantic sector and Barents Sea). While most of the GCM CMIP5 long-term studies seem to suggest that the average wind speeds seem to increase over the Arctic Ocean, there are still no studies that look at more extreme event-based Arctic cyclone events under climate change modelling approach (i.e. pseudo-climate method).

3 Study Areas

3.1 North Atlantic

The North Atlantic region is situated between the North American and Eurasian continents, where air masses mostly follow Westerlies from west to east. The large scale winds in the area are highly influenced by the Icelandic Low (low pressure system) and Azores High (high pressure system), where air flows are counterclockwise and clockwise, respectively. When the generated air currents meet, they determine much of the wind patterns over Atlantic and Europe. In the winter time, the breaking cold air masses from Canadian Arctic and warm air masses from low latitudes create a strong temperature contrasts at the zones where they meet (fronts). In return ETC are formed at these zones that usually move towards northeast direction, often diverging towards Iceland and further north, or towards further east over the Northern Europe. The intensity of these cyclones is largerly determined by the amplitude in temperature differences at the front (because of this, the generated storms tend to be stronger in the winter months when the contrasts are the highest). However, the because the North Atlantic pressure distribution can greatly vary (e.g. interannual variability, and various upstream teleconnection at much larger scale), then the climate and prevailing wind and storm tracks can also vary. For instance, when the dominant low pressure fields over Iceland are replaced with high pressure fields, then the storms path is blocked by that and they move towards south (usually West-Southwest Europe). In this case the mild weather that the warm Atlantic airs bring are replaced by the cold air masses moving in from the European Arctic and continental Russia (e.g. Barnes et al. 2019).

These movements and changes in the North Atlantic weather patterns are described by the North Atlantic Oscillation (NAO), which determines and shapes all the atmospheric variability in the area (Barnston & Livezey 1987). As previously noted, this mode is more pronounced during winter and more than one-third of the interannual winter total variance in sea level pressure (Cayan, 1992; Hurrell et al., 2003, and references therein) is governed by it. The changes in Atlantic Ocean, ecosystems and in meteorological parameters are influenced and associated with NAO (Bader et al. 2011; Hurrell & van Loon, 1997; Alexandersson et al. 1998; Hurrell 2002; Hurrell & Deser 2009; Frankcombe et al. 2010; Woollings 2010). The NAO influence to ETCs is closely linked, during the positive phase of NAO stronger and more frequent ETCs will make their way Iceland and Norwegian Sea (Serreze et al. 1997; Deser et al. 2000). The same extension applies to Baltic Sea region, which is more

susceptible to ETCs during the positive phase (Fig. 3). In this case, more moisture and precipitation is carried to these areas. In contrast the low latitude areas will have drier conditions and less storms reach those areas (Mediterranean and northern Africa).

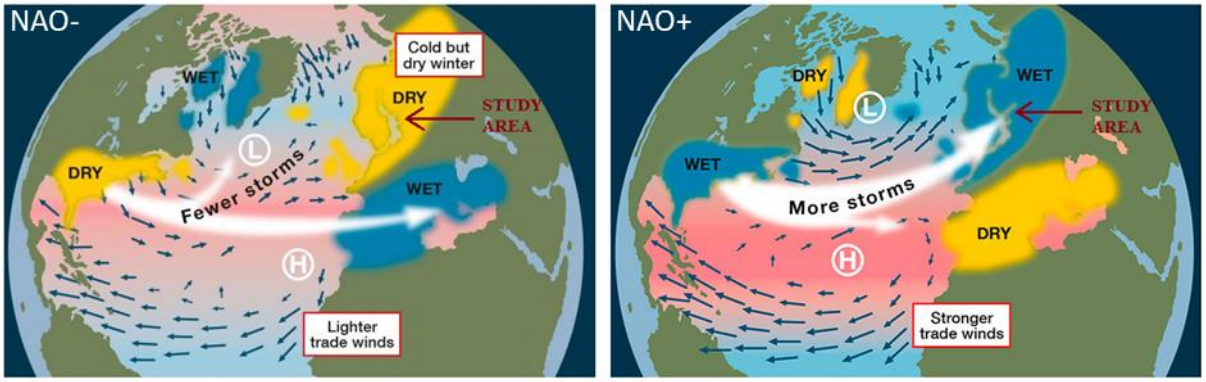

Figure 3. Simplified illustration on the effects of NAO phases to regional weather patterns around the North Atlantic area (image after Nelson 2017).

3.1.1 Baltic Sea

Lying at high latitudes under the so-called North Atlantic storm track (Schernewski et al. 2011), the relatively compact, cyclone-prone Baltic Sea (Fig. 4) is a suitable model area for testing interdisciplinary approaches to study the parameters and impacts of future ETCs. Such atmospheric low pressure systems form near the polar front in the Northern Atlantic Ocean, between Iceland, Greenland and Newfoundland Peninsulas, during the colder half of the year. While travelling along the westerlies towards the Baltic Sea region, the ETCs can pose a great threat to the British Isles, Scandinavia and other parts of Northern Europe. In addition to bringing heavy wind and rain, ETCs may cause storm surges of 2–4 m height in certain locations of the Baltic Sea (Averkiev & Klevannyy 2010). The other concurrent impacts are inundation of low-lying urban and coastal areas, loss of life, damage of infrastructure, coastal erosion, siltation of naval channels and secondary pollution (Cormier et al. 2013). The recent most influential ETC that affected Estonia was 9 January 2005 storm Gudrun (Suursaar et al. 2006).

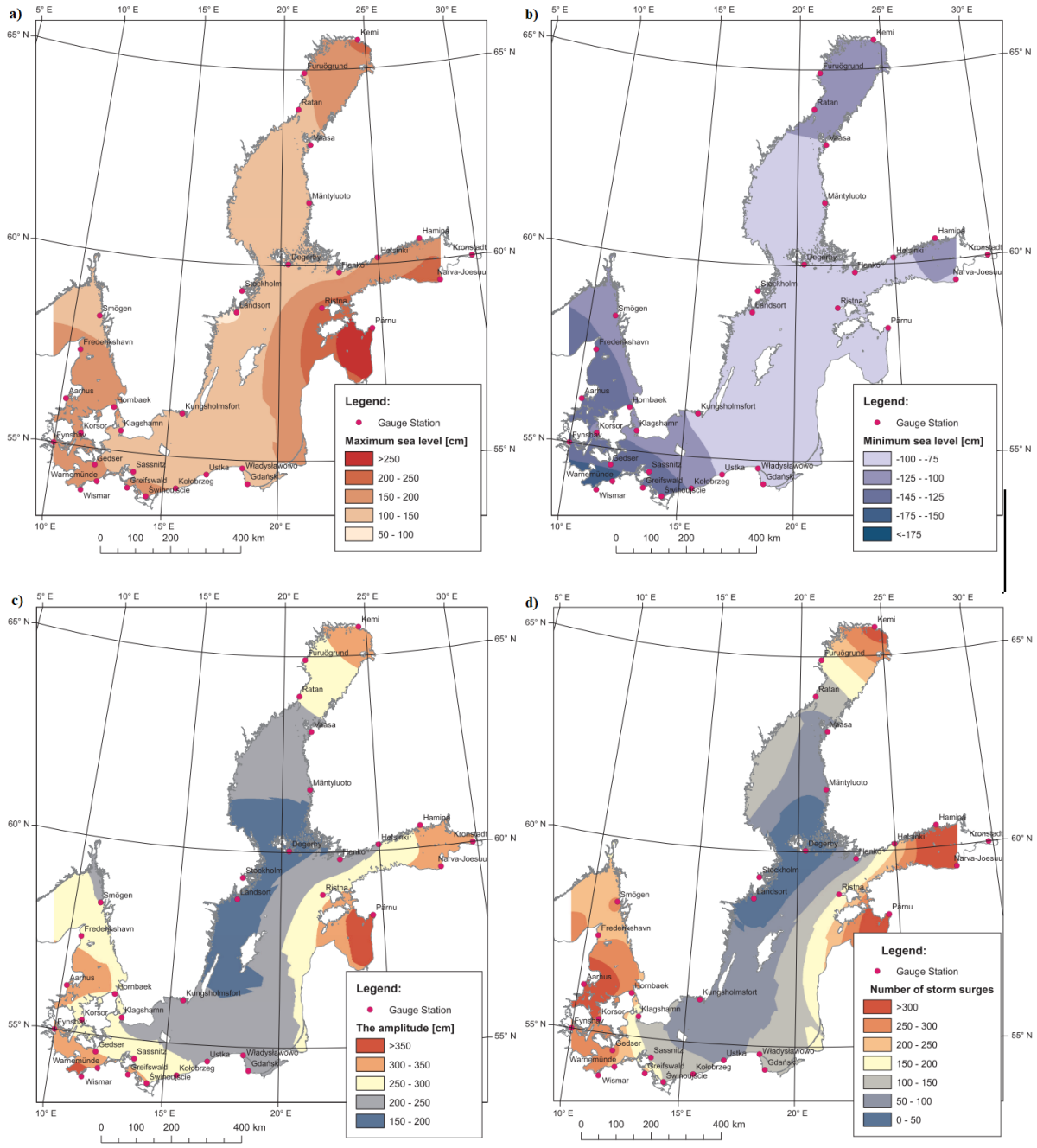

Figure 4. Surface water topography of the Baltic Sea for maximum levels (a), minimum levels (b), the amplitude of variations (c) from the period 1960–2010 and d) number of storm surges ≥70 cm above zero Normal Amsterdam Peil (after Wolski et al. 2013).

3.1.1.1 Pärnu (Estonia)

Pärnu Bay is a shallow marine area on the NE corner of the Gulf of Riga, Baltic Sea (Fig. 4). The maximum depth of the 14 x 14 km^2 inner Pärnu Bay is just 8 m. The bay receives some freshwater input from the Pärnu River; on the banks of the river mouth, Pärnu resort town (pop. 45 000) and port are located. The most serious hazards for the Pärnu Bay

area are related to occasional, south-westerly storms in autumns or early winters, which are mainly caused by the ETCs of the North Atlantic origin. Such storms may cause power cuts, toppling of woods and rooves, and storm surges of up to 2–3 m height (Suursaar et al. 2006).

Sea level observations at Pärnu tide gauge have been carried out since autumn 1923. At present the hourly measurements are operated by the Estonian Environmental Agency (EEA). The long-term average sea level at Pärnu in 1923–2014 was 1.2 cm according to the Baltic Height System 1977 with its reference zero-benchmark at Kronstadt near St. Petersburg (Bogdanov et al. 2000). Approximately 90 % of the (hourly) data falls between -40 and 50 cm (Suursaar & Sooäär 2007). However, the sea level variability range at Pärnu is up to 400 cm (from -125 to +275 cm), being the highest in the Estonian coastal sea and one of the largest in the Baltic Sea (Suursaar et al. 2015). Yet the amplitude of tides is less than approximately 5 cm in the Baltic Proper (Magaard & Krauss 1966), because Danish Straits are too shallow and narrow for letting considerable amount of tidal flows through before the astronomically forced flow direction reverses. On the other hand, the Baltic Sea is not large enough for developing its own tides.

The impacts of storms are usually track-dependent, they mainly include so-called inverse barometer effect and influence of wind stress in reaction with the coastal topography (Wiśniewski & Wolski 2011). A sea level inclination within the elongated, but practically isolated from the World Ocean (in cyclonic time scales 1-2 days) Baltic Sea is created. The strongest winds of a travelling cyclone occur to the right from the cyclone track (on the northern hemisphere). While invading from west to northeast across the British Isles and Southern Scandinavia, the tracks of most dangerous cyclones pass Estonia about 100–500 km to the north, which yields local SW-W winds with sustained speeds up to 20–30 m s^{-1} and, occurring roughly each winter, sea levels of up to 150–200 cm. For the even higher total sea levels, gradually pre-elevated (by up to 50–70 cm) mean Baltic Sea level as a result of prolonged periods of intense westerlies or a series of preceding cyclones is needed. The sea level build-up is duplicated on a smaller scale within the Gulf of Riga and it is strongest in the far ends of windward bays. Thus, a crucial feature is two-tier morphological configuration of the Baltic Sea – Gulf of Riga system and the south-westerly exposure of the Pärnu Bay in the end. The length of the Pärnu Bay measures approximately 40 km. Its width converges from 25 to 10 km and the cross-section average depth vanishes from 15 to 3 meters. These basin measures alone let the barotropic wave height to grow by a factor of 2.3 within the bay (approximated using e.g. the Green's Law; LeBlond & Mysak 1978).

Over the period of 1923–2015, the Pärnu sea level record (Fig. 5) includes 21 individual events higher than the critical value of 160 cm. As the north-south extent of the Baltic Sea is quite considerable (approx. 1400 km) the list of most influential historical storms in the Estonian coastal waters may differ from those of European extreme wind catalogues (e.g. Roberts et al. 2012). The two highest sea level events off the Estonian coast (since 1923) were both registered at Pärnu: 253 cm on 19 October 1967 and 275 cm on 9 January 2005. The long-term trend of maximal sea levels (both on annual and monthly basis) has been slightly increasing since 1923 with a linear trend rate 1.7 mm yr^{-1} (Fig. 5). One must also consider the influence of vertical land movements in the area, which partly compensates the influence of the global sea level rise. Locating on the edge of Fennoscandian postglacial uplift zone, the crustal uplift rates vary in Estonia between (0–3 mm yr^{-1}; Kall et al. 2016). Consequently, the long-term relative sea level variations in Pärnu in future will depend on regional land uplift, global sea level rise, and regional influence of changing wind climates.

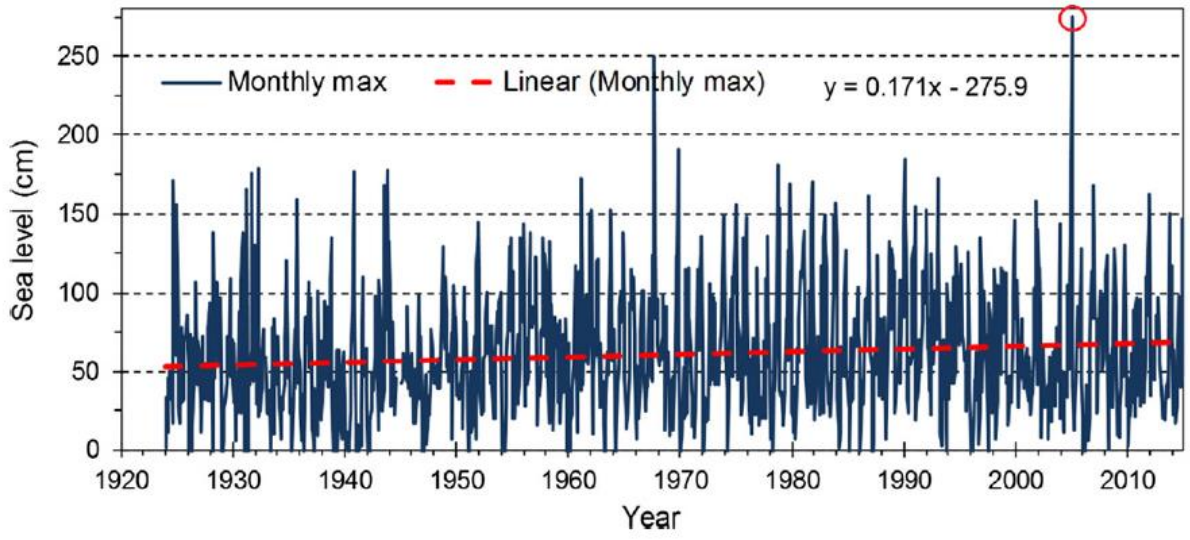

Figure 5. Variations in observed monthly maximum sea levels (1924–2014) at Pärnu tide gauge. The storm surge of Gudrun (January 2005) is marked with a circle. The linear trend is 1.7 mm year-1; no land uplift correction is introduced.

3.1.2 Case studies

This subsection presents a review on ETCs considered for the case studies. The development and impacts of these storms are discussed in detail, and storm tracks over much of Europe can be seen on Figure 6.

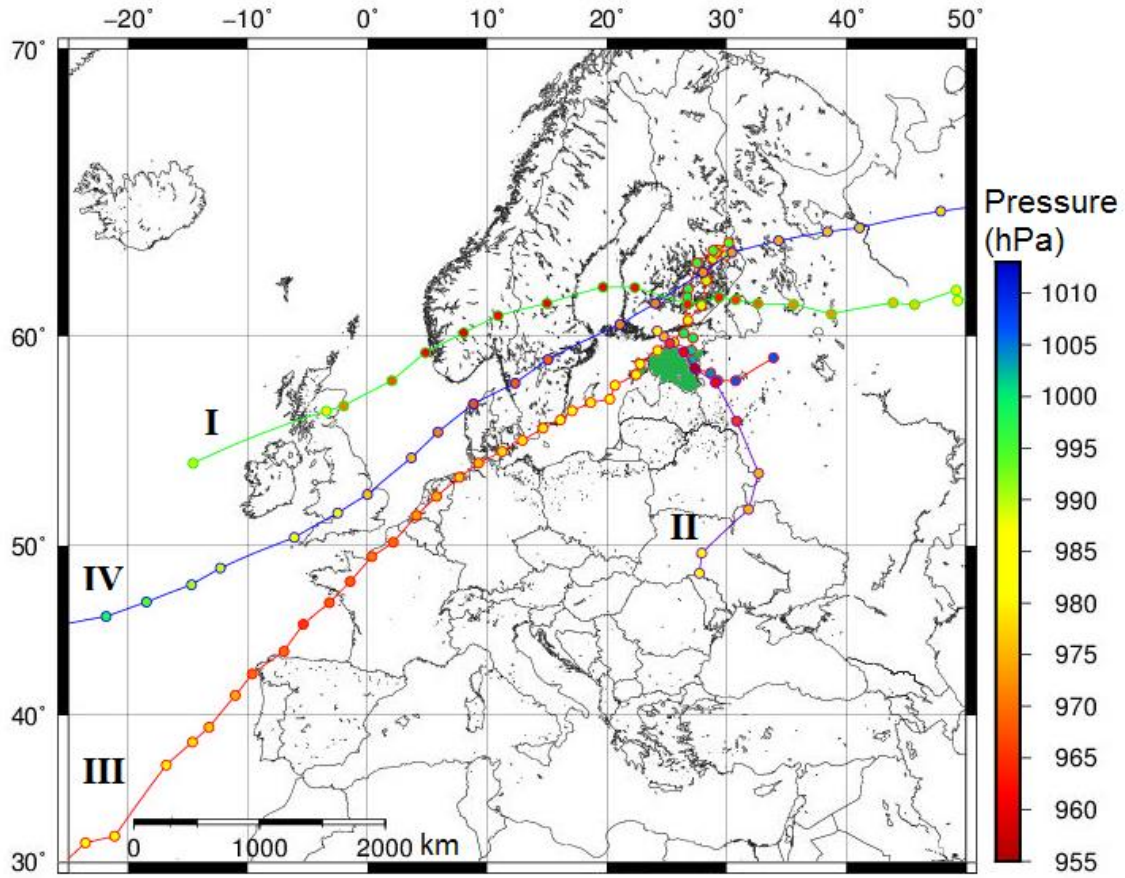

Figure 6. Tracks of four studied European ETCs. I – January 2005 storm ("Gudrun"), II – November 2008 (snowstorm), III – February 2010 ("Xynthia"), IV – October 2013 ("St. Jude"). The colours in circles show MSLP values and the location of Estonia is marked in green. The cyclone II actually originated more southward than shown, however its track identification was complicated in earlier stages. Atlantic storm track data are from XWS Catalogue (Roberts et al. 2014) and 2008 storm track is compiled from pressure charts (www.wetterzentrale.de).

3.1.2.1 2005 "Gudrun"

The hurricane known as Gudrun in the Nordic Countries and Erwin in the British Isles and Central Europe crossed the Baltic Sea on 8–9 January 2005. Over the course of the storm, at least 17 people lost their lives in Nordic Countries, including one senior citizen in Pärnu, Estonia (Carpenter 2005). Gudrun formed as a gradually deepening perturbation of the polar front in a region West of Ireland in the afternoon of 7 January 2005 and moved fast eastward over the British Isles, Scandinavian Peninsula and Finland. The nadir point of 957 hPa was reached northeast of Oslo at 20.00 UTC on 8 January 2005 (Post & Kõuts 2014). According to the Saffir-Simpson classification, the cyclone reached hurricane strength based upon the

maximum mean wind speed measurements both in Denmark and Sweden. According to the Danish Meteorological Institute (DMI), the highest sustained wind speeds reached 34 m s^{-1}. Estonian territory also fell into the zone of the cyclone's strongest wind speeds. Maximum average speeds of SW and W winds went up to 28 m s^{-1} on the West Estonian coast and gusts reached 38 m s^{-1} (Suursaar et al. 2006). Actual maximum wind speeds could have been even higher as the malfunctioning measurement equipment due to power outage left gaps in several wind speed records interposed among some very high readings. Also, there were missing or distorted data from some of the tide gauges (such as Ristna). Therefore, many of the storm parameters were later needed to be evaluated with models (Suursaar et al. 2006). The average Baltic Sea level had already been high since December 2004 as a result of the strong cyclonic activity that forced the water from Kattegat through the Danish Straits into the Baltic Sea. As a result of high (+70 cm) initial sea level (Fig. 7) and the fast travelling cyclone with a favourable trajectory, the new highest recorded storm surge occurred in Pärnu, as well as in many other locations along the West Estonian coast. Sea level height reached 275 cm at 04 UTC, 9 January 2005 according to the Pärnu mareograph data. The sea was ice-free as a result of warm and windy weather conditions that preceded the event. Wave hindcasts indicated that record-high waves (significant wave heights up to 9.5 m) could have occurred in the Baltic Sea (Soomere et al. 2008).

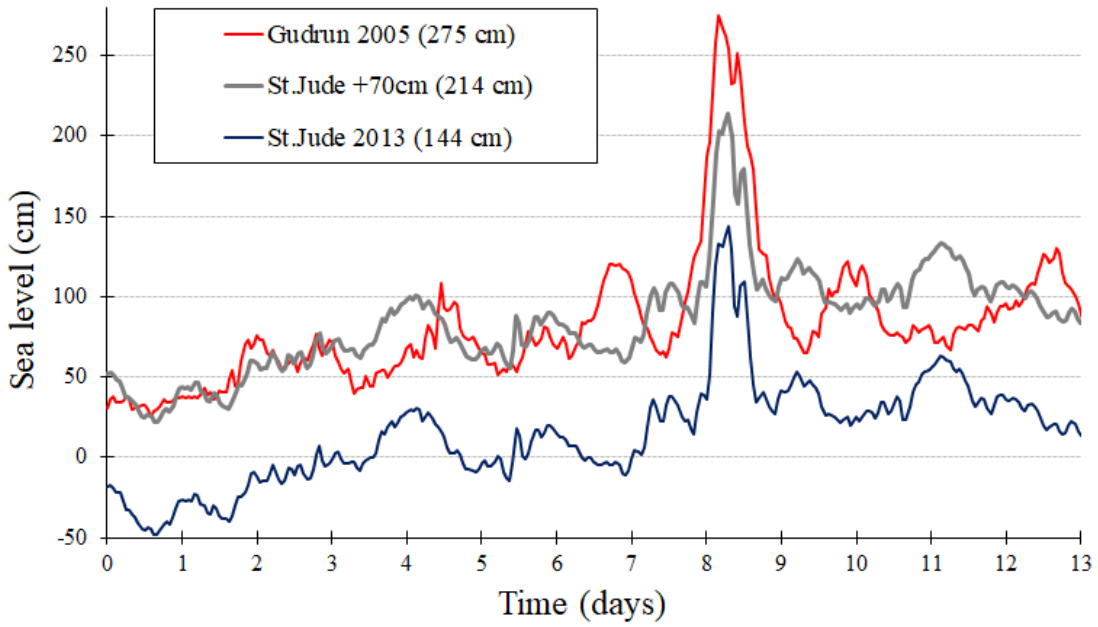

Figure 7. Comparison on sea level variations at Pärnu during Gudrun and St. Jude storm. Gudrun time starts 1 January 2005 (00:00 UTC), St. Jude time starts 21 October 2013 (00:00 UTC); Zero sea level – BHS77 zero; Pärnu average was 1.5 cm in 1924-2016, and 0.0 cm in 1924-1985.

Estimated losses due to wind damage and flooding of the urban areas reached 0.7% of the GDP in Estonia (Tõnisson et al. 2008). The scale and consequences of the new flooding were quite unexpected both for the population and authorities, as the previous highest surge (253 cm) took place nearly 38 years earlier (Figs. 5,8). Following the dissolution of the Soviet Union in 1991, some previous building standards and planning acts were discontinued due to the changes in political and economic courses. There has been a rapid increase in the number of holiday houses built as close as possible to the seashore and numerous new-rise blocks appeared to be within even less than 200 cm above mean sea level. Considering the shallow sea, low-lying hypsometric curve of Pärnu, and virtual absence of tides, the local residents were not sufficiently prepared for such an event. Essentially it became the most influential natural disaster for recorded history in Estonia, which received even more local media coverage than the Asian tsunami (on December 2004) or the New Orleanian hurricane Katrina (on August 2005) did. The event activated a broad discussion, as some serious deficiencies in flood forecasting and mitigation abilities in Estonia were revealed.

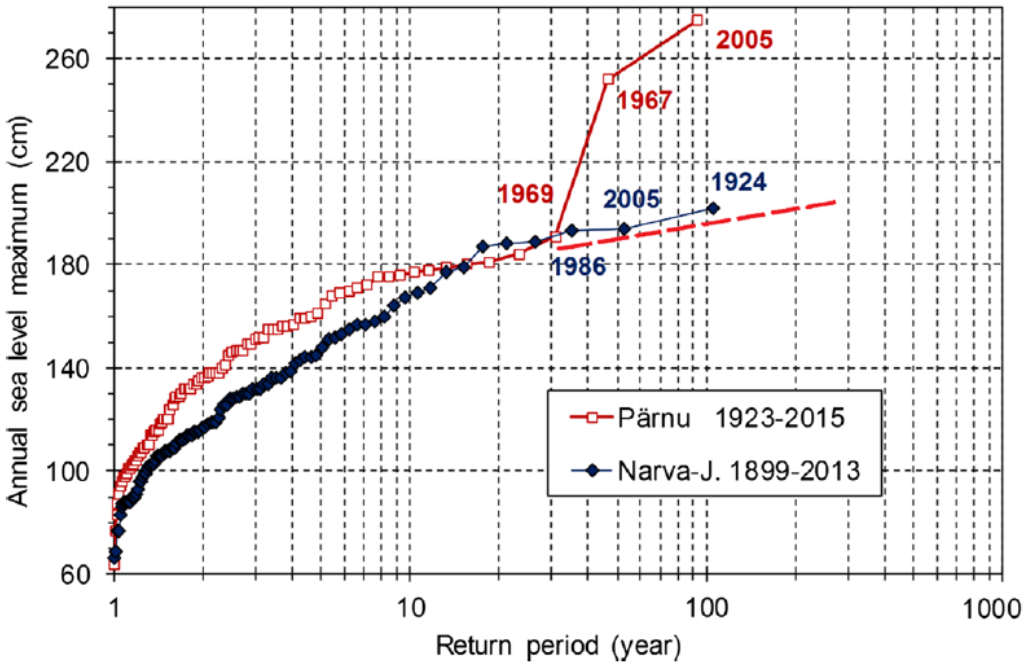

Figure 8. Comparison of empirical return graphs based on annual maximum sea levels for tide gauges at Pärnu (1923–2015) and Narva-Jõesuu (NE Estonia, Gulf of Finland). For Pärnu, an extrapolation according to generalized (Gumbel-type) theoretical distribution (indicated using dashed line) seems to poorly accommodate the two outlying events.

After this event, operational, model-based short-range forecasts and alert systems were established, but the preparedness towards long-range climate change induced hazards remained low in Estonia (Kont et al. 2011).

Study of various Estonia based storm related met-ocean datasets revealed that while the data on general "storminess" followed certain long-term quasi-cycles, the most extreme events were unexpected (Suursaar et al. 2015).

3.1.2.2 2008 "Snow Storm"

The storm predominantly affected Estonia, Finland, and Russia's Pskov and Leningrad oblasts. It started to develop near the Black Sea area on the 21st November, and approached Estonia from the southeast by 23th November (Fig. 9). At first, an undulating upper-tropospheric jet stream extended southward to the Mediterranean Sea, allowing cold air-masses to spread south, and warm moist air towards north on its eastern side. The wave-like structure developed into a closed circulation and formed a cyclone at surface, which started to shift northwards. According to meteorological analysis (Nevalainen 2012), the cyclone deepened with a "bomb" rate (more than 12 hPa in 12h, according to Sanders & Gyakum, 1980) and probably reached 952 hPa. Until the cyclone occluded above Finland on 24 November, it brought heavy winds and 24h snowfall accumulation of up to 33 cm at Helsinki, Southern Finland. It caused power cuts in 41 000 households in Finland alone, numerous traffic accidents and damage to buildings (Rauhala & Juga 2010).

According to Estonian data, the lowest atmospheric pressure (951-952 at several stations) was measured on 23 November (20:00 UTC), the 24h deepening rate being 36.8 hPa and a 12h drop of 23.0 hPa. As the cyclone approached, wind direction rotated counter-clockwise from W to S and E (22 Nov.), and finally to N (23 Nov.; Fig. 9a). Bringing cold air, the northerlies reached 16-18 m s^{-1} (as 1 hour averages), while maximum gusts reached 30 m s^{-1} at Pakri (Fig. 9a). The wind direction continued to turn, when the storm moved away to Finland and started to occlude. The heaviest snowfall was associated with northerlies during 23-24 November. The depth of the snow-cover reached 30-50 cm in most of the Estonia's continental stations (Fig. 9b). Although the precipitation amount was everywhere considerable, in West Estonia it partially fell down in liquid state, thus not adding much to snow-cover.

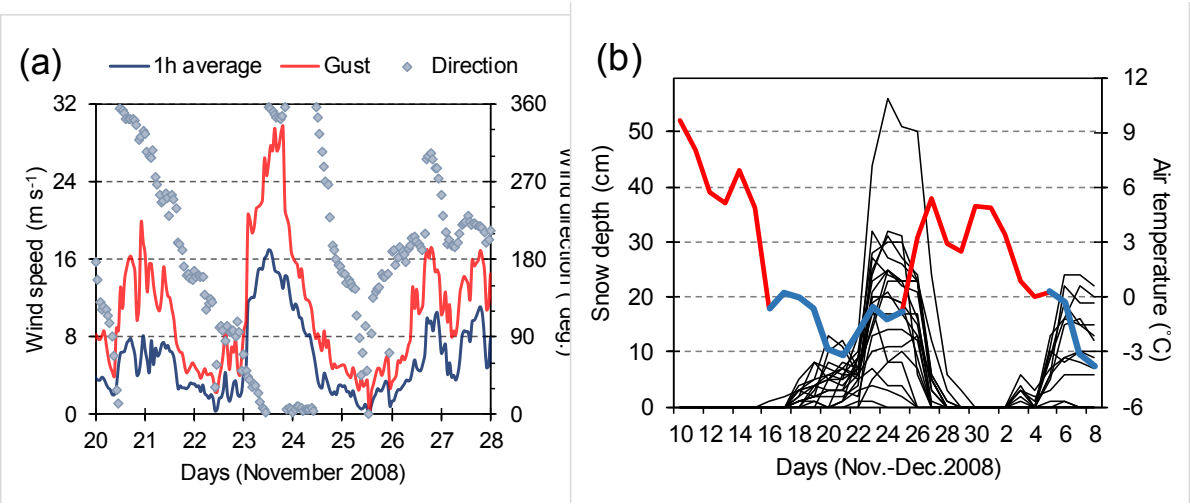

Figure 9. (a) Variations in hourly average wind speeds, directions and maximum gusts at Pakri station. During the cyclone, wind direction rotates from east to north (bringing cold air) and later on to west (for warmer air). (b) Variations in snow cover depth at 21 Estonian meteorological stations (non-specified thin black lines; maximum 56 cm was measured at Kuusiku on 25 Nov. 2008). Daily average air temperatures at Türi (25 km from Kuusiku) showing positive (red) and sub-zero (blue) temperatures.

3.1.2.3 2010 "Xynthia"

Xynthia was the severest European windstorm in 2010, which crossed Western Europe between 27 February and 1 March 2010, causing 64 reported casualties (Liberato et al. 2013). It was generated close to Madeira Islands, from there it moved across to the Canary Islands, Portugal, northern Spain, and southwestern France (Fig. 10). The highest gust wind speeds reached 44 m s^{-1} in France. Although the minimum sea level pressure was 965 hPa, the storm impacts included storm surge and rough seas hitting coastal regions of France at high tide (Bertin et al. 2012), as well as river floods in France, Spain, Switzerland and Germany.

Being considerably weakened by that time, the storm reached the Baltic Sea from south-west on 1-2 March 2010. It was detectable in Estonia by moderately low (980-990 hPa; Fig. 10a) atmospheric pressure and fresh wind conditions (1h average wind speeds 11-12 m s^{-1} at coastal stations, max. gusts up to 17 m s^{-1}; Fig. 10b). The cyclone also brought warm (+2˚C) and moist air from south, and the wind direction abruptly changed from SE to NW, as the center of the cyclone crossed Estonia. Even if its impacts as an occluding depression were not noteworthy in Estonia's context, it still was an interesting case due to its long course and

preceding history. An interesting question is, would the storm retain its strength further north in future climates?

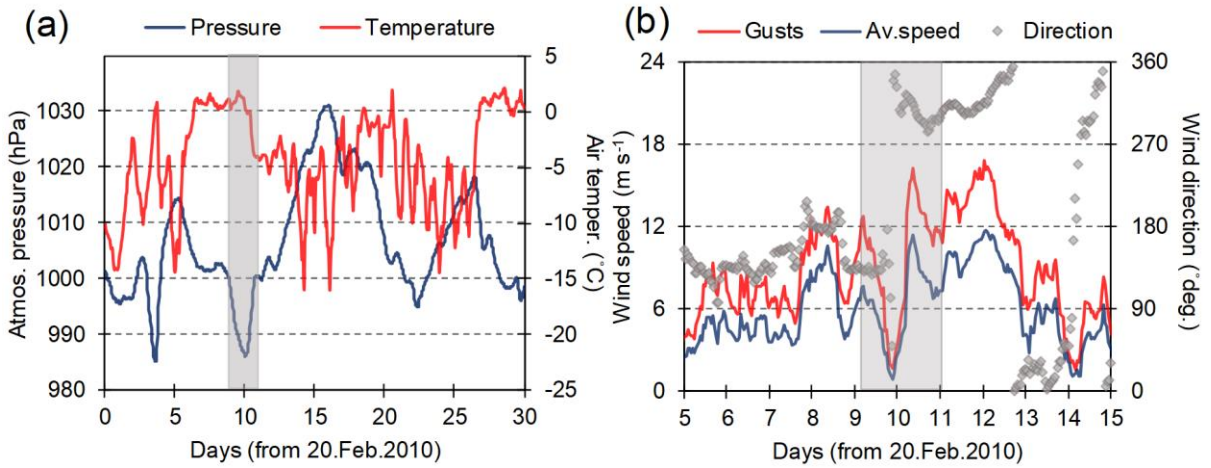

Figure 10. (a) Variations in hourly atmospheric pressure and air temperature at Kihnu station. Approaching Xynthia (1-2 March is marked by grey area) brought warm air from south to Estonia. (b) Variations in wind speed and direction at Vilsandi. The centre of the weakened cyclone crossed West Estonia, which is also stressed by the abrupt wind direction change (SE->NW).

3.1.2.4 2013 "St. Jude"

Prolonged stormy period above northern Europe began in October 2013 and lasted until the middle of January 2014. Originated at the polar front in the region south of Iceland, a series of extratropical cyclones (including St. Jude, Hilde, Xavier and some others) crossed the Baltic Sea from west to east. The storms were highly destructive over most of the northern Europe, however reached Estonia in somewhat dissipative state. The first in this series was the St. Jude storm, known also as Cyclone Christian (in Germany), Carmen (in UK), or Allan (in Denmark). Forming on the 26 October, the atmospheric depression travelled eastward as an explosive cyclone and made its landfall in the early 28 October near the Isle of Wight, UK. Quite similarly to storm Gudrun, the cyclone continued across the North and Baltic Sea (Fig. 6). The record breaking gust-wind speeds were recorded both in Netherlands (up to 41 m s^{-1}) and Denmark (up to 53 m s^{-1}). In Estonia, the strongest recorded 1h-sustained wind speeds (from SW-W) were 22.1 m s^{-1} at Sõrve and 23.2 m s^{-1} at Roomassaare on 29 October. The gust wind speeds reached 32 m s^{-1}. Although much weaker than Gudrun, the St. Jude was still the most powerful autumn storm in Estonia over many years.

The cyclone also caused a storm surge and high waves in the eastern Baltic Sea (Viitak et al. 2016). At Pärnu tide gauge, the maximum sea level of 144 cm was recorded at 07:00 UTC (Fig. 7). At Narva, within 10 hours the sea level rose from the initial -21 cm to the final 132 cm at 10:00 UTC. The sea level heights remained relatively modest only because St. Jude was the first cyclone of the season and the background sea level of the Baltic Sea was not elevated yet (in fact, it was even below long-term mean). If the Baltic background sea level would have been similar to that of Gudrun (Fig. 7), the Pärnu maximum sea level could have been 214 cm, which is well over the 160 cm critical value and ranking third (after 275 cm in 2005 and 253 cm in 1967) since the beginning of the measurements in 1923.

3.2 Arctic

The North Pole region contains the smallest ocean of the world – Arctic Ocean. Its total area is around 14.09 million km2, making it around 6 times smaller than the next largest ocean (Indian Ocean), and 5 time larger than the Mediterranean Sea (largest sea in the world). The deepest part that has been measured reaches depths as low as 5502 meters; the average is 987 meters. Arctic Ocean consists number of more notable marginal seas – Beaufort, Chukchi, Laptev, East Siberian, Barents, Kara, Baffin and Greenland. These regional bodies of water are one of the least known in the world, mainly because of the harsh and remote environment they are in. Furthermore, up until recent times the longstanding and seasonal sea ice cover has made it difficult to further the understanding of these waters. However, the situation is changing. Due to the global warming effects, the regional climate and its wide range of ecosystems are rapidly shifting and undergoing changes. Because of the polar amplification effect, the thermodynamic changes have an impact to virtually every aspect of Arctic as we currently know it. The cold southward moving ocean currents, the oceanic thermohaline circulation and global albedo from decreased ice cover will likely all go through changes in the near future (Ostenso 2018). While large scale environmental changes are already happening and expected to increase, the area is also attracting new attention from governments and other interest groups for economic exploration (Berkman & Young 2009).

As in North Atlantic, in Arctic the climate variability is determined by the Arctic Oscillation (AO) – a phenomenon that describes the effect varying pressure gradients on temperature and storm tracks. Similarly, it consists of a positive and negative phases where strong winds circulate and are confined to polar region (around North Pole) or the belt weakens, distorts and allows cold air masses to break towards lower latitudes, respectively

(NOAA, 2019). Aside from AO, a more Arctic specific index called Arctic Ocean Oscillation (AOO) also has also been developed that looks simulated sea surface heights driven by winds all over Arctic (Proshutinsly & Johnson 1997). AOO looks at the Arctic Ocean wind driven circulation from the view point of sense (either cyclonic or anticyclonic) and intensity. For instance during the positive phase the less storms reach the Arctic from the North Atlantic storm tracks (similar response with the positive NAO phase), because the storm tracks are shifted eastwards (e.g. Fig. 12; Proshutinsky et al. 2015). During the negative phase however, the situation is opposite, and more North Atlantic storm tracks reach Arctic region bringing warm and humid conditions (Proshutinsky & Johnson 1997; Proshutinsky et al. 1999; WHOI 2019).

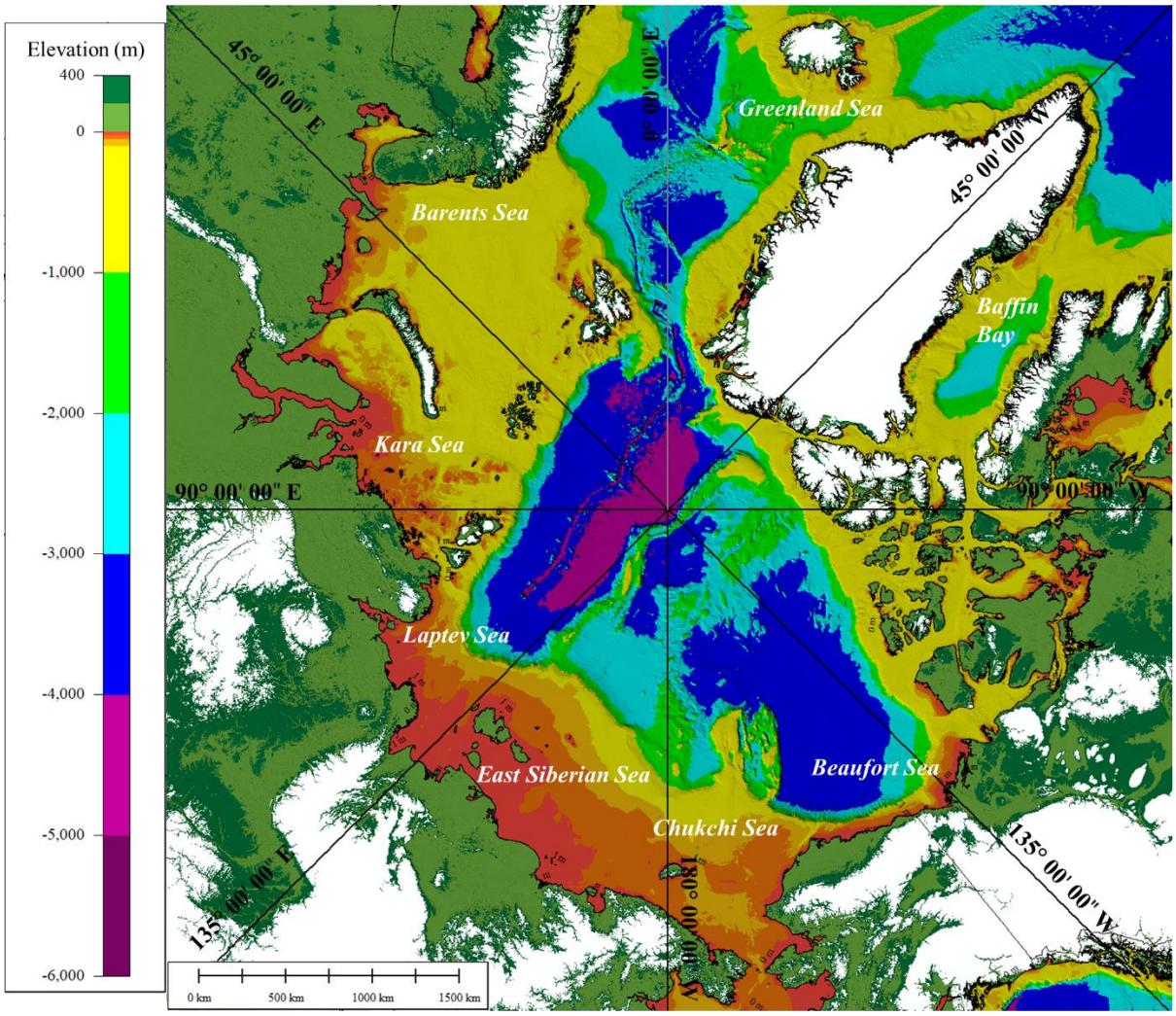

Figure 11. Elevation map of Arctic region and its surrounding seas. Map created from IBCAOv3 data. The white areas show elevations higher than 400 m.

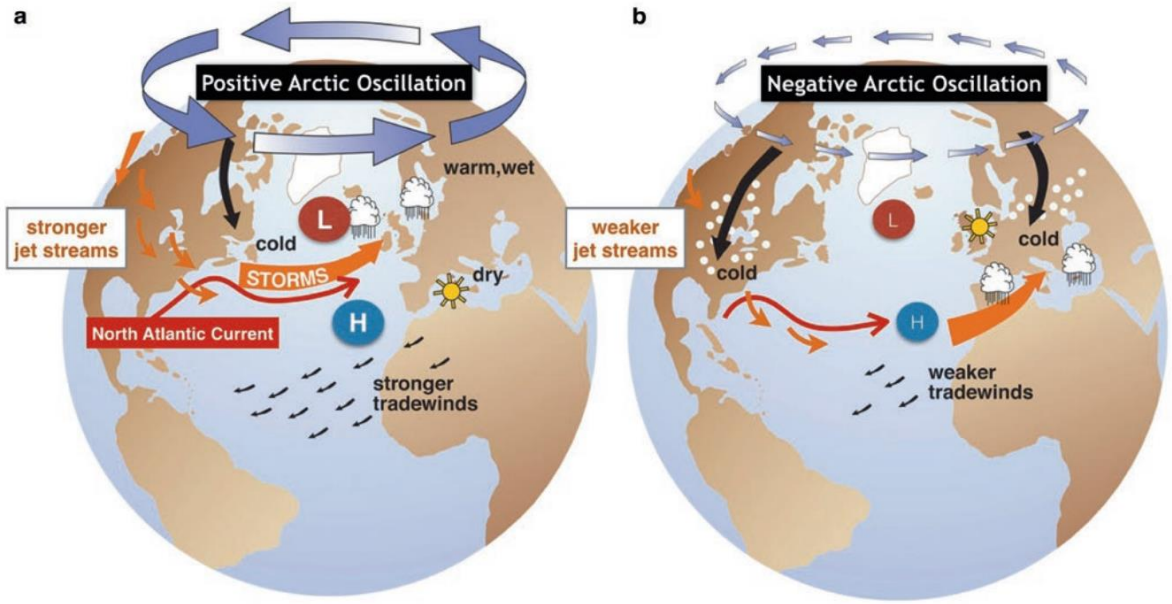

Figure 12. Illustration of the Arctic Oscillation and its effects. Positive Arctic Oscillation (a) and negative Arctic Oscillation (b). The centres of low (L) and high (H) pressure systems over the North Atlantic indicate the corresponding North Atlantic Oscillation phases (Campos 2018).

3.2.1 Beaufort Sea

Beaufort Sea (Fig. 11), is one the marginal sea within the Arctic Ocean, located north of Canada and Alaska. The surface area covers around 476000 km2. The water depth in most of the area is rather deep (4682 m maximum, 1004 m average), and that is mainly due to the relatively narrow continental shelf, especially around Barrow, however widens eastwards to Canadian side (near Makenzie River Delta). However nowhere is it wider that 145 km, and the most common depth is at around 64 m. Near the Canadian coastline the average water depth can be extremely shallow for many kilometres seaward direction. The coasts along the Beaufort are low-lying and for the most part covered in tundra (Britannica 2019). According to studies on changes in Beaufort coastal dynamics, the average rate of coastal retreat has been observed at 1.4 m/yr and local maximum is at 18.5 m/yr over (1600 km; Gibbs & Richmond 2015). Depending on the local study sites, temporal extent considered and other environmental drivers, these retreat values can vary greatly.

3.2.1.1 Tuktoyaktuk (Canada)

Tuktoyaktuk is a port hamlet situated in the Northwest Territories (Canada) next to the Beaufort Sea. The Mackenzie River delta is roughly 32 km to its west and one of the largest settlements, Inuvik, is 160 km to southwest. The hamlet was first established in 1936

as transport depot and trading post for the Hudson's Bay Company. The main economic drivers for the settlement are in trapping, whaling, reindeer herding, sealing and handicrafts. During summer months the port is major transhipment point for cargo that come from the Mackenzie River and transfer goods open sea vessels (Britannica 2017).

Like rest of the Arctic (and Beaufort) coastal areas, Tuktoyaktuk also struggles with erosion problems (Figure 13). The erosion issue in the hamlet is not a recent problem. However, in the past decades due to the decrease of the seasonal sea ice coverage, the hamlet has been left open to longer periods of open sea water that further increase erosion from high waves and potential surges. Historically the hamlet has tried various coastal defences they could implement (mainly various forms of rip rap, sandbags etc.).

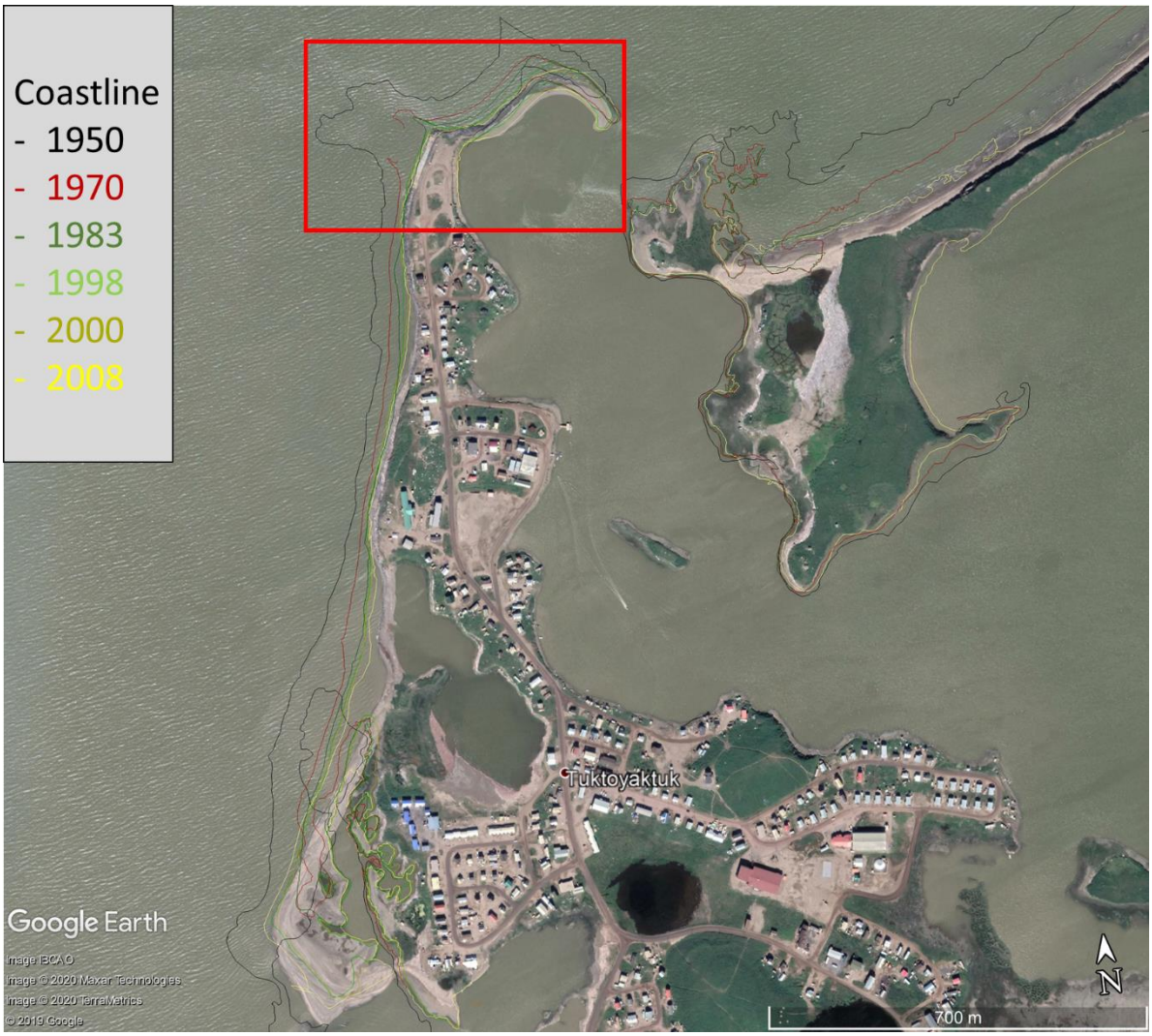

Figure 13. Coastal erosion in Tuktoyaktuk. The black line shows the 1950 coastline position and yellow line in 2008. Compiled from data provided by Hynes et al. 2014. Red box shows more closer look at the northern tip of Tuktoyaktuk peninsula (see figure 14).

Although during more extreme weather conditions they have been almost always undermined. The more effective defensive measures have been the usage of 40 concrete slabs at the northern stretch of Tuktoyaktuk, that were donated to the community in 1998 by an oil company (Figure 14). While proven to be successful in dissipating in-coming wave energy, they are economically expensive to produce on site and would need heavy equipment to move around (McClearn 2018).

In terms of potential climate change effects, the Tuktoyaktuk area can also expect the effects of relative local sea level rise. Many areas at high latitudes (including Baltic Sea region and Estonia) are still undergoing postglacial rebound since the retreat of continental ice mass from the last ice-age, which can even out the relative local sea level change during considering the global projection through the 21st century. Tuktoyaktuk however (and other coastal regions in the Northwest Territories), is located near the periphery of the former ice sheet where the vertical land uplift can be slower there (ENR 2019). Along the North Coast Region, the projected sea level changes differ greatly from location to location, and only Tuktoyaktuk, Inuvik and Sachs Harbour are projected to experience the relative sea-level rise at, or close to, the global mean (Fig. 15, James et al. 2014).

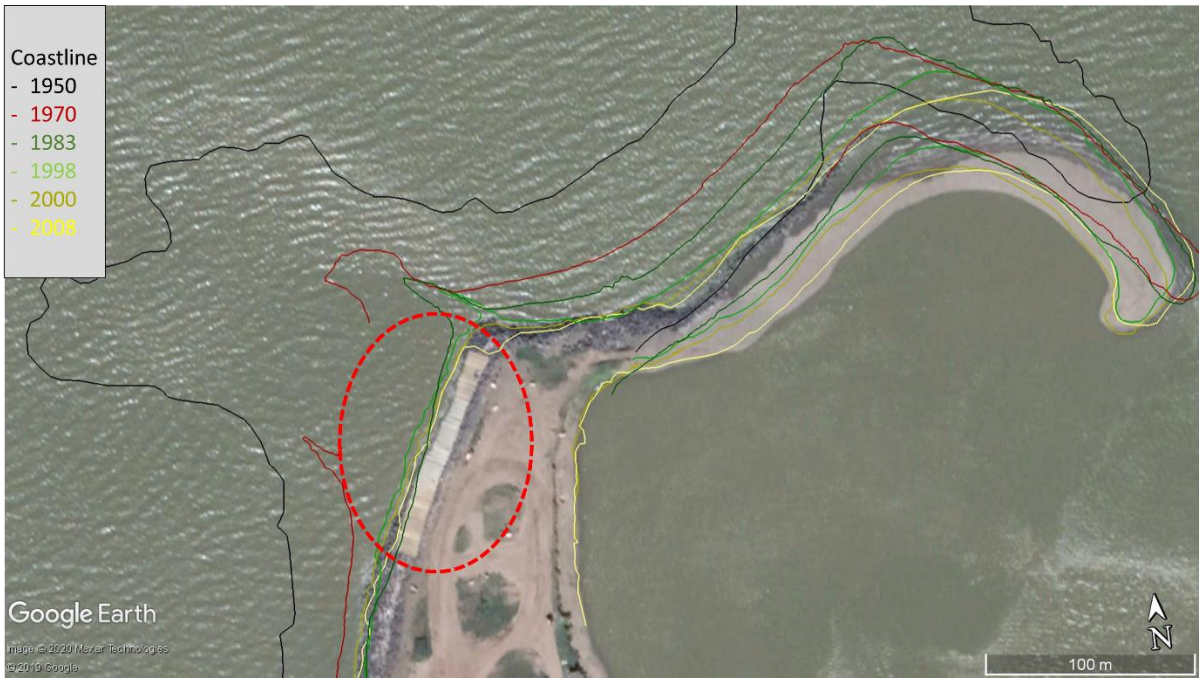

Figure 14. Over the years various approaches have been tried to protect the coastline of Tuktoyaktuk. One of the more successful protective measures have been using concrete slabs (red circled area). The relative effect can be seen with surrounding area to east, where changes have been more pronounced. Compiled from data provided by Hynes et al. 2014.

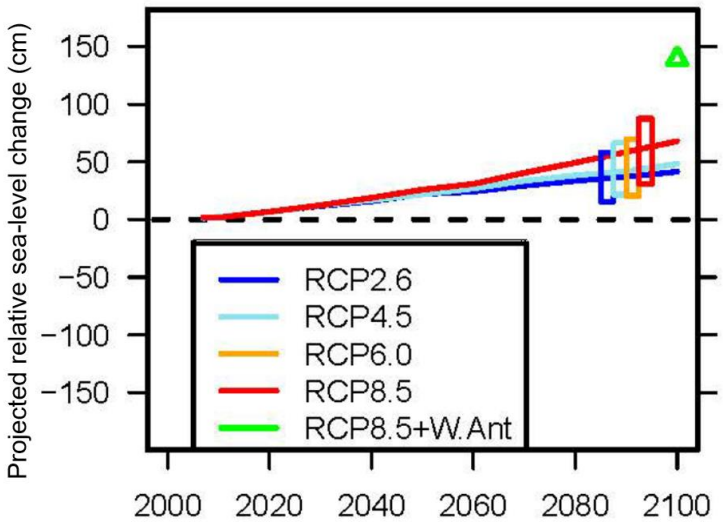

Figure 15. Relative sea-level change projections for Tuktoyaktuk (based on the IPCC AR5; after Church et al., 2013a, 2013b). Rectangles show the range of projections at 2081-2100 relative to 1986-2005.

3.2.2 Case study

3.2.2.1 1999 "Arctic Storm"

Historically in the Arctic region the storms have not been named and are poorly documented (currently named "Arctic Storm" by the author). Most of the reliable data in determining high impact weather events comes usually from the weather and tide station data near the study area, if available. Additional information can sometime also be found from various research studies or newspaper articles that often study and report such events, respectively.

In this research the available station data timeseries were investigated first, however lot of the high surge recordings fell under the winter season when the sea ice was fully covered the Beaufort Sea (Fig. 16). Furthermore, the available datasets show large data gaps. According to personal correspondence with the officials from the Fisheries and Oceans Canada, the data gaps are mostly due to the challenges in operating a gauge in the Arctic.

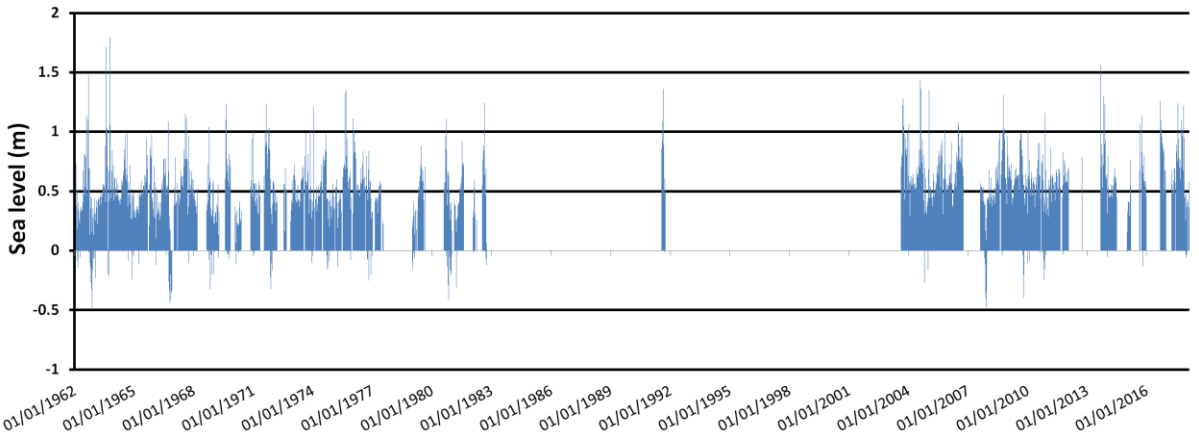

Figure 16. Historical sea level records from Tuktoyaktuk tide gauge. The data series include large gaps in measurements (data source: Fisheries and Oceans Canada, 2019).

Secondary source of information on historical high impact events can be found by looking at high quality modelled hindcast data products for wind, wave and surge. One such available product is the Meteorological Service Canada Beaufort (MSCB) Wind and Wave Reanalysis data (Swail et al. 2006). This dataset provides historical surface winds and ocean surface wave for the Canadian Beaufort Sea for the period 1970-2015. The hourly data can be obtained through a request from the Meteorological Service of Canadas's Climate Services. A closest grid point to the hamlet of Tuktoyaktuk is labelled MB000181 (Fig. 17b) and is roughly 5 km away from the hamlet, inside the Kugmallit Bay. From that data it becomes clear that in Tuktoyaktuk particularly there are not many extreme surge-wave events in the late summer month when the sea ice is at its minimum and the coastline is open for wave attacks. From the whole 45 year hindcast period (Fig. 18), only two notable events are present: 14 September 1970 (max surge 2.45 m, max wave 2.5 m) and 25 September 1999 (max surge 2.13 m, max wave 1.9 m). Among research studies, the late September storm surge was investigated by Pisaric et al. (2011) in terms of storm surge damage to Mackenzie Delta's ecosystem (~100 km west from Tuktoyaktuk). While their study did not focus on Tuktoyaktuk itself, they did found that the 1999 storm surge caused an ecological impact, unmatched over the > 1,000-year history of this lake ecosystem.

With above presented considerations, and since coastal processes are extremely rapid in the area, the most recent suitable study period is desirable. In addition, by investigating the 1999 storm case, more accurate and higher quality data can be used for simulation processes (e.g. much of the atmospheric reanalysis data start from the 1979).

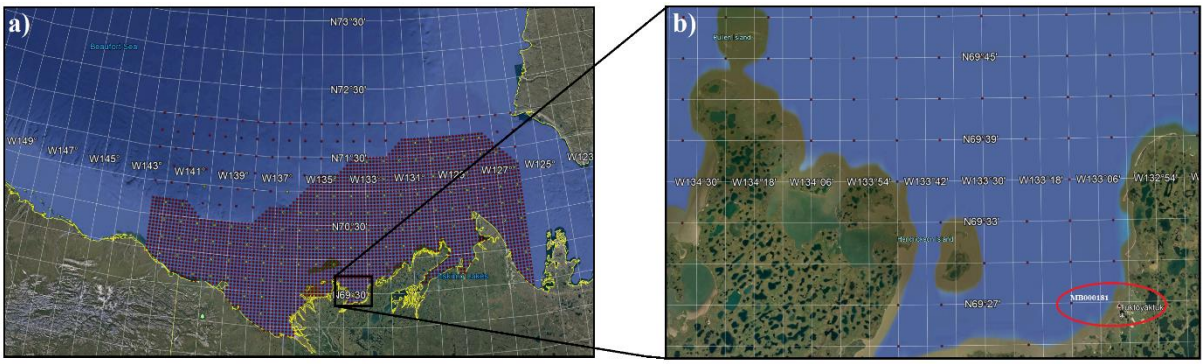

Figure 17. Beaufort MSCB domain (a), and the location grid point MB000181 used to analyse the hindcast data (b). The red circle marks the locations of the grid point and Tuktoyaktuk (~ 5 km distance; Google Earth).

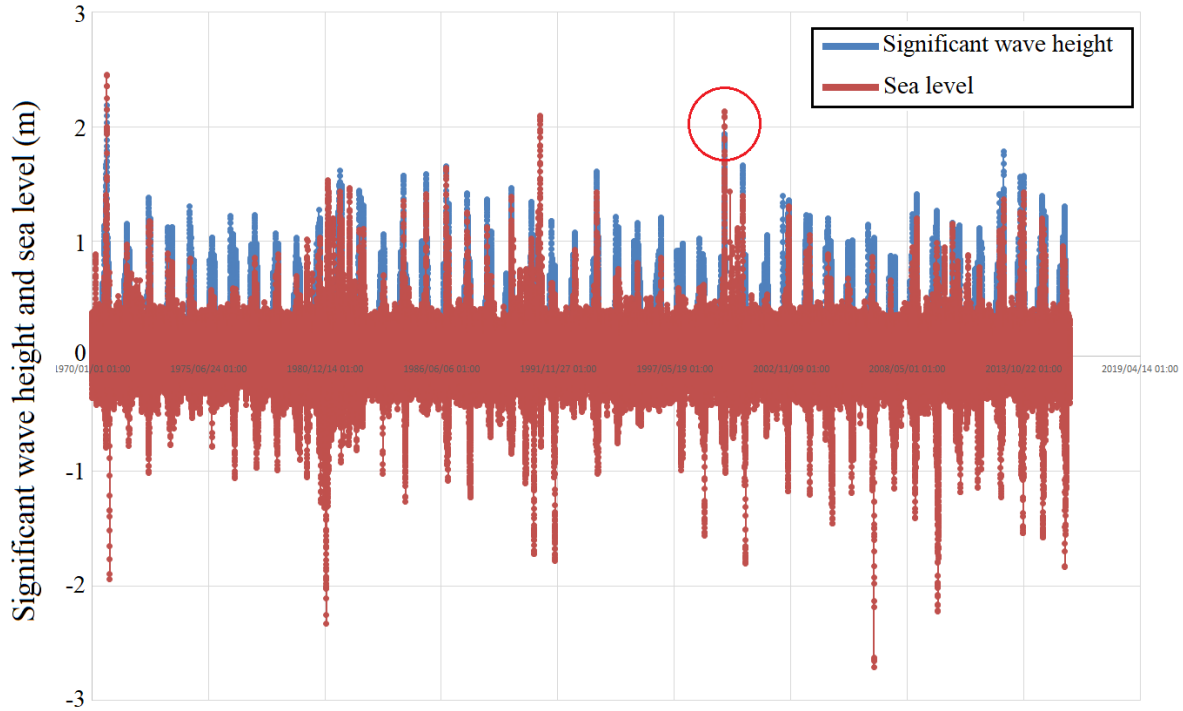

Figure 18. The significant wave height and sea level output from Beaufort MSCB model at grid point MB000181 (see also Fig. 17 for location). The temporal extent of the data is 1970-01 – 2015-12. Data provided by Isabella Gaboury, Fisheries and Oceans Canada.

4 Methodology

4.1 The modelling system

The modelling system and data flows between its various components are depicted in Figure 19. The top-down methodology for estimating both (past) hindcast and projected (future) storm surge parameters is similar to that of Nakamura et al. (2016) and Mäll et al. (2017). Basically, using either realistic or a combination of realistic and manipulated forcing data, the atmosphere model is run first to study storm parameters and the resulting output The main tools of the current research were the ARW-WRF atmospheric model (ver. 3.9.1.1; Skamarock et al. 2008) for simulating the atmospheric conditions throughout the investigated storms life cycle, and the updated FVCOM ocean model (ver. 4.1), including the wave-current interaction (hereafter: FVCOM-SWAVE; Chen et al. 2003, Qi et al. 2009, Wu et al. 2010), for simulating sea level variations along the West coast of Estonia. For Arctic study domain, an slightly more advanced FVCOM setup is used – FVCOM-SWAVE model. Furthermore, the SWAN model version 41.20 (Booji et al. 1999, Björkqvist et al. 2018) was used to simulate the future changes in significant wave heights (Hs) and its spatial distributions in the Baltic Sea area for the 2005 and 2013 storms.

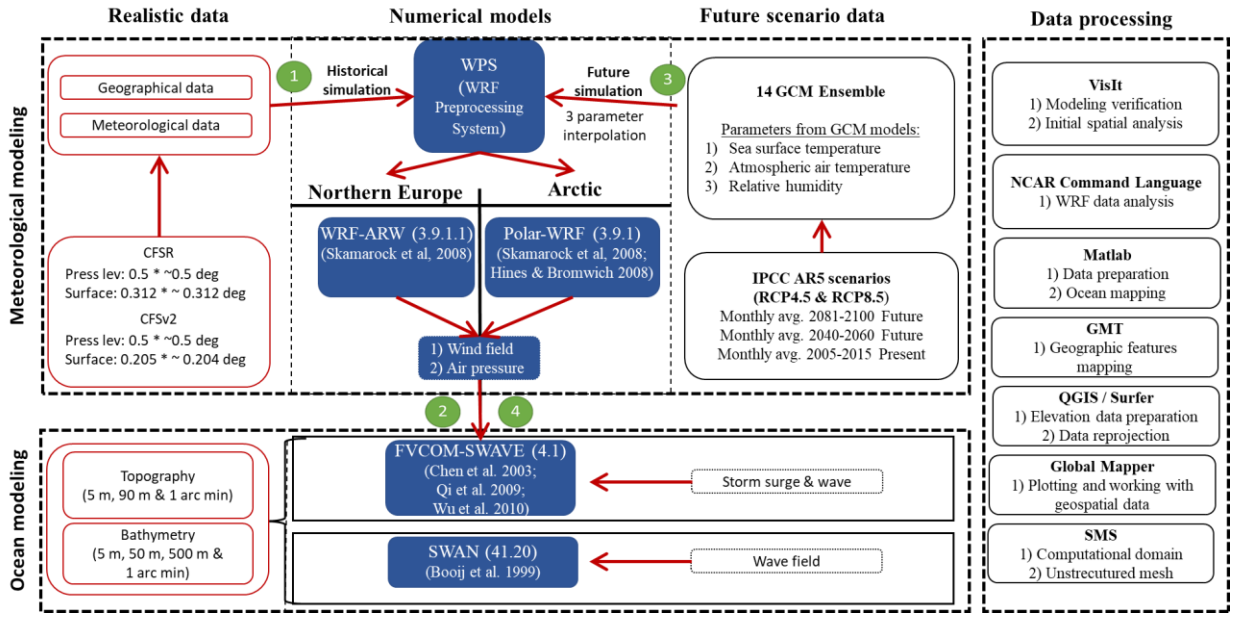

Figure 19. Flowchart of models, data and processing tools used for hindcast and future simulations. The green numbers show priority flow of models (1-2 hindcasting and 3-4 future scenarios).

4.2 Atmospheric models

4.2.1 WRF

One of the key components of this research method is the mesoscale numerical weather prediction model called the Advanced Research Weather Research and Forecasting Model (ARW-WRF). A detailed description of WRF was provided by Skamarock et al. (2008). For weather calculation (WRF), there are eight equations including three momentum conservation equations (three directions), a mass conservation equation, a potential temperature equation, a geo-potential equation, a scaler conservation equation and a state law equation. These equations are solved based on the terrain following scheme and staggered Arakawa C grid. The WRF has two dynamical solvers known as NMM (Nonhydrostatic Mesoscale Model) and ARW (Advanced Research WRF) core, therefore enabling atmospheric simulations with idealized conditions or using realistic data, respectively. In this study the ARW dynamical solver was used which is most suitable for case study and regional climate study research.

4.2.1.1 Governing equations

According to Sakamarock et al. (2008) the ARW equations are formulated using a terrain-following hydrostatic-pressure vertical coordinate denoted by η and defined as:

$$\eta = (p_h - p_{ht})/\mu \qquad \text{where } \mu = p_{hs} - p_{ht} \tag{1.1}$$

p_h is the hydrostatic component of the pressure, and p_{hs} is the value along the surface, p_{ht} is the value along the top boundaries. η has a value of 1 at the surface and 0 at the upper boundary of the model domain (see Fig. 20). The flux form variables can be defined as follows by using μ:

$$V = \mu v = (U, V, W), \quad \Omega = \mu\dot{\eta}, \qquad \Theta = \mu\theta \tag{1.2}$$

, where v is the covariant velocities in the 3 directions- 2 horizontal and 1 vertical directions, respectively, Ω is the contravariant vertical velocity, and θ is the potential temperature. Furthermore, in the governing equations of ARW also the non-conserved variables $\phi = gz$ (the geopotential), p (pressure) and $\alpha = 1/\rho$ (the inverse density) appear.

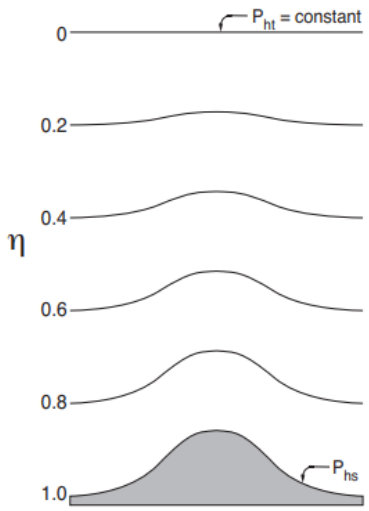

Figure 20. WRF-ARW η coordinate (Skamarock et al. 2008).

The governing equations, including map factors and rotational terms are as follows:

Momentum conservation

$$\frac{\partial U}{\partial t} + m_x\left[\frac{\partial(Uu)}{\partial x} + \frac{\partial(Vu)}{\partial y}\right] + \frac{\partial(\Omega u)}{\partial \boldsymbol{\eta}} + \left(\frac{m_x}{m_y}\right)[\mu_d \alpha \frac{\partial p}{\partial x} + \left(\frac{\alpha}{\alpha_d}\right)\frac{\partial p}{\partial \eta}\frac{\partial \phi}{\partial x}] = F_U \tag{1.3}$$

$$\frac{\partial V}{\partial t} + m_y\left[\frac{\partial(Uv)}{\partial x} + \frac{\partial(Vv)}{\partial y}\right] + \left(\frac{m_y}{m_x}\right)\frac{\partial(\Omega v)}{\partial \eta} + \left(\frac{m_y}{m_x}\right)[\mu_d \alpha \frac{\partial p}{\partial y} + (\frac{\alpha}{\alpha_d})\frac{\partial p}{\partial \eta}\frac{\partial \phi}{\partial y}] = F_V \tag{1.4}$$

$$\frac{\partial W}{\partial t} + \left(\frac{m_x m_y}{m_y}\right)\left[\frac{\partial(Uw)}{\partial x} + \frac{\partial(Vw)}{\partial y}\right] + \frac{\partial(\boldsymbol{\Omega} w)}{\partial \boldsymbol{\eta}} - m_y{}^{-1} g[\left(\frac{\alpha}{\alpha_d}\right)\frac{\partial p}{\partial \eta} - \mu_d] = F_W \tag{1.5}$$

Potential Temperature Conservation Law

$$\frac{\partial \Theta}{\partial t} + m_x m_y\left[\frac{\partial(U\theta)}{\partial x} + \frac{\partial(V\theta)}{\partial y}\right] + m_y\frac{\partial(\boldsymbol{\Omega}\theta)}{\partial \eta} = F_\Theta \tag{1.6}$$

Mass Conservation

$$\frac{\partial \boldsymbol{\mu_d}}{\partial t} + m_x m_y\left[U_x + V_y\right] + m_y\frac{\partial \Omega}{\partial \eta} = 0 \tag{1.7}$$

The Geopotential

$$\frac{\partial \phi}{\partial t} + \mu_d{}^{-1}[m_x m_y\left(U\frac{\partial \phi}{\partial x} + V\frac{\partial \phi}{\partial y}\right) + m_y\Omega\frac{\partial \phi}{\partial \eta} - m_y g W] = 0 \tag{1.8}$$

Scaler Equation

$$\frac{\partial \boldsymbol{Q_m}}{\partial t} + m_x m_y \left[\frac{\partial (U q_m)}{\partial x} + \frac{\partial (V q_m)}{\partial y}\right] + m_y \frac{\partial (\Omega q_m)}{\partial \eta} = F_{\boldsymbol{Q_m}} \quad (1.9)$$

State equation

$$p = p_0 \left(\frac{R_d \theta_m}{p_0 \alpha_d}\right)^{\Upsilon} \quad (1.10)$$

, where a represents a generic variable, $\gamma = c_p/c_v = 1.4$ is the ratio of the heat capacities for dry air, R_d is the gas constant for dry air, and p_0 is a reference pressure (typically 10^5 Pascals). The right-hand-side (RHS) terms F_U , F_V , F_W , and F_Θ represent forcing terms arising from model physics, turbulent mixing, spherical projections, and the earth's rotation. α_d is the inverse density of the dry air ($1/\rho_d$) and α is the inverse density taking into account the full parcel density $\alpha = \alpha_d(1 + q_v + q_c + q_r + q_i + ...)^{-1}$, where q_* are the mixing ratios (mass per mass of dry air) for water vapor, cloud, rain, ice, etc. Additionally, $\theta_m = \theta(1 + (R_v/R_d)q_v) \approx \theta(1 + 1.61q_v)$, and $Q_m = \mu_d q_m$; $q_m = q_v, q_c, q_i, \ldots$.

4.2.1.2 Modelling setup

The initial step was to run the atmospheric model WRF in order to validate the accuracy of the model output. To control the modelling biases between four different storm cases, the authors used as homogenous initial and boundary condition settings as possible (Table 1). All the WRF physics, calculation time steps and resolutions were the same for all events. For storms approaching the Atlantic Ocean (2005, 2010 and 2013 events) fixed homogeneous domains were used (Fig. 21a) and for the 2008 snow storm, approaching from the SE Europe, a different domain configuration was employed (Fig. 21b). The models were forced with the NCEP's Climate Forecast System Reanalysis (CFSR) datasets in 0.5 x 0.5 deg. and 0.312 x ~0.312 deg. resolution for pressure levels and surface, respectively. The CFSR data extended until the end of 2010. Therefore, for the 2013 storm case NCEP's Climate Forecast System version 2 (CFSv2) was used, with 0.5 x 0.5 deg. and 0.205 x ~0.204 deg. resolution for pressure levels and surface, respectively. The simulation results (hindcast) were then validated against observed data (provided by the Estonian Environmental Agency; www.ilmateenistus.ee) at Estonian weathers stations and tide gauges (Vilsandi, Kihnu, Ruhnu, Pärnu; Fig. 23). The main study parameters were precipitation, wind speed and direction. Wind fields were studied in depth for the storm surge related 2005 and 2013 cases.

Furthermore, precipitation amount and spatial distribution comparisons were conducted for all the cases, with main incentive to see the precipitation spread and the differences between hindcast and future scenario simulations. The precipitations distribution maps were plotted as a total sum of convective (cumulus scheme) and non-convective (physics scheme) values at each grid point. For descriptions on selected physics schemes, see appendix 1.

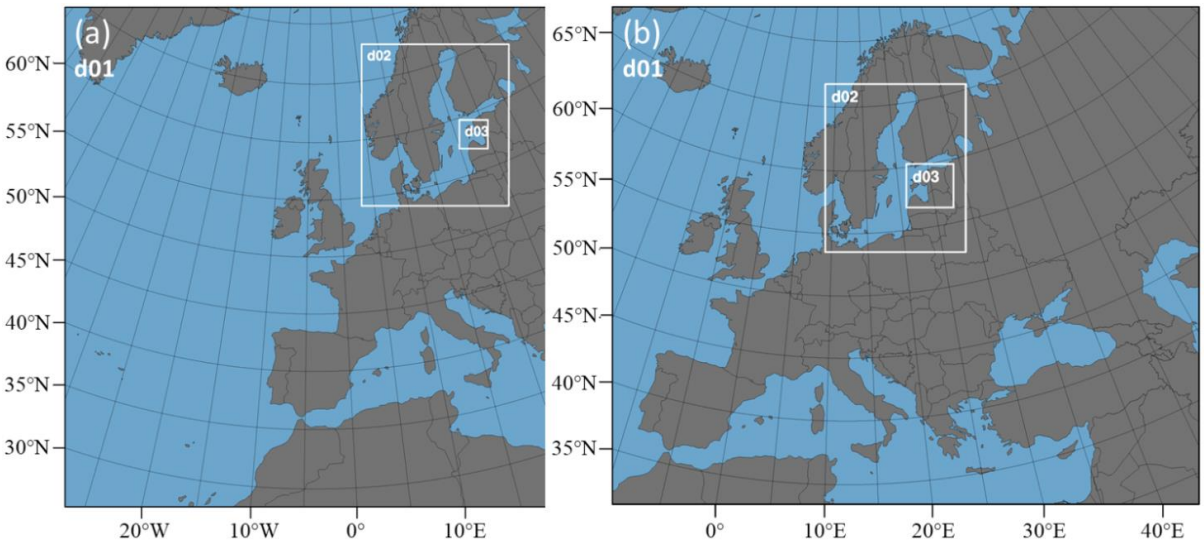

Figure 21. WRF modelling domains (d01, d02, d03) for 2005, 2010 and 2013 case studies (a), and for the 2008 case study (b).

4.2.2 PWRF

Polar-optimized version of the WRF model is known as Polar WRF. The PWRF has been updated and developed since the release of WRF version 3.0.1.1 by The Ohio State University Polar Meteorology Group (Hines & Bromwich 2008). The key modification for PWRF are as follows (Polar Meteorology Group 2019): Optimal surface energy balance and heat transfer for the Noah LSM over sea ice and permanent ice surfaces; and a fix to allow specified sea ice quantities and the land mask associated with sea ice to update during a simulation. Polar optimizations are mainly done for the Noah LSM scheme and improve the representation of heat transfer through snow and ice. Fractional sea ice was implemented in Polar WRF by Bromwich et al. (2009) and from version 3.1 and onwards has been part of the standard release of the model. Therefore, to fully utilize the PWRF, it is necessary to use Noah LSM physics scheme for land surface parameterization. Similar to Northern European

case studies, the meteorological forcing for PWRF simulation in the Arctic is initialized through NCEP CFSR data. The horizontal resolution and number of nested domains is also the same (Fig. 22). However, additional parameters were set in the model configurations. Namely the sea ice thickness, sea ice albedo and snow cover of sea ice were also enabled. The sea ice thickness data was acquired from PIOMAS version 2.1 daily data. The temporal extent of the data is from 1978-present, and horizontal resolution is 25 km. The PIOMAS data was interpolated to PWRF metgrids and sea ice parameter flags were enabled (albedos, thickness and extent). The PWRF initial and boundary conditions can be seen in Table 2.

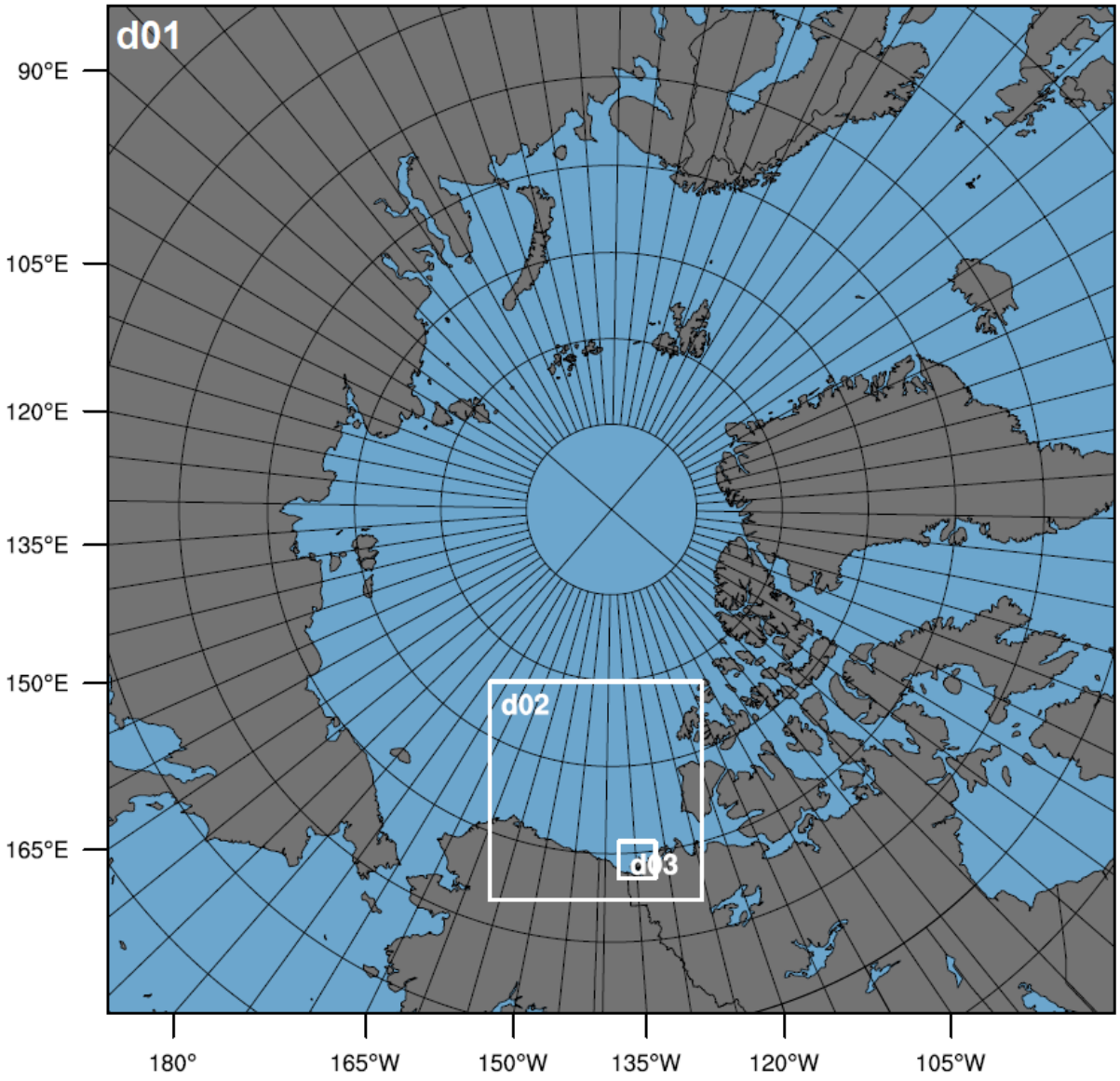

Figure 22. PWRF modelling domains (d01, d02, d03) for the 1999 Arctic storm event. The d01 and d02 output was used to force the regional and local FVCOM-SWAVE simulations, respectively.

4.3 Ocean models

4.3.1 FVCOM-SWAVE

Hydrodynamic parameters (sea level variations in this case) were simulated using the Finite Volume Community Ocean Model (FVCOM) which is a prognostic, unstructured-grid, finite-volume, 3D primitive equation coastal ocean circulation model developed originally by Chen et al. (2003a). The model consists of momentum, continuity, temperature, salinity and density equations (governing equations in chapter 4.3.1.1) and is closed physically and mathematically using turbulence closure submodels (Chen et al. 2013). The horizontal grid is comprised of unstructured triangular cells and the irregular bottom is presented using generalized terrain-following coordinates. In this study, FVCOM version 4.1 was used. FVCOM solves the governing equations on Cartesian (used in this study) or spherical coordinates in integral form by computing fluxes between non-overlapping horizontal triangular control volumes. According Chen et al. (2003, 2013), this finite-volume approach combines the best of finite-element methods (FEM) for geometric flexibility and finite-difference methods (FDM) for simple discrete structures and computational efficiency. This numerical approach also provides a much better representation of mass, momentum, salt, and heat conservation in coastal and estuarine regions with complex geometry. The study employed FVCOM-SWAVE version of the model which converts structured grid surface wave model SWAN into the FVCOM-based unstructured grid system.

4.3.1.1 Governing equations

This chapter presents the FVCOM governing equation in cartesian coordinates. Further details can be found in the FVCOM Users Manual 3rd Edition (Chen et al. 2011). The following are the momentum, continuity, temperature, salinity and density equations without consideration for snow and ice.

Momentum conservation

$$\frac{\partial u}{\partial t} + u\frac{\partial u}{\partial x} + v\frac{\partial u}{\partial y} + w\frac{\partial u}{\partial z} - fv = -\frac{1}{\rho_0}\frac{\partial(p_H+p_a)}{\partial x} - \frac{1}{\rho_0}\frac{\partial q}{\partial x} + \frac{\partial}{\partial z}\left(K_m\frac{\partial u}{\partial z}\right) + F_u \quad (2.1)$$

$$\frac{\partial v}{\partial t} + u\frac{\partial v}{\partial x} + v\frac{\partial v}{\partial y} + w\frac{\partial v}{\partial z} - fu = -\frac{1}{\rho_0}\frac{\partial(p_H+p_a)}{\partial y} - \frac{1}{\rho_0}\frac{\partial q}{\partial y} + \frac{\partial}{\partial z}\left(K_m\frac{\partial v}{\partial z}\right) + F_v \quad (2.2)$$

$$\frac{\partial w}{\partial t} + u\frac{\partial w}{\partial x} + v\frac{\partial w}{\partial y} + w\frac{\partial w}{\partial z} = -\frac{1}{\rho_0}\frac{\partial q}{\partial z} + \frac{\partial}{\partial z}(K_m\frac{\partial w}{\partial z}) + F_w \quad (2.3)$$

Mass conservation

$$\frac{\partial u}{\partial x}+\frac{\partial v}{\partial y}+\frac{\partial w}{\partial z}=0 \tag{2.4}$$

Potential temperature

$$\frac{\partial T}{\partial t}+u\frac{\partial T}{\partial x}+v\frac{\partial T}{\partial y}+w\frac{\partial T}{\partial z}=\frac{\partial}{\partial z}\left(K_h\frac{\partial T}{\partial z}\right)+F_T \tag{2.5}$$

Salinity

$$\frac{\partial S}{\partial t}+u\frac{\partial S}{\partial x}+v\frac{\partial S}{\partial y}+w\frac{\partial S}{\partial z}=\frac{\partial}{\partial z}\left(K_h\frac{\partial S}{\partial z}\right)+F_S \tag{2.6}$$

Density

$$\rho=\rho(T,S,p) \tag{2.7}$$

, where *x, y*, and *z* are the east, north, and vertical axis in Cartesian coordinates, *u, v,* and *w* are the *x, y, z* velocity components, respectively, *T* is temperature, *S* is salinity, ρ is density, p_a is air pressure at the sea surface, p_H is the hydrostatic pressure, q is the non-hydrostatic pressure, *f* is the Coriolis parameters, *g* is the gravitation acceleration, $K_m$is the vertical eddy viscosity coefficient, K_h is the thermal vertical eddy diffusion coefficient, and F_u, F_v, F_T, and F_S is the horizontal momentum, thermal, and salt diffusion terms, respectively. The wave action density (*N*) is given as follows:

$$\frac{\partial N}{\partial t}+\frac{\partial c_x N}{\partial x}+\frac{\partial c_y N}{\partial y}+\frac{\partial c_\sigma N}{\partial \sigma}+\frac{\partial c_{\hat{\theta}} N}{\partial \hat{\theta}}=\frac{S_{tot}}{\sigma} \tag{2.8}$$

, where (σ, $\hat{\theta}$) is the relative frequency and wave direction in spectral space; (*x*, *y*) is the Cartesian coordinate in geographic space. S_{tot} is the source/sink term representing the effects of wind-wave generation, wave breaking, bottom dissipation, and nonlinear wave-wave interactions (See also chapter 4.3.2.1; Booij et al. 2004; Qi et al. 2009)

4.3.1.2 Modelling setup

For the Northern Atlantic storms, the wind field and pressure values from fine resolution (0.8 km) WRF domain 3 were used to force the FVCOM-SWAVE model in two storms (2005 and 2013) that caused a storm surge in the Pärnu city. For Arctic case study, the wind and pressure field from PWRF domain 2 (4 km resolution) was used to model surge and wave parameters in the Canadian Beaufort Sea and Tuktoyaktuk. Simulations were conducted for hindcast, RCP4.5 and RCP8.5 scenario studies. The FVCOM-SWAVE modelling domain (Fig. 23) used the same bathymetry and topography data as in Mäll et al. (2017). The main reasoning for using the same modelling domain was output quality allowing accurate results in simulating the storm surge at Pärnu city (-2.2% peak bias compared to observations). For the 2005 storm Gudrun, initial sea level height (70 cm above the long-term mean sea level) was taken as an average from the tide gauge data before the event (Suursaar et al. 2006) and added to zeta levels to represent the elevated background water levels. Water flux through the open boundary during the event was allowed. The study by Mäll et al. (2017) used air-sea drag coefficient proposed by Honda-Mitsuyasu (1980), as opposed to default coefficient used in FVCOM. In this study the authors however considered the coefficient proposed by Wu (1982) with upper limitation of 0.003. Among the three coefficients, this yielded the most accurate results in the study area. The parameter selections for FVCOM-SWAVE can be seen in Table 1 and Table 2, for North Atlantic and Arctic study areas, respectively.

The input data for creating the bathymetry files was gathered from a wide range of sources. For Estonian coastal water the 5m and 50 m bathymetry was provided by Estonian Maritime Administration (EMA). The outer edges (near the open boundaries) were created from the ETOPO1 1-arc minute data. Also land surface levels were included in the Pärnu city by including the 5m DEM LiDAR data provided the Estonian Land Board. For Arctic, the a single source of bathymetry was used. The highest available data in the Arctic region is provided in the International Bathymetric Chart of the Arctic Ocean version 3 (500 m resolution; Jakobson et al. 2012). The unstructured bathymetry files were all created with Surface-water Modelin System (SMS), where the bathymetry files in are interpolated to generated unstructured meshes via the nearest 4-point inverse distance weighting method.. Recent versions of SMS (e.g. 13.0) allow to plot datasets with different projection and convert them into a desirable projected output. This was utilized for the Arctic simulation domain, where the bathymetry and coastline data were projected to North Pole Lambert Azimuthal Equal Area. The PWRF projection used polar stereographic projection, however

no specification are made as to which EPSG convention is used. Therefore the PWRF output coordinates were linearly adjusted to computational grid x,y coordinates through Matlab scripting.

The Arctic simulations consist of two different setups, where 1) is of Canadian Beaufort with and without the presence of sea ice, and 2) Arctic Ocean with and without the presence of sea ice. The sea ice edge was built from 1999 September monthly mean shapefile (25 km resolution) Sea Ice Index Version 3 (NSIDC 2019; Fetterer et al. 2017). The figures 24 and 25 show the regional bathymetry and open boundaries used for the FVCOM-SWAVE simulations. From modelling standpoint, the Arctic region presents difficulties from a computation domain standpoint, with the main issue being effectively representing the complex coastal geometry of the area while also using relatively large resolution meshes (e.g. 20 km in the relatively smooth coastal areas and around 8km in more complex areas such as the Canadian Archipelago).

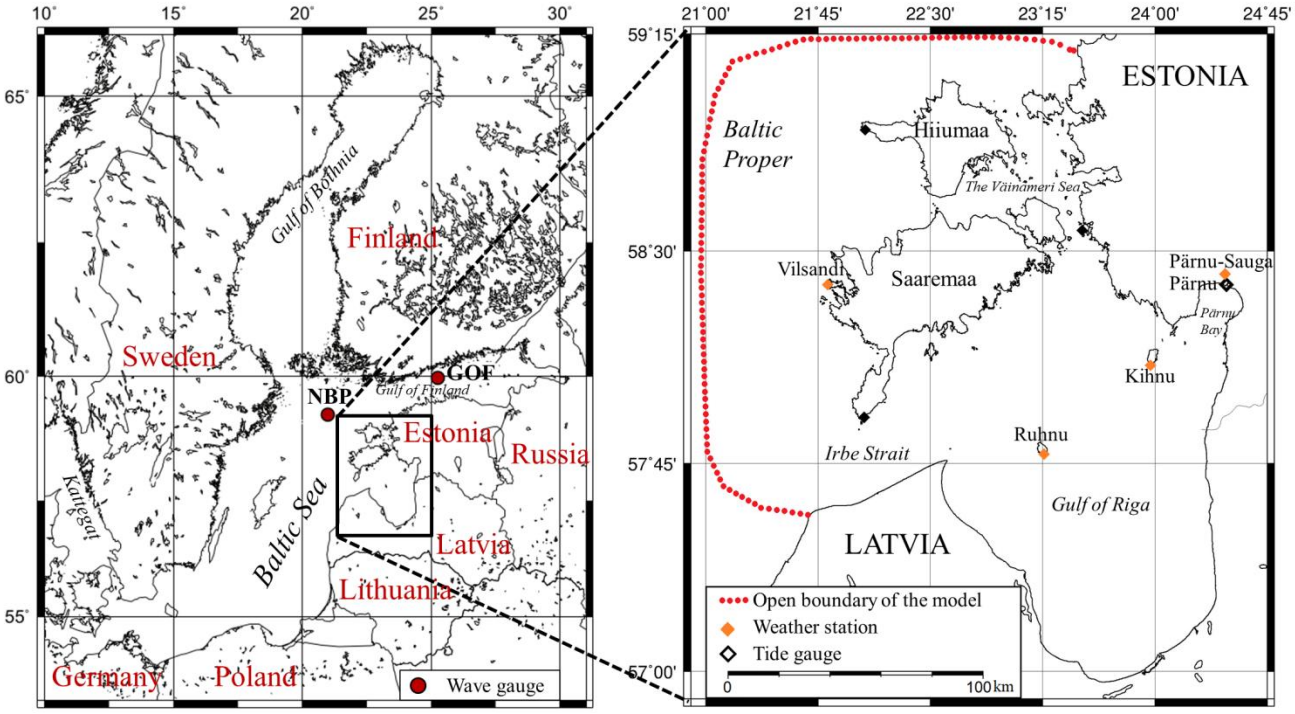

Figure 23. Area map of the Baltic Sea with its surrounding countries is shown on the left. The wave gauges are marked NPB (Northern Baltic Proper) and GOF (Gulf of Finland). The modelling domain (same as d03 in WRF) of FVCOM-SWAVE model with validation locations is shown on the right.

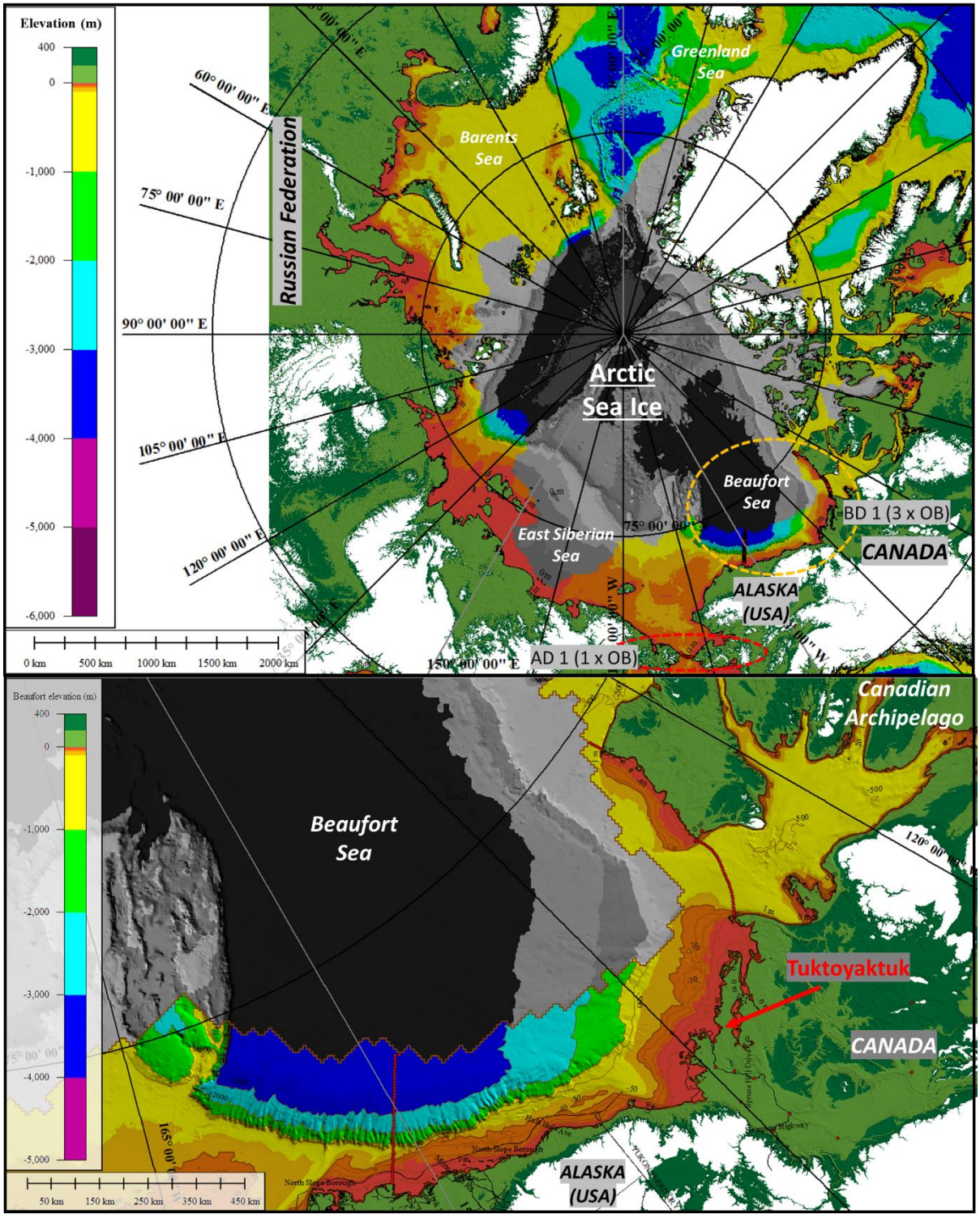

Figure 24. Area map of the entire Arctic region with modelling setup for hindcast scenarios. The hindcast scenarios studies include the presence of 1999 September month Arctic sea ice extent (Greyscale; 6.12 x 10^6 km^2; extent data by Fetterer et al. 2017). The AD and BD stand for Arctic domain and Beaufort domains open boundary locations, respectively.

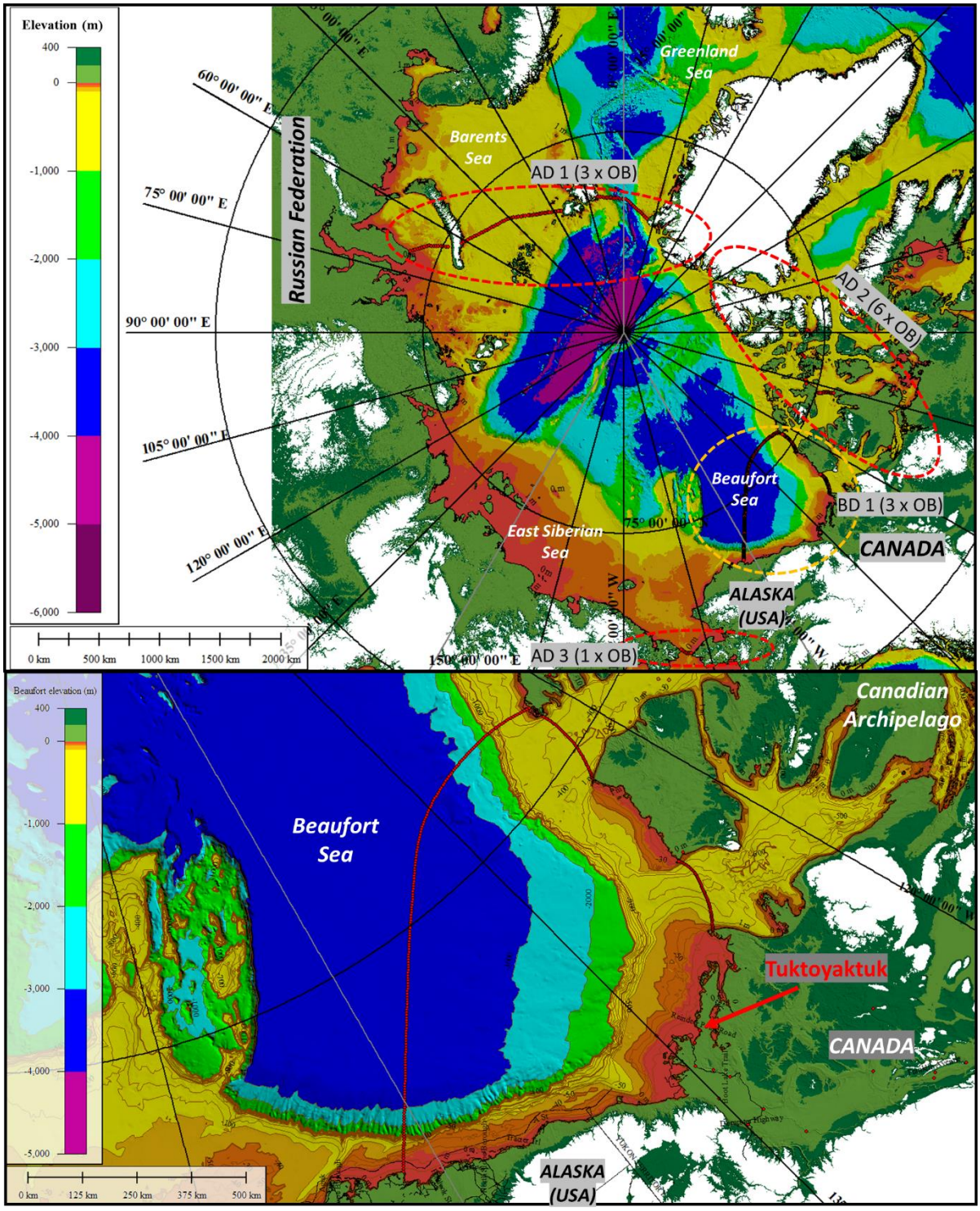

Figure 25. Area map of the entire Arctic region with modelling setup for future scenarios. The image shows ice free Arctic Ocean and open boundaries used in the RCP future scenario modelling. The modelling open boundary clusters are shown in circles, where AD and BD stand for Arctic domain and Beaufort domains open boundary locations, respectively.

4.3.2 SWAN

Simulating WAves Nearshore (SWAN) is a third-generation wave model, developed at Delft University of Technology (http://www.swan.tudelft.nl), that computes random, short-crested wind-generated waves in coastal regions and inland waters. It incorporates the state-of-the-art formulations for the deep-water processes of wave generation, dissipation and the quadruplet wave-wave interactions from the WAM model (Komen et al., 1994). In shallow water, these processes have been supplemented with the state-of-the-art formulations for dissipation due to bottom friction, triad wave-wave interactions and depth-induced breaking (Booij et al., 1999). SWAN model solves the spectral action balance equation without any a priori restrictions on the spectrum for the evolution of wave growth. This model is widely used all over the world for the calculation of wave parameters on various scales (Akpinar et al. 2012; Arkhipkin et al. 2014; Rusu 2011; Zijlema 2010).

4.3.2.1 Governing equations

The basic equation of SWAN is the spectral action balance equation. For large-scale computations, including global scales, the spectral action balance equation in SWAN is optionally formulated in terms of spherical coordinates. It is formulated in terms of Cartesian coordinates for small-scale computations. The equation in terms of Spherical coordinates is

$$\frac{\partial}{\partial t}N + \frac{\partial}{\partial \lambda}c_\lambda N + (\cos\varphi)^{-1}\frac{\partial}{\partial \varphi}c_\varphi \cos\varphi N + \frac{\partial}{\partial \sigma}c_\sigma N + \frac{\partial}{\partial \theta}c_\theta N = \frac{S}{\sigma} \qquad (3.1)$$

where, N is action density spectrum ((energy density spectrum)/(relative frequency)), σ is wave relative frequency, θ is wave direction, λ is longitude and φ is latitude.

In Equation (3.1), the first term represents the local rate of change of wave action density spectrum in time while the second and third terms state propagation of wave action in geographical space with velocities c_λ and c_φ in longitude and latitude. The fourth term represents shifting of the relative frequency due to variations in depths and currents with propagation velocity c_θ in θ-space. The fifth term states depth-induced and current-induced refraction. The term in right hand side represents the source term of energy density (S) representing wave generation, energy dissipation and non-linear wave-wave interactions as follows:

$$S = S_{in} + S_{ds} + S_{nl} \quad (3.2)$$

, where, S_{in} is wind-wave interaction, S_{ds} is dissipation of wave energy, and S_{nl} is non-linear wave-wave interactions.

For energy dissipation, SWAN model has three processes: depth-induced wave breaking, white-capping and bottom friction. In the shallow water areas, bottom friction is the main source for energy dissipation. In the deep water, the main source for energy dissipation is white-capping. Through non-linear interaction the energy is transformed between waves. Furthermore, triad wave-wave interactions have a major role to play in the shallow water, whereas quadruplet wave-wave interactions become a dominant mode in deep water. SWAN is comprehensive in that it is capable of performing computations ranging from large-scale, time dependent cases with the two-dimensional action balance equation in spherical coordinates to small-scale, stationary cases with the one-dimensional energy balance equation in Cartesian coordinate (SWAN, 2019).

4.3.2.2 Modelling setup

For wave height validation, observation data from two stations were retrieved from the website of the Finnish Meteorological Institute (https://en.ilmatieteenlaitos.fi/download-observations#!/). The stations equipped with Datawell Waveriders are located in the Northern Baltic Proper (59°15’ N 21°00’ E) and Gulf of Finland (59°58’ N 25°14’ E; Fig. 4). The SWAN simulations in this study are forced by the 4 km resolution winds from the WRF domain 2 (Fig. 23). The physical settings are shown in Table 1.

For the 2005 Gudrun and 2013 St. Jude SWAN simulation, bathymetry data from the Baltic Sea Bathymetry Database (BSBD) v0.9.3. BSBD is collaboration effort to among Baltic Sea countries to compile homogeneous up-to-date bathymetry (500 m) from official sources. in un-projected geographic (latitude/longitude) coordinates in EPSG:4258 referencing to ETRS89. Matlab script was used to re-project the extracted forcing wind field to match the x, y coordinates of the bathymetry data.

Table 1. Initial and boundary conditions of the models used for Northern Europe study area.

WRF	**2005**	**2008**	**2010**	**2013**
Domain 1 (res. 20 km)	01/06 00:00 – 01/10 12:00 (108 h)	11/19 18:00 – 11/26 00:00 (150 h)	02/26 00:00 – 03/03 18:00 (138 h)	10/26 00:00 – 10/31 00:00 (120 h)
Domain 2 (res. 4 km)	01/07 06:00 – 01/10 12:00 (78 h)	11/20 06:00 – 11/25 12:00 (126 h)	02/28 12:00 – 03/03 18:00 (78 h)	10/27 12:00 – 10/31 00:00 (84 h)
Domain 3 (res. 0.8 km)	01/08 06:00 – 01/10 12:00 (54 h)	11/21 12:00 – 11/25 06:00 (90 h)	03/01 12:00 – 03/03 18:00 (54 h)	10/28 06:00 – 10/30 12:00 (54 h)
Time step	d01 - 120 seconds, d02 - 24 seconds, d03 - 4.8 seconds			
Map projection	Lambert conformal			
Pressure top; vertical layers	1 hPa; 61			
Micro physics	WRF Single-moment 6-class scheme (Hong and Lim 2006a)			
Planetary boundary layer	Yonsei University Scheme; YSU (Hong and Lim 2006b)			
Cumulus parameterization	Grell-Freitas Ensemble Scheme (Grell and Freitas 2014)			
Shortwave and longwave	RRTMG Shortwave and Longwave Schemes (Iacono et al. 2008)			
Land surface option	Unified Noah Land Surface Model (Tewari et al. 2004)			
Surface layer option	Revised MM5 Scheme (Jimenez et al. 2012)			
Forcing data	Climate Forecast System Reanalysis (CFSR)			CFSv2
Forcing data res.	Pressure levels (1): 0.5 * 0.5 deg Surface (2): 0.312 * ~0.312 deg			(1): 0.5 * 0.5 (2): 0.205 * ~0.204
FVCOM-SWAVE	**2005**			**2013**
Simulation time	01/08 06:00 – 01/10 12:00 (54 h)			10/28 06:00 – 10/30 12:00 (54 h)
Calculation time step	Sea level – 2 seconds; Significant wave height – 30 seconds			
Nodes	63 189			
Cells	123 533			
Mesh size	50 – 2000 m			
Coastline data	Pärnu City – 5 m (DEM LiDAR); Pärnu Bay – 90 m (SRTM90); Rest of the study area – 1 arc min (ETOPO1)			
Bathymetry data	Pärnu Bay and Pärnu River – 5m (EMA); Gulf of Riga, Väinameri and Irbe Strait – 50 m (EMA); Rest of the study area 1 arc min (ETOPO1)			
SWAN/SWAVE	**2005**			**2013**
Frequency range (Hz)	0.05 -0.5			
Direction	Full circle			
Bottom friction	Madsen formulation (Madsen et al. 1988)			
Friction parameter	0.067			
Min water depth (m)	0.05			
SWAN bathymetry	500 m (BSBD v0.9.3)			
SWAN simulation time	01/07 06:00 – 01/10 12:00 (78 h)			10/27 12:00 – 10/31 00:00 (84 h)

Table 2. Initial and boundary conditions of the models used for the Arctic study area (SWAVE parameter selection is the same as in Table 1).

PWRF	**1999**
Domain 1 (res. 20 km)	11/19 18:00 – 11/26 00:00 (150 h)
Domain 2 (res. 4 km)	11/20 06:00 – 11/25 12:00 (126 h)
Domain 3 (res. 0.8 km)	11/21 12:00 – 11/25 06:00 (90 h)
Time step	d01 - 80 seconds, d02 - 16 seconds, d03 - 3.2 seconds
Map projection	Polar stereographic
Pressure top; vertical layers	1 hPa; 71
Micro physics	WRF Single-moment 6-class scheme (Hong and Lim 2006a)
Planetary boundary layer	Mellow-Yamada Nakanishi Niino 2.5 (Nakanishi & Niino 2006, 2009; Olson 2019)
Cumulus parameterization	Grell-Freitas Ensemble Scheme (Grell and Freitas 2014)
Shortwave and longwave	RRTMG Shortwave and Longwave Schemes (Iacono et al. 2008)
Land surface option	Unified Noah Land Surface Model (Tewari et al. 2004)
Surface layer option	MYNN Scheme
Forcing data	Climate Forecast System Reanalysis (CFSR)
Forcing data res.	Pressure levels (1): 0.5 * 0.5 deg Surface (2): 0.312 * ~0.312 deg
FVCOM-SWAVE	**1999**
Simulation time	**SD***: 09/23 12:00 - 09/28 00:00 (108 h) **LD***: 09/23 12:00 - 09/25 12:00 (48 h)
Calculation time step	Sea level – 5 seconds; Significant wave height – 30 seconds
Nodes	**SD***: Hindcast: 25 570 RCPs: 40 800; **LD***: Hindcast: 33 380 RCPs: 88 862
Cells	**SD***: Hindcast: 49 752 RCPs: 80 351; **LD***: Hindcast: 63 374 RCPs: 172 347
Mesh size	Hindcast: 500 - 8 000 m RCPs: 500 - 20 000 m
Coastline data	OpenStreetMap
Bathymetry data	500 m (IBCAOv3)

* SD - Small domain (Canadian Beaufort)
* LD - Large domain (Arctic Ocean)

4.4 Future scenarios

4.4.1 CMIP5 framework – models and data

In this study, 14 general circulation models (GCMs) were considered for future scenario calculations. The main selection criteria were based on the study by Zappa et al. (2013a), which suggested that among current CMIP5 GCMs, high resolution setup (~ T106/N96) might be needed to better capture the extratropical North Atlantic storm track in winter months. Another necessary criteria was that all the GCMs need to have RCP4.5 and RCP8.5

projection data available for years 2081-2100 (hereafter "2090") and 2040-2060 (hereafter "2050") and have experiment data on AAT, SST and specific humidity (converted to RH). An exception was made for HadGEM2-CC model, which data extends from 2081-2098, however met other set parameters. Accordingly, 14 GCMs were considered for the current study (Table 3) and their data was downloaded from The Earth System Grid Federations website (https://esgf-node.llnl.gov).

Future scenario calculations were done for both RCP4.5 and RCP8.5 pathways (IPCC 2014). Firstly, the ensemble mean was calculated for applicable models. Multi-model ensemble mean was calculated based on the 14 GCMs for each event month and future scenario. The GCM data was monthly averaged, therefore each of the four storm months corresponded to specific months extracted from GCMs. For example, the 2005 storm occurred in January, therefore only January values were used for this storm (and similarly, 2008 November, 2010 February, 2013 October, and 1999 September). The data for each month was divided into two groups – control period (CP) and future period (FP). The CP corresponded to monthly average values between 2006-2015 and the FP corresponded to data from 2081-2100 (with the exception of HadGEM2-CC) for NA study area and 2040-2060 for the Arctic study area. The FP and CP differences were then calculated and interpolated onto meteorological grids (created with the WRF pre-processing system, WPS), thus producing new initial conditions for the WRF simulations.

Table 3. List of CMIP5 models including resolution and ensemble information. Same models were used for North Atlantic and Arctic future case studies.

ID	Model name	Model institution	Atmospheric resolution		Ensemble number	Ensemble name
			Horizontal	Vertical levels		
G1	ACCESS1.0	Commonwealth Scientific and Industrial Research Organization (CSIRO) and Bureau of Meteorology (BOM), Australia	192 x 145 (N96)	38	1	r1i1p1
G2	ACCESS1.3				1	r1i1p1
G3	BCC-CSM1.1 (m)	Beijing Climate Center, China Meteorological Administration	T106	26	1	r1i1p1
G4	CCSM4	National Centre for Atmospheric Research	0.9 x 1.25 deg	27	6	r1i1p1, r2i1p1, r3i1p1, r4i1p1, r5i1p1, r6i1p1
G5	CESM1(BGC)	NFS-DOE-NCAR	0.9 x 1.25 deg	27	1	r1i1p1
G6	CESM1(CAM5)				3	r1i1p1, r2i1p1, r3i1p1
G7	CMCC-CM	Centre Euro-Mediterraneo per I Cambiamenti Climatici	0.75 x 0.75 (T159)	31	1	r1i1p1
G8	EC-EARTH	EC-EARTH consortium	1.125 long. Spacing, T159L62	62	4	r1i1p1, r6i1p1, r8i1p1, r12i1p1
G9	GISS-E2-H-CC	NASA Goddard Institute for Space Studies	Nominally 1 deg	40	1	r1i1p1
G10	GISS-E2-R-CC				1	r1i1p1
G11	HadGEM2-AO	National Institute of Meteorological Research/Korea Meteorological Administration	1.875long x 1.25lat (N96)	60	1	r1i1p1
G12	HadGEM2-CC	UK Met Office Hadley Centre (additional HadGEM2-ES realizations contributed by Instituto Nacional de Pesquisas Espaciais)	1.875long x 1.25lat (N96)	60	3	r1i1p1, r2i1p1, r3i1p1
G13	HadGEM2-ES			38	4	r1i1p1, r2i1p1, r3i1p1, r4i1p1
G14	MRI-CGCM3	Meteorological Research Institute	320 x 160 (TL159)	48	1	r1i1p1

4.5 Statistical analysis methods

The observational data was compared against WRF and FVCOM output data, where the hourly values of wind speed, direction and surge height were picked from the closest nodes corresponding to the coordinates of the meteorological stations and the tide gauge (Fig. 1). Data visualization and variables point extraction was done with VisIt software version 2.9.2. WRF provides u and v wind components at a 10 m height, which is also the height of the wind instrument in weather stations. The storm surge height at Pärnu city and significant wave height at Northern Baltic Proper and Gulf of Finland was were also extracted from the closest geographical grid point form the FVCM-SWAVE and SWAN, respectively. At each of the observational station locations, quality analysis and scenario comparisons were conducted to aid the visual assessment (timeseries graphs) through statistical analysis by quantifying modelled changes in the storm events' parameters.

The study cases are investigated in two parts; first, for the cases of four storm events (2008 Snow Storm not included), it is estimated, whether the acquired hindcast data for the measurement parameters of wind direction, wind speed and wave height are similar enough ($\alpha<=0.05$) to the observed set to be considered satisfactory for use in future climate scenario treatments of the data (RP4.5 and RCP8.5). Second, for each storm event, each parameter's hindcast is individually compared to the climate scenarios ($\alpha<=0.05$) to estimate the significance of changes between the events given the different conditions and across the different locations.

The data were assessed by storm and measurement station location. First, the dataset for each parameter (ranging from n=29 to n=168) measured was tested individually for parametricity using the Shapiro-Wilk test (Appendix 3). The complete-event comparison between hindcast and observed data, as well as between hindcast and the RCP scenarios was conducted using either the paired-samples t- (if both sets were parametric), or the Wilcoxon signed-rank test (if at least one set was non-parametric). The paired t-test (two-tailed), chosen for parametric samples, compares the mean difference between samples ($H_0^{\alpha=0.05}: \mu_\delta = 0$). It is an appropriate test based on its assumptions of the data: the dependent variable is continuous, does not contain any outliers and is approximately normally distributed (as determined by Shapiro-Wilk). Lastly, it can be reasonably assumed, that observations are independent of one another

The results quantify whether the visually observed differences in the storm events between scenarios are significant (α<0.05). For each storm event and for every parameter observed at each measurement station, the following hypotheses were tested (Appendix 3-5 for tables):

Hindcast verification:

$H_0^{0.05}$: There is no difference between the observed and hindcast dataset.

$H_1^{0.05}$: There is a difference between the observed and hindcast dataset.

Scenario comparison between parameters:

Hindcast and RCP4.5.

$H_0^{0.05}$: There is no difference between the hindcast and RCP4.5 scenario.

$H_1^{0.05}$: There is a difference between the hindcast and RCP4.5 scenario.

Hindcast and RCP8.5.

$H_0^{0.05}$: There is no difference between the hindcast and RCP8.5 scenario.

$H_1^{0.05}$: There is a difference between the hindcast and RCP8.5 scenario.

RCP4.5 and RCP8.5.

$H_0^{0.05}$: There is no difference between the RCP4.5 and RCP8.5 scenarios.

$H_1^{0.05}$: There is a difference between the RCP4.5 and RCP8.5 scenarios.

5 Results

The performance of the modelling system was validated using partly different aspects of each storm. Once the model performance was on adequate level, it was not necessary to compare (validate) all the possible output data. Strictly speaking, the study does not analyse the future (year 2081-2100) simulation results in comparison with the past measurements, but past and future simulations obtained with the same model. The current section is divided into three main subsections: (1) description and analysis of CMIP5 output, (2) analysis of wind, wave plus surge simulations, and (3) precipitation simulations. The future GCM output analysis is presented first since hindcast and future simulation results are presented together for a more efficient presentation.

5.1 CMIP5 GCM analysis

5.1.1 North Atlantic domains

An essential part in understanding how the studied extreme weather events might change under potential climate change conditions, is to know to what degree the initial conditions would change. The previous study by Mäll et al. (2017) used data from a single GCM, the MIROC5 (not included in this study). However, using a single GCM output comes with an inherent bias factor to it, as the various GCM outputs tend to vary greatly as can be seen from the Figure 26 and Table 4.

A comparative analysis for all the future scenarios (8 in total) included horizontally averaged pressure levels of AAT and RH. Since all the considered storms occurred under diverse thermal conditions, the vertical distributions based on the ensemble mean also differed to an extent. For AAT, the RCP4.5 and RCP8.5 differences were more apparent, where the RCP8.5 values were almost 2 °K higher compared to RCP4.5 (Fig. 27). At around 250 hPa height (about 11 km), the differences started to decrease, and turned into decrease in stratospheric heights. Highest increase occurred in 2013RCP8.5 (October month) and in 2008RCP8.5 (November), respectively. Roughly similar vertical tendencies occurred in the RCP4.5 scenarios as well.

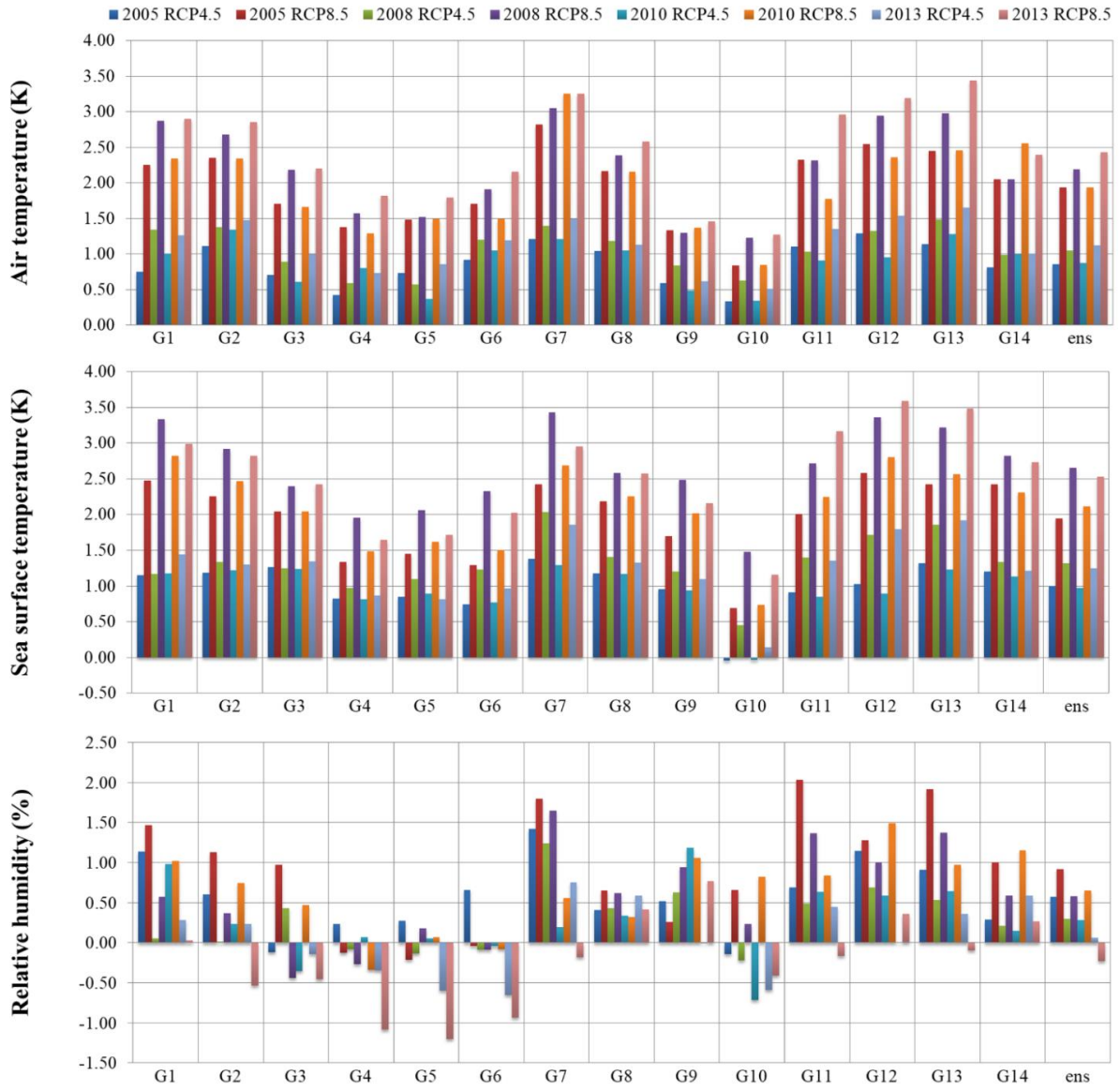

Figure 26. Projected changes from all the 14 GCMs for AAT, SST, and RH (see Table 2 for model reference and Table 3 for statistics).

The mean SST rise relative to the CP (2006-2015) showed larger changes in the RCP8.5 case (Fig. 28), and similar in increase to that of the AAT cases (Fig. 27; Table 4). For RCP4.5, the SST extremes were rather modest when compared to RCP8.5. All scenarios exhibited similar patterns in change, where the semi-enclosed water bodies (e.g. the Baltic Sea and Mediterranean Sea, also the Norwegian Sea) showed the highest increases. The SST differences became less apparent or even slightly negative (2005 and 2010 scenarios) in the North Atlantic, SW from Iceland. This negative tendency was more pronounced for the months January and February. Overall, the most pronounced changes occurred in October and November.

Table 4. Averages (Av.), standard deviations (SD) and coefficients of variance (CV) of all 14 GCM models for AAT (°K), SST (°K), and RH (%) over the WRF domain 1.

		AAT			SST			RH		
		Av.	SD	CV(%)	Av.	SD	CV(%)	Av.	SD	CV(%)
2005RCP4.5	Jan	0.86	0.30	35	0.99	0.36	36	0.58	0.47	81
2008RCP4.5	Nov	1.06	0.32	30	1.31	0.39	30	0.30	0.41	137
2010RCP4.5	Feb	0.88	0.32	36	0.97	0.34	35	0.29	0.50	172
2013RCP4.5	Oct	1.13	0.36	32	1.24	0.47	38	0.07	0.48	686
2005RCP8.5	Jan	1.95	0.56	29	1.95	0.57	29	0.92	0.75	81
2008RCP8.5	Nov	2.21	0.64	29	2.64	0.58	22	0.58	0.63	109
2010RCP8.5	Feb	1.95	0.64	33	2.11	0.60	28	0.65	0.51	78
2013RCP8.5	Oct	2.45	0.69	28	2.53	0.72	28	-0.23	0.59	256

Compared to RCP4.5, the overall parameter changes in RCP8.5 were more pronounced, and also more reliable, as estimated on the basis of coefficients of variation (CV, calculated as SD/Av. ratio and presented as percentages) among the 14 CMIP5 model output values (Table 3). For instance, the CVs were smaller in RCP8.5 calculations than in RCP4.5 (e.g. 22-28% vs. 30-38% in SST). The same basically applied for AAT and RH as well. On the other hand, the RH changes were least reliable due to relatively high SDs (and thus, CVs).

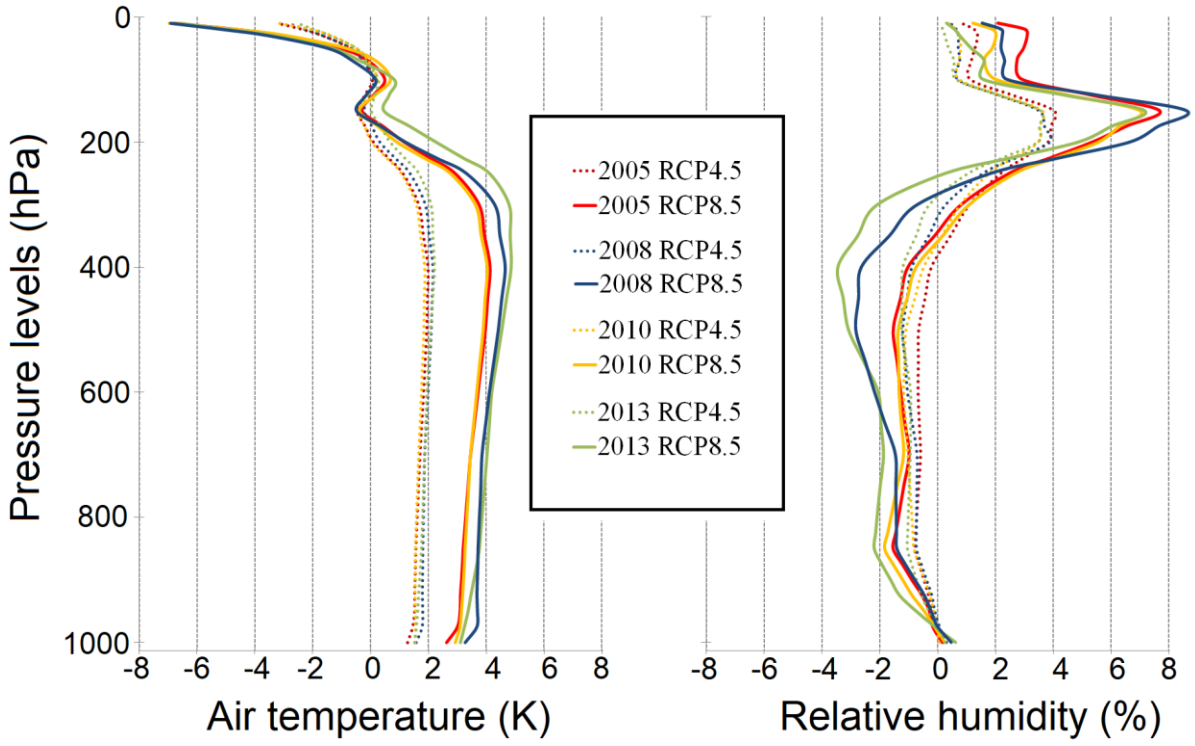

Figure 27. Horizontally averaged AAT and RH differences over the Northern Atlantic WRF parent domain.

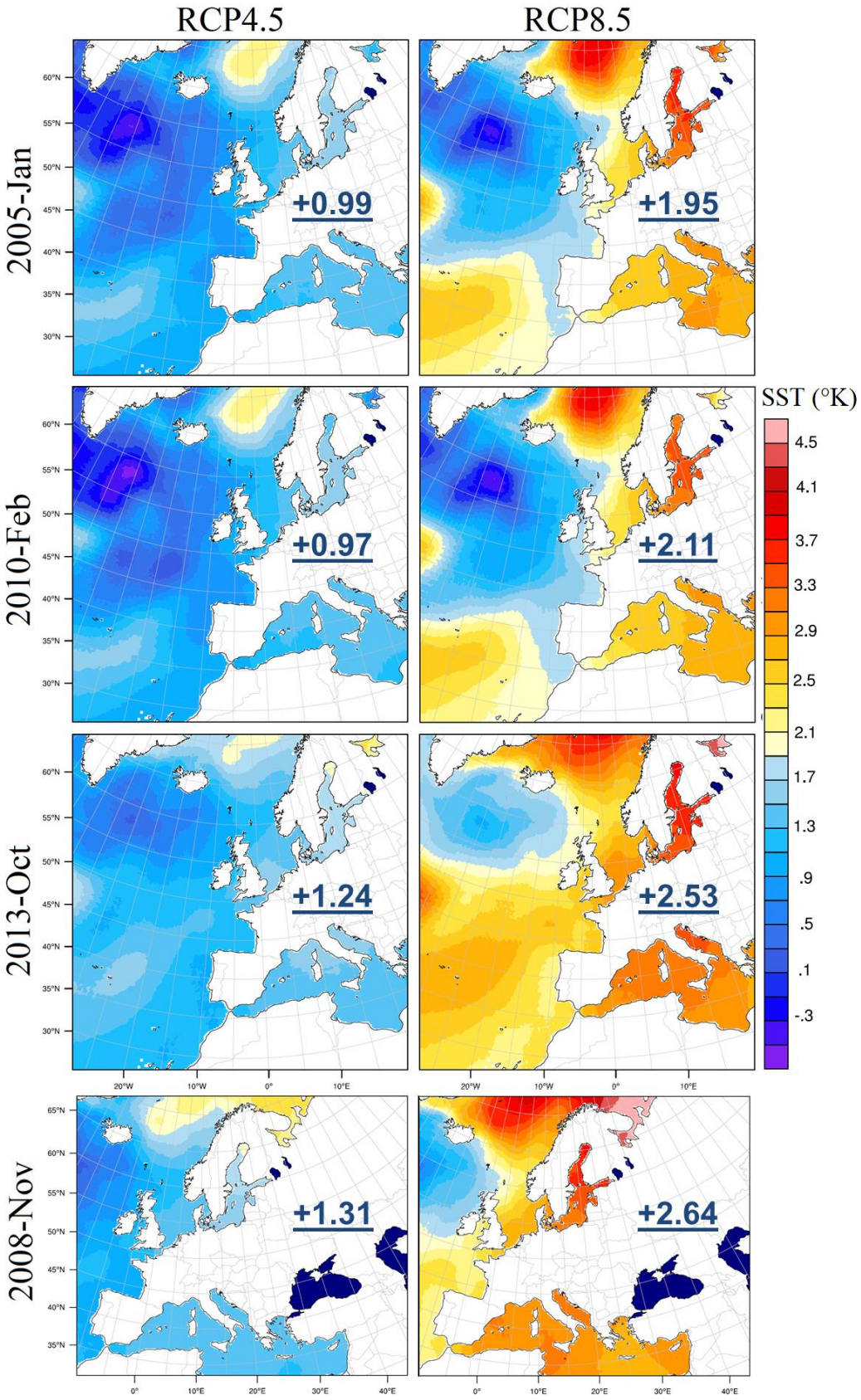

Figure 28. SST spatial distribution changes among all the future scenario calculations with indicated average SST differences (°K) over the corresponding domain by year 2090 relative to CP. Note that light blue still marks temperature rise; GCM data did not include information on inland water bodies.

5.1.2 Arctic domains

Within in the Arctic domain a single 1999 September storm event was studied. The subsequent GCM output differs further (besides the study month) in regard to future period, while in the North Atlantic the future period looked at was at around 2090, then for the Arctic it was 2050 (FP 2040-2060), against the 2006-2015 CP. Since this timeframe looks at mid-century, then the observed changes are also more modest.

For AAT (Fig. 29), the ensemble differences are not as large when compared to values looked at NA case studies (where RCP4.5 and RCP8.5 scenarios had almost two times the difference for AAT AND SST averaged fields). In the Arctic, for 2050, the expected AAT rise under current method is 1.04 K and for RCP4.5 0.83 K. For SST, the changes are 1.28 and 0.75 K for RCP8.5 and RCP4.5, respectively. Changes in atmospheric relative humidity can also be expected, similarly to NA, the positive changes start to occur at the 250 hPa pressure levels (Fig. 30). In general, for the 2050 Arctic RCP8.5 scenario, the changes are similar to that of 2100 RCP4.5 NA scenarios. However, the 14 model output variability is far larger for the Arctic in the case of SST and RH changes, where some of the models project very little change, and some in contrast, large changes.

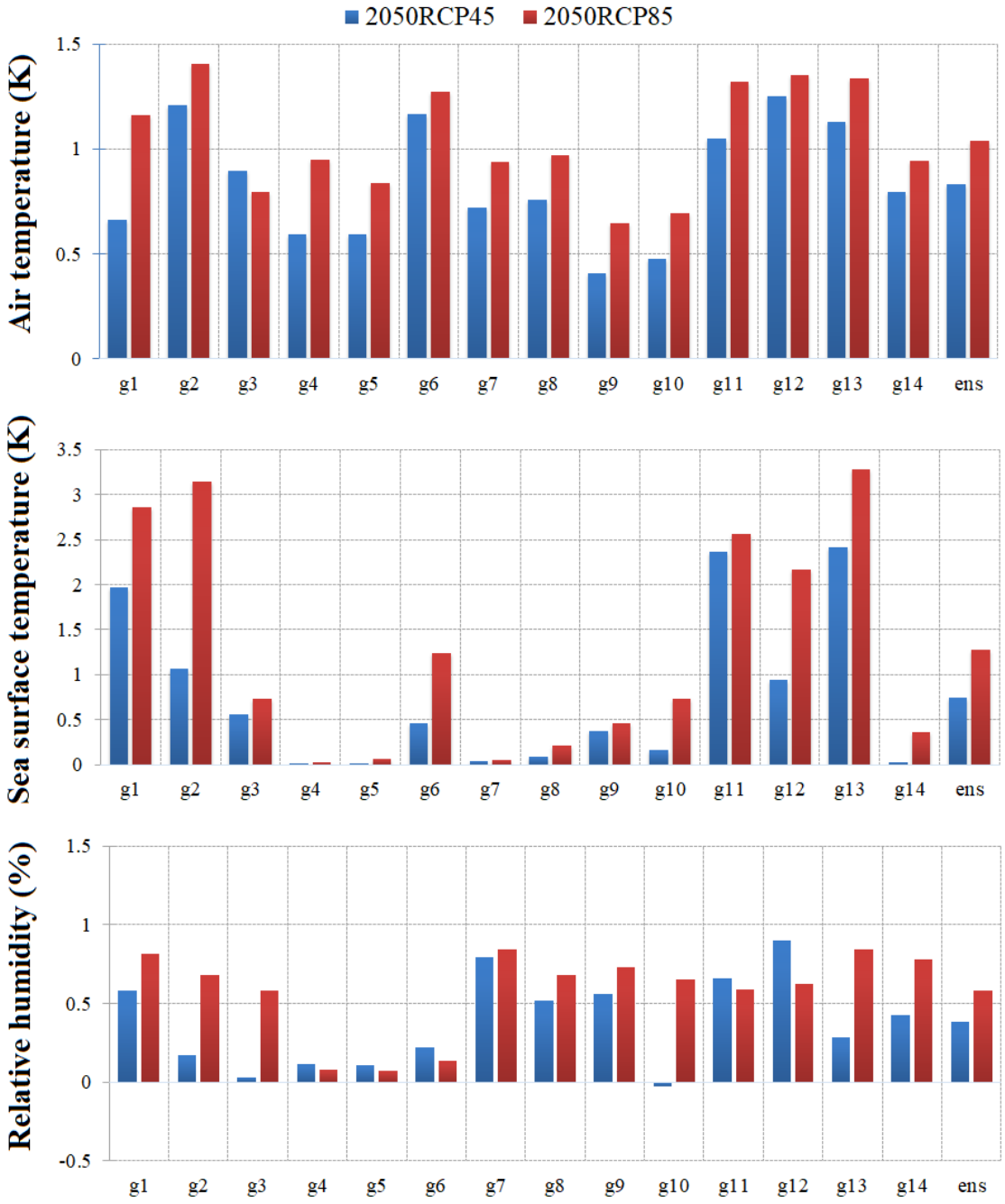

Figure 29. Projected changes from all the 14 GCMs for AAT, SST, and RH in the Arctic study domain.

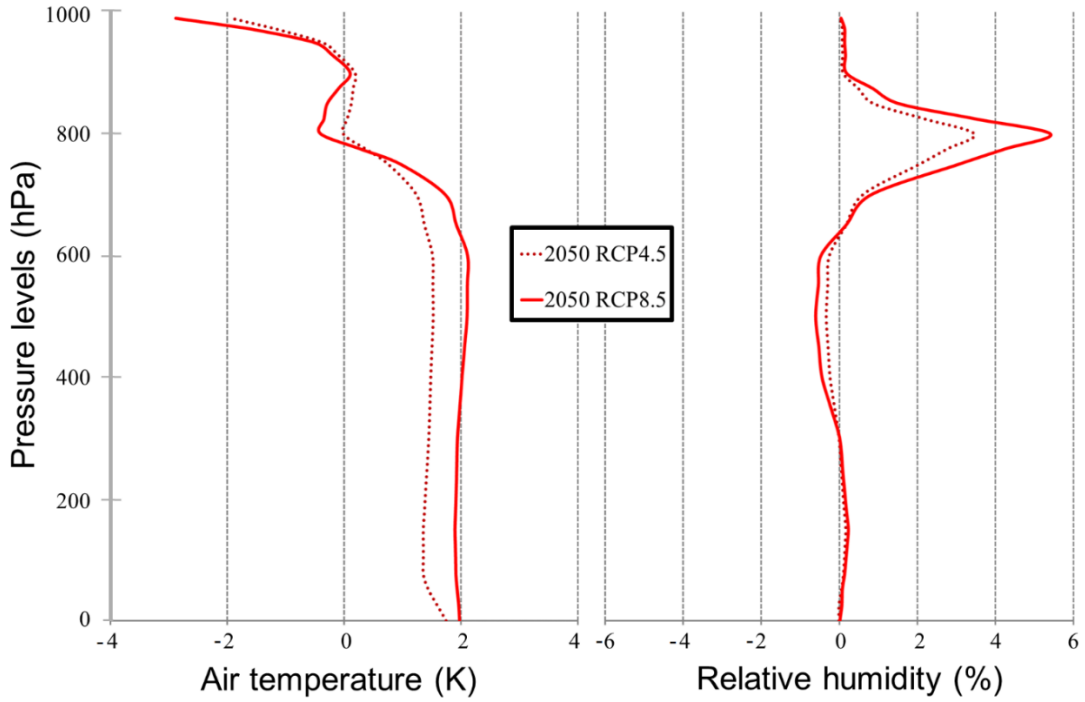

Figure 30. Horizontally averaged AAT and RH differences over the WRF parent domain for the Arctic PWRF parent domain.

5.2 Metocean results for 2005 storm Gudrun

The hindcast modelling results for the 2005 storm Gudrun were slightly different when compared to previous study by Mäll et al. (2017). The differences were probably attributed to changes made in initial and boundary conditions and use of 14 model ensemble. In the current study, higher horizontal and vertical resolutions were applied, and the domain 1 and 2 sizes have been increased. In particular, the increase in domain sizes influenced greatly the accuracy of local wind values (smaller domains yielded better results). The main argument for using larger domains and therefore accepting somewhat decreased accuracy was that larger parent domains allow better to capture the changes in cyclogenesis processes invoked by the new calculation conditions. Furthermore, for the sake of homogeneity, the single domain setup for Atlantic storms needed to encompass all the locations where the three storms originated from.

Although a backward shift in the wind speed peak timing for the Kihnu and Ruhnu stations were observed (Fig. 31), the maximum values were captured with good accuracy. Results for Vilsandi and Pärnu-Sauga stations showed the best fit with the observed values. The prominent drop in observed wind speed at Vilsandi station occurred due to the stations proximity to a lighthouse, which dampened the wind measurements from 210˚-250˚ sector.

Concurrently to the results at Kihnu and Ruhnu station locations, which possesses the largest potential for evoking storm surge in Pärnu Bay (Fig. 31), the simulated FVCOM-SWAVE results showed higher initial increase in the sea level and reached its first peak maximum of 2.41 m at 9 January 00:20 UTC (observed was 2.75 m at 9 January 04:00 UTC). The almost 4 hour difference can be attributed to the wind field quality which also reached its first peak maximum 3 hours before the observed measurements.

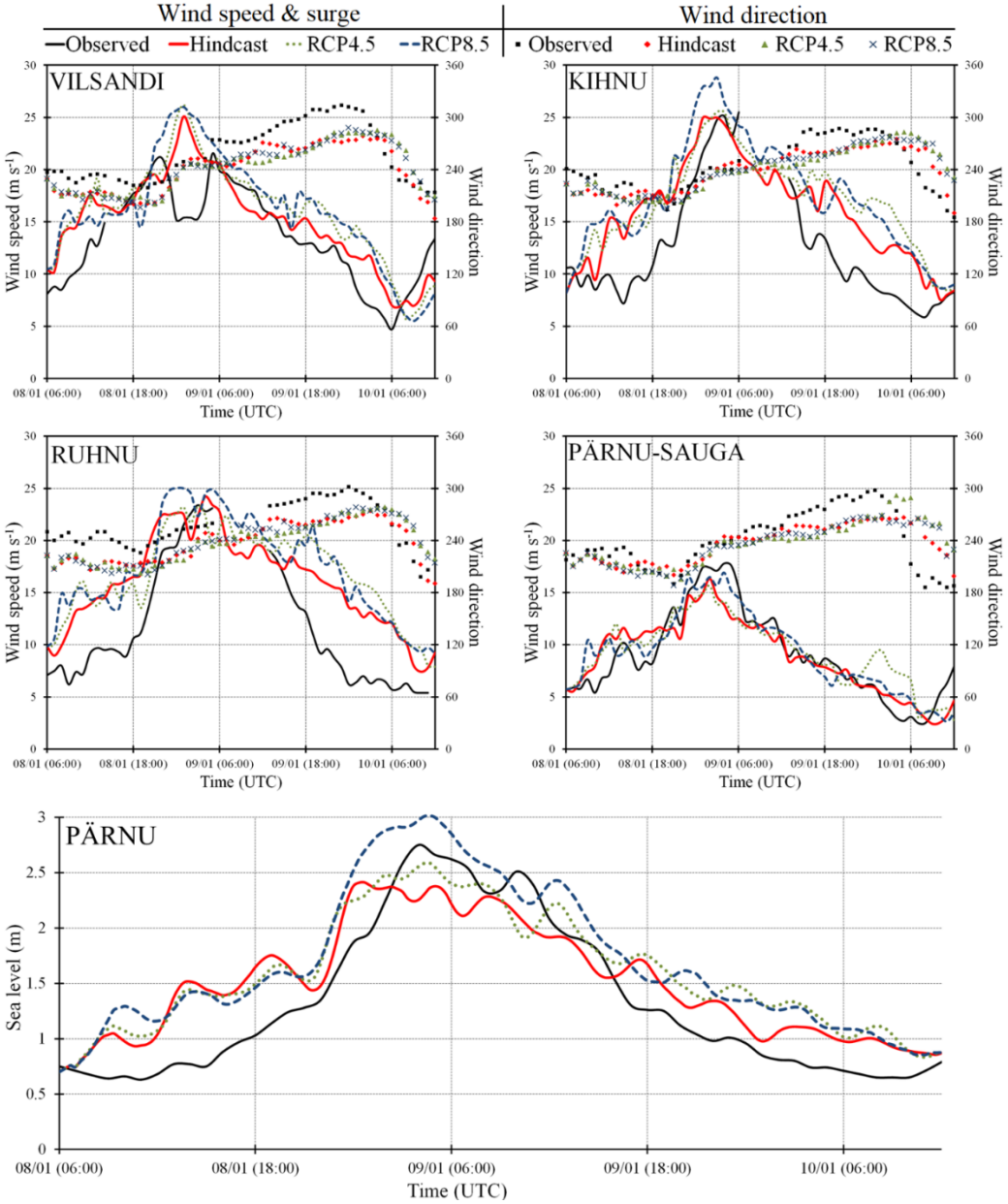

Figure 31. Modelling results for the 2005 storm Gudrun. The upper two rows show wind speed and direction at selected stations and the bottom image shows the surge results at Pärnu (see also Fig. 21).

The future simulations, on the other hand, showed more pronounced outcome, compared to the previous study, where no increase in intensity was observed. Interestingly, among the stations, the future increase occurred in the stations situated in the Gulf of Riga. Furthermore, in the location of Kihnu (closest to Pärnu Bay; Fig. 23) the peak hourly sustained wind values reached as high as 28.8 m s^{-1}, while RCP4.5 and hindcast peak values reached 25.5 and 25.0 m s^{-1}, respectively. This difference also translated into surge height increment (Fig. 32; Table 5), yielding in maximum surge values of 3.0 m for RCP8.5 and 2.59 m for RCP4.5, as opposed to 2.41 m in hindcast simulation (Figure 32). Hence, the peak surge height increased 19.7% under RCP8.5, while under RCP4.5 the increase was 7%. Considering the scatter among the individual model outputs (Table 4), the increase in RCP4.5 was not significant, but it was under RCP8.5.

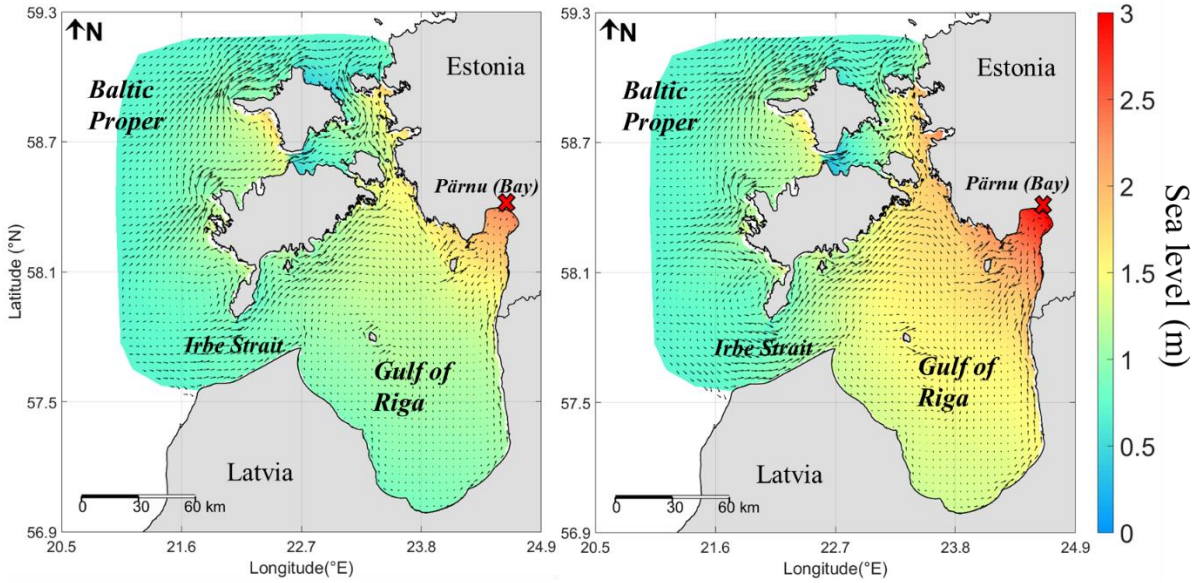

Figure 32. Spatial distribution of storm surge max during the hindcasted (9-January 00:40 UTC; 2.41 m) and future RCP8.5 (9-January 04:40 UTC; 3.01 m) scenarios as shown in left and right figures, respectively. The red x marks the tide gauge and Pärnu city approximate location.

Table 5. Maximum surge heights and surge increments (relative to hindcast) in different scenarios by the year ~2090.

Scenario	Max. (cm)	Increment (%)
RCP4.5 Gudrun	259	6.9
RCP4.5 St. Jude	122	2.5
RCP8.5 Gudrun	301	19.9
RCP8.5 St. Jude	142	16.2

Since the RCP8.5 case showed significant station-based changes (Fig. 31), the hindcast and RCP8.5 simulations on a regional scale (WRF domain 2) were also compared to see whether there were any significant changes in cyclone track and/or wind field (Fig. 33). In terms of pressure field, the RCP8.5 had an equal or slightly higher (by up to 2 hPa) minimum sea level pressure (MSLP) values at the cyclone core, compared to the hindcast. However, the MSLP area of RCP8.5 was more symmetrical compared to hindcast and thus, covering somewhat larger area. This, in turn, could strengthen pressure gradient on the southern side of the cyclones core (due to more densely packed isobars; Fig. 33), and hence, also local winds. The extent of high wind speed field (≥ 24 m s^{-1}) stretched further southwards from the core boundary. Stronger winds extensively occurred over Baltic Proper, Gulf of Riga, and Danish straits.

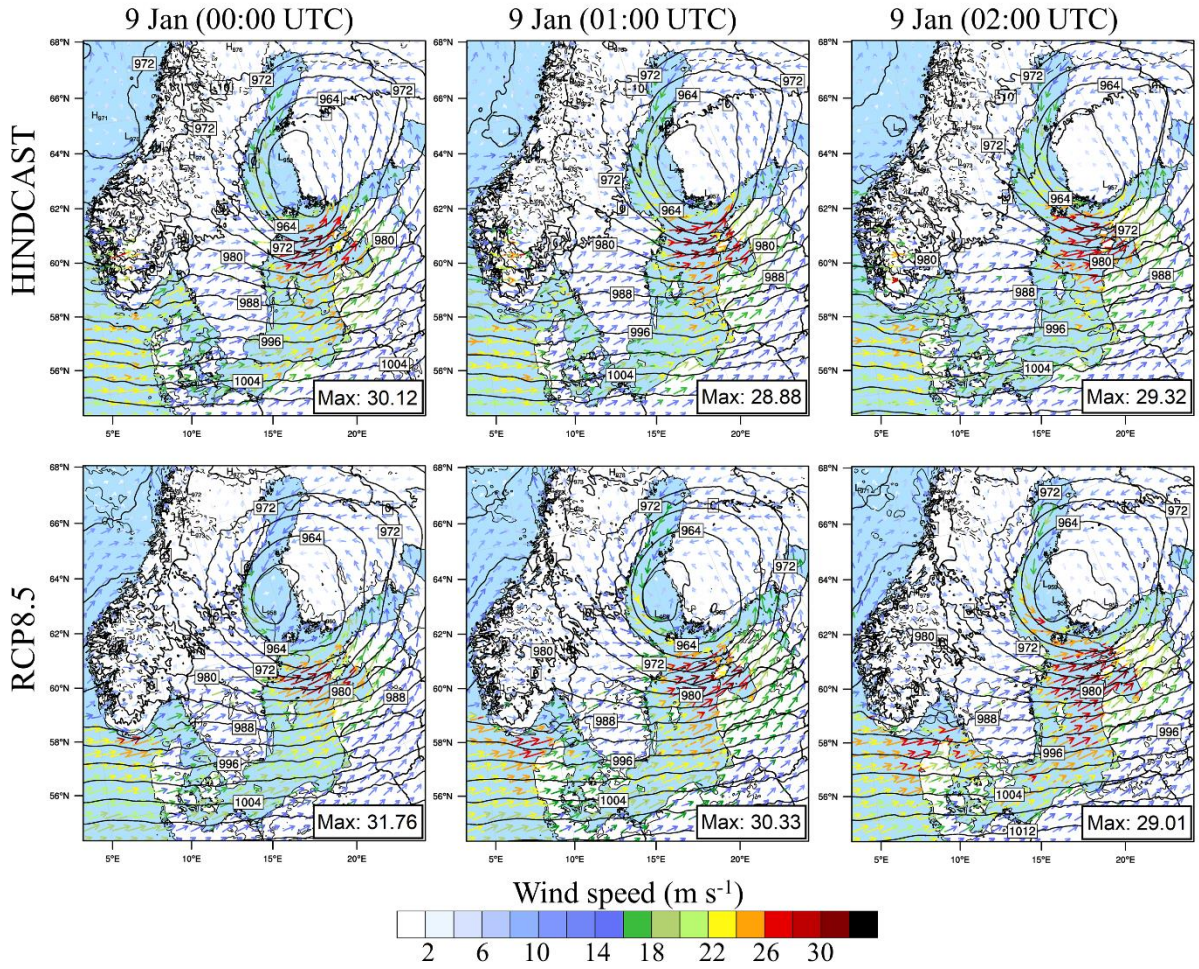

Figure 33. Wind and MSLP fields over WRF d02 for hindcast and RCP8.5 simulations (2005 case). The "Max" values indicate maximum hourly wind speed values at a given time-step.

The hindcast simulation results for wind waves at the station which has the longest fetch area (Northern Baltic Proper; NBP) generally showed good agreement with the observed significant wave height values (Fig. 34). However, the peak heights were overestimated by 1.2 m (7.2 m observed vs. 8.4 m simulation). Similar model overestimations for the NBP were forecasted by various meteorological institutes at the time of the event, as discussed and presented by Soomere et al. (2008). In fact, our modelling results were very close to those forecasts (by DMI, DWD and FIMR; Soomere et al. 2008; Fig. 34). While the measurements and hindcasts generally behave similarly in "normal" conditions, during the peak wave conditions either the models are overestimating or the Waverider underestimating the actual wave heights. It is possible that the Waverider measurements were, in some reason, not quite representative during the peaks of the extreme storms. In particular, the measured wave heights around 3 m in the Gulf of Finland seems to be much too low for such an extreme storm (Fig. 34), while 5.2 m H_s has been attained several times, before and after the 2005 storm (Björkqvist et al. 2018). Gulf of Finland comparison could suffer from measurement gaps during the storms, due to specific configuration of the Baltic Sea and narrow fetch geometry of the Gulf of Finland itself (Björkqvist et al. 2018).

Compared to hindcast, the future simulations showed no significant change in H_s maximums at either station locations. However, under RCP8.5 the calculated wave field patterns showed a notable southward extension of the high wave zone, increase in maxima within the Baltic Proper (9.2 m vs 8.7 m; Fig. 35), and also in the Gulf of Riga. This was directly related to the south-ward extension of stronger wind fields as shown in figure 33.

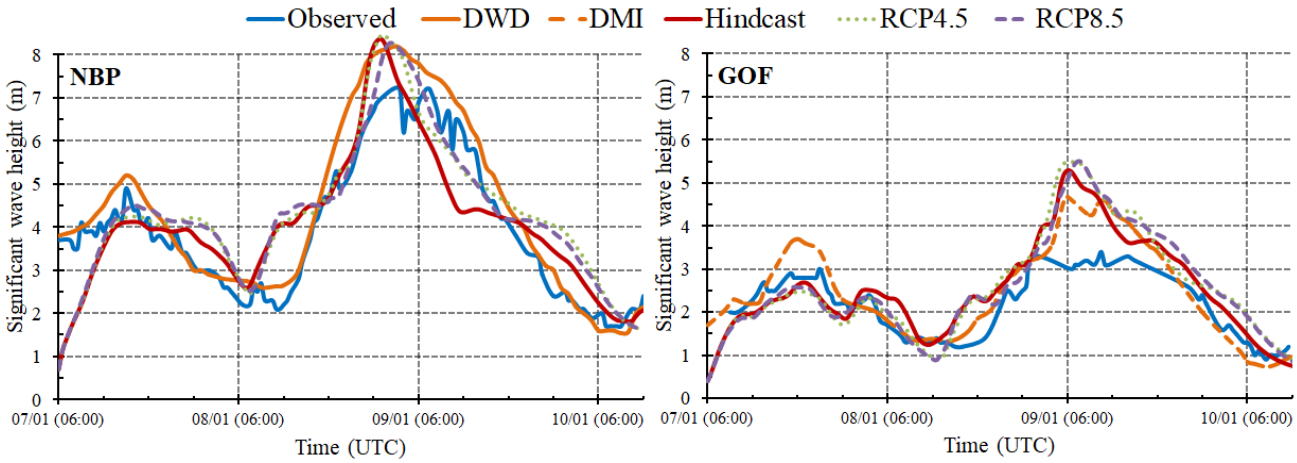

Figure 34. SWAN simulation and observed significant wave height comparisons at the two wave gauge stations (see also Fig. 4). The Deutscher Wetterdienst (DWD) and DMI data were reproduced from Soomere et al. (2008).

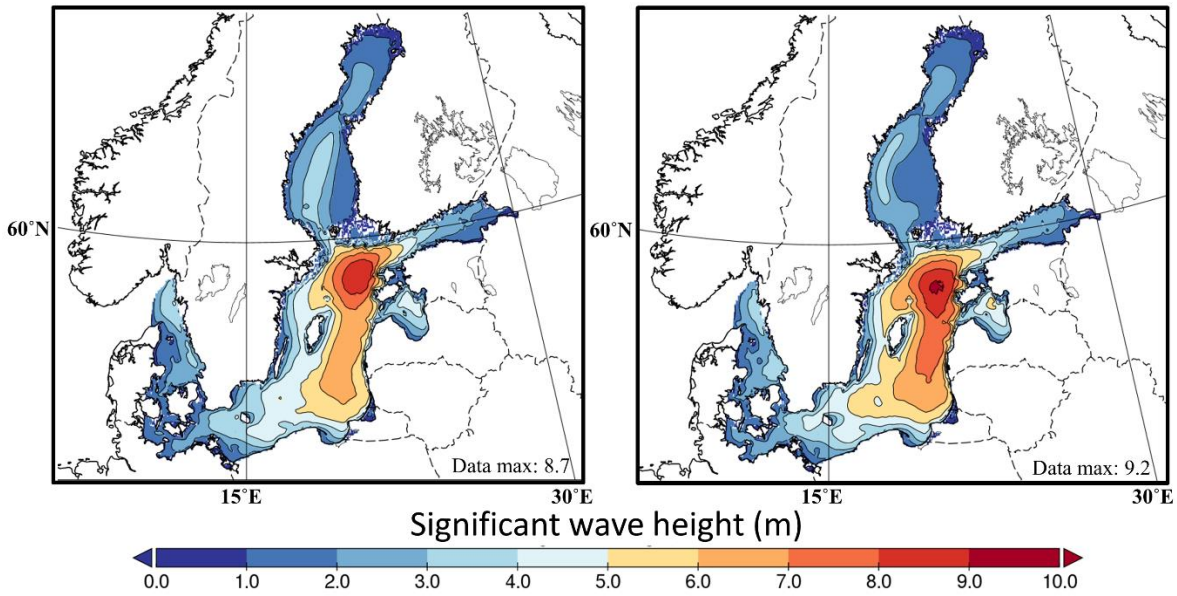

Figure 35. Spatial distribution of SWAN simulation results for the hindcast and RCP8.5 case at Jan-9 01:00 UTC, during the occurrence of highest simulated significant wave heights. Left figure is for hindcast and right figure is for RCP8.5 scenario calculations.

5.3 Metocean results for 2013 storm St. Jude

The analysis section for Gudrun explained how configuring simulation conditions can affect the simulation accuracy. In the 2013 storm case, on the other hand, simulated wind speed curves at the four stations showed a remarkably good fit with the observed values (Fig. 36). The peak wind speed values and their timings were well captured, showing no significant deviations. Also the wind speed values before and after the peak were more concurrent with observations. The observed drop in Vilsandi was caused by the same reason as for the 2005 case (lighthouse shade). The observed surge peak at Pärnu was 1.44 m (29 Oct. 07:00 UTC). The FVCOM-SWAVE hindcast simulation peak maximum was 1.19 m (29 Oct. 04:00 UTC). Furthermore, in both 2005 and 2013 cases, the observed second peak at Pärnu was caused by the 5 hour seiche period of the Gulf of Riga sub-basin (Suursaar et al. 2002), which the ocean model was unsuccessful in capturing. In terms of relationship between surge potential and wind direction, Pärnu Bay is most susceptible to winds from 220˚ (Suursaar et al. 2006). The 9-hour average wind directions at Ruhnu station were 210˚ and 226˚ for hindcast and observations, respectively (Fig. 36). At Kihnu, the hindcast wind directions were close to the most suitable 220˚ mark as well.

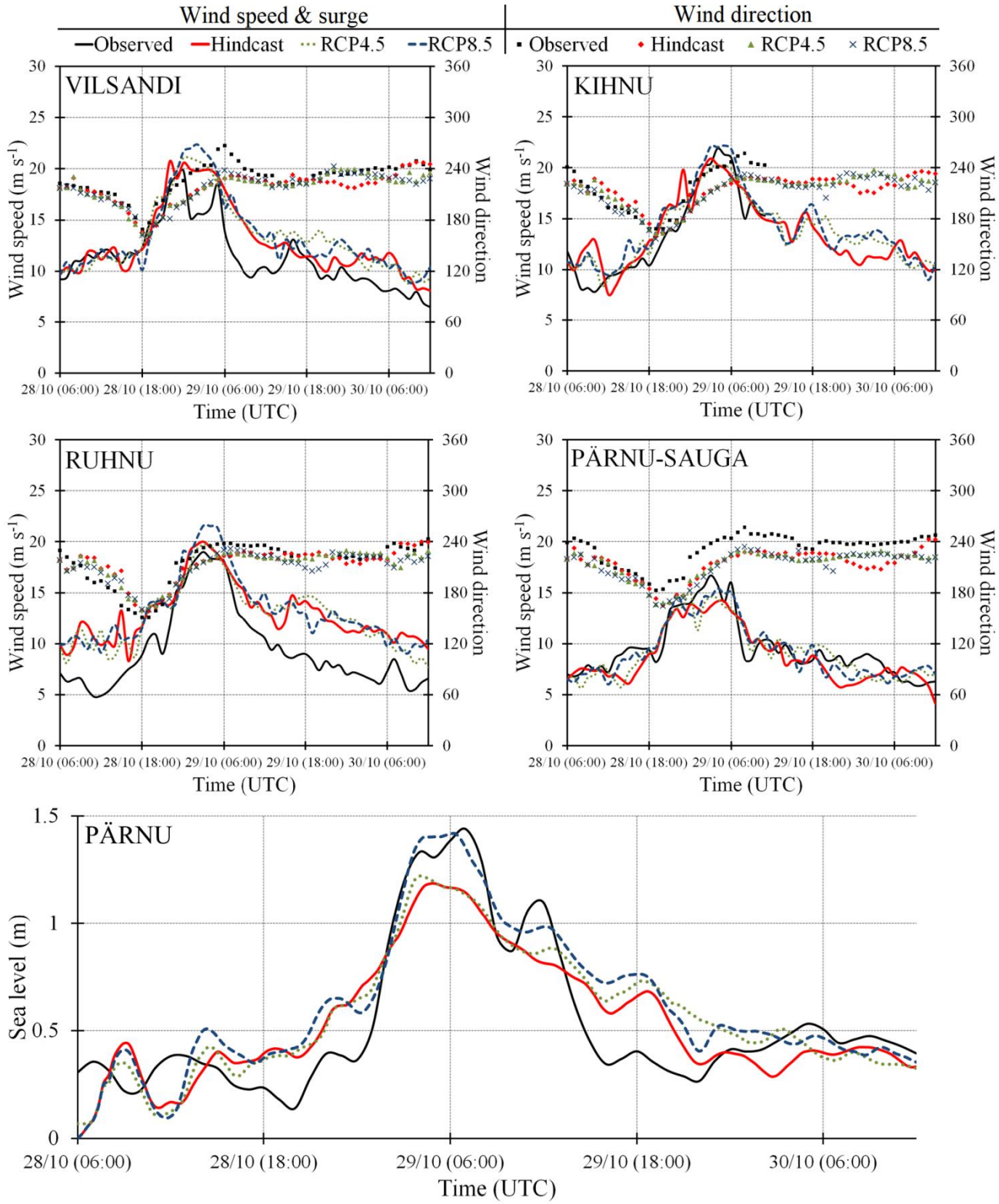

Figure 36. Modelling results for the 2013 storm St. Jude (see also Fig. 11).

Similar to the 2005 case, future scenario calculations under RCP4.5 scenario had little to no increase in wind speed, while RCP8.5 showed clear increase over the Gulf of Riga (Fig. 36). Also, a slight increase at peak value occurred at Vilsandi station. These higher wind

speed values were also translated into higher storm surge simulation results (Fig. 36; Table 5). The peak differences for RCP8.5 wind speeds were 0.7, 1.6 and 1.0 m s^{-1} for Vilsandi, Ruhnu and Kihnu stations, respectively. The changes, especially at Kihnu station, were not as profound as was for the 2005 case (3.8 m s^{-1} increase at Kihnu for the 2005 RCP8.5). The RCP4.5 surge simulation yielded peak value of 1.22 m (just 0.03 m increase over the CP), while RCP8.5 surge simulation yielded 1.41 m (0.22 m or 15.6% increase; Fig. 37).

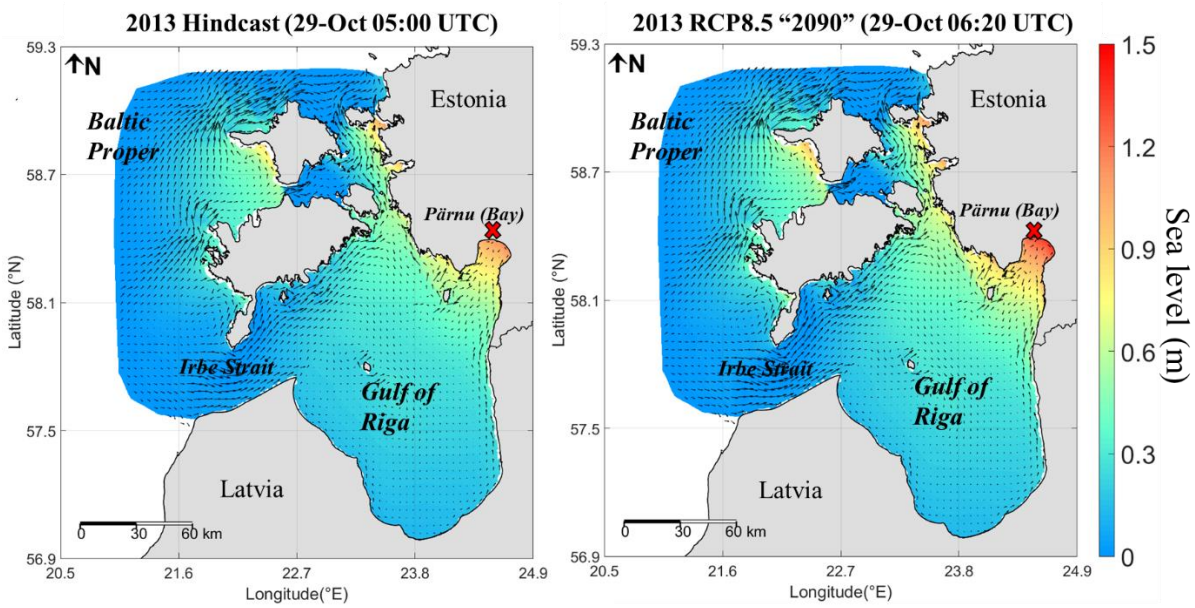

Figure 37. Spatial distribution of storm surge max during the hindcasted (29-October 05:00 UTC; 1.19 m) and future RCP8.5 (29-October 06:20 UTC 1.41 m) scenarios. The red x marks the tide gauge and Pärnu city approximate location.

The 2013 regional pressure field (Fig. 38; WRF domain 2) differences between hindcast and RCP8.5 had less apparent changes than during the 2005 storm. The core pressure levels stayed the same (968 hPa) for both hindcast and RCP8.5 throughout the investigated 4 hour period. Furthermore, the central pressure area location, spread and pattern remained almost unchanged, with the more notable exception of slightly elongated isobars spread from the core. The maximum wind speed values also remain largely unchanged, with an exception where significant increase of 3 m s^{-1} for the RCP8.5 at 29 October 05:00 UTC occurred. In terms of strong wind speed ($\geq$ 22 m s^{-1}) spatial distribution, the RCP8.5 showed a slight southwards extension of stronger winds (therefore stronger winds over the Gulf of Riga) which seemed to be related to the aforementioned elongated spread of near core pressure isobars. The strong wind speed values started to form and extend from the 976 hPa isobar line, which explains the wind speed differences over the Gulf of Riga stations and therefore the increase in surge height at Pärnu.

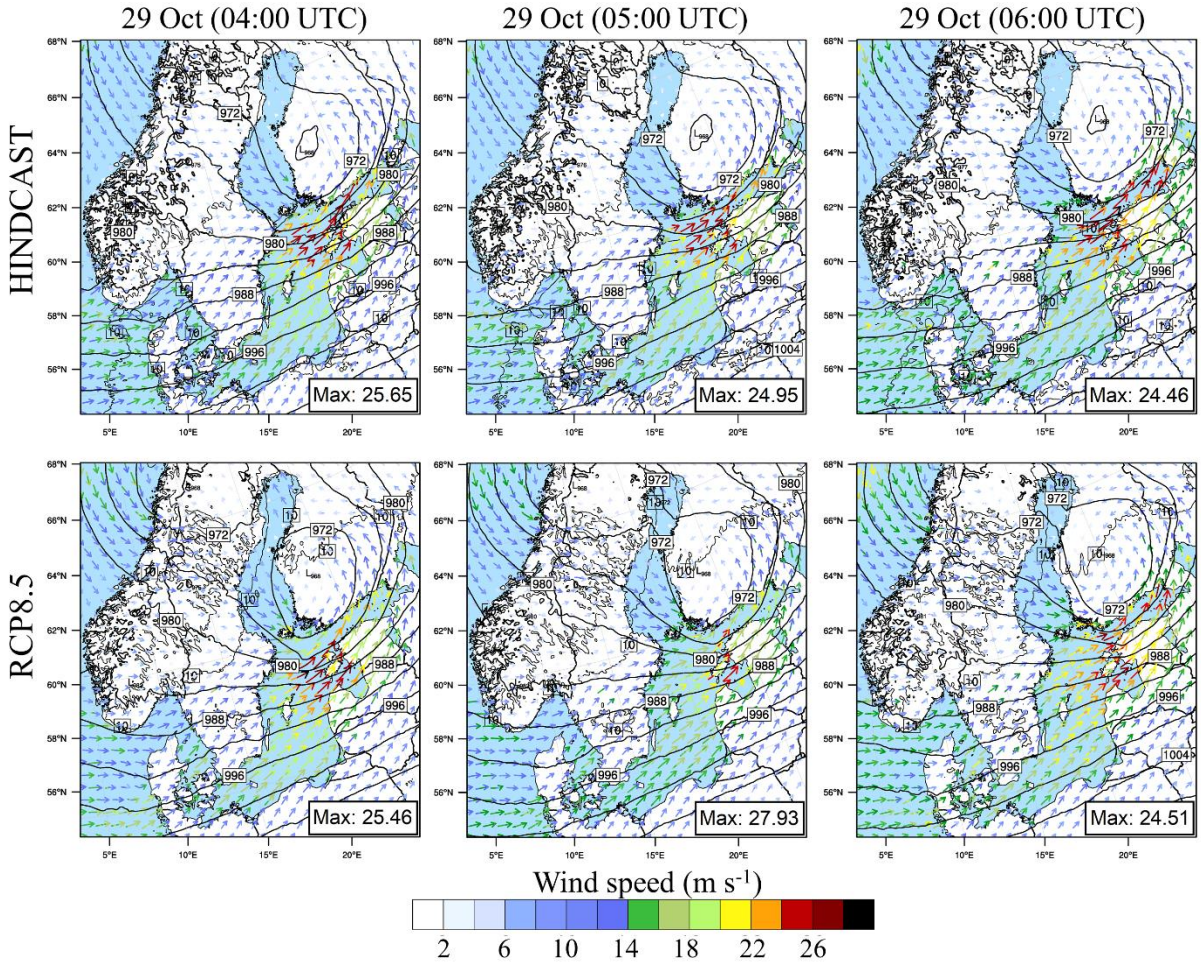

Figure 38. Wind and MSLP fields over WRF d02 for hindcast and RCP8.5 simulations (2013 case; see also Fig. 12).

The SWAN hindcast simulation results for the 2013 storm also show overestimation of H_s at the location of wave gauges (5.2 m vs. 7.3 m at NPB and 2.8 m vs. 4.5 m at GOF for observation and hindcast, respectively; Fig. 39). The problems of comparison were quite similar to those already described in case of 2005 storm wave modelling. It should also be noted that in terms of modelling it is challenging to achieve high order of accuracy when considering the complex configuration of the study area.

In terms of future simulations, the changes were not as apparent as they were for the stronger 2005 storm Gudrun. However, a small increase in H_s maximum (7.8 m vs. 7.4 m; Fig. 40) can be still seen. Also, a slight south-ward extension of high wave fields occurred within the Baltic Proper. The expanded effect of the high wave zone could be more pronounced in the most extreme storm events (i.e. 2005 Gudrun; Fig. 35) and less so for weaker but still strong storms (i.e. 2013 St. Jude; Fig. 40).

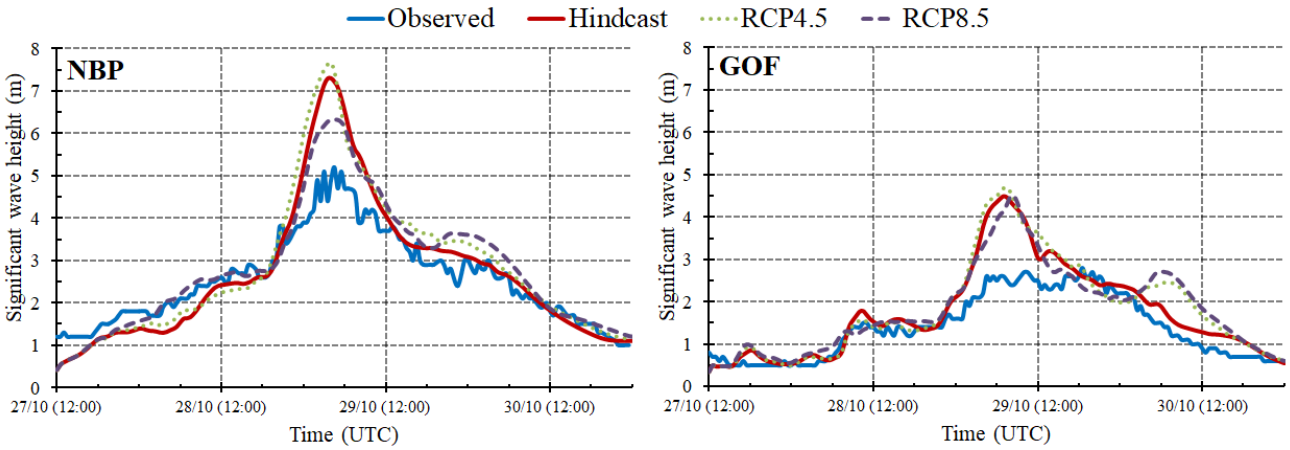

Figure 39. SWAN simulation and observed significant wave height comparisons at the two wave gauge stations (see also Fig. 4).

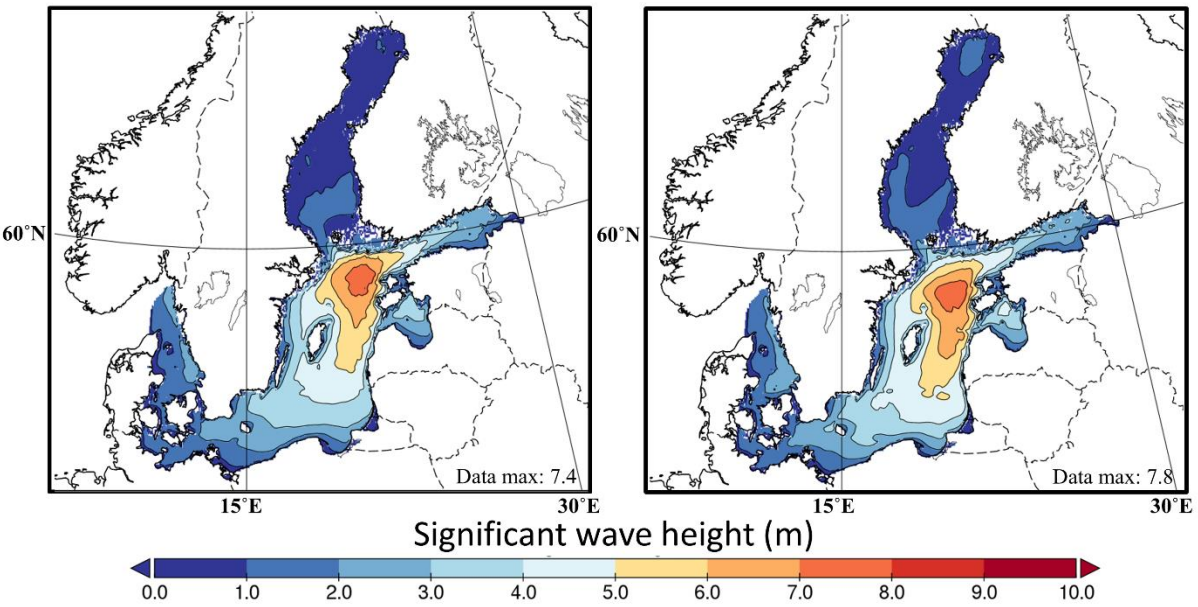

Figure 40. Spatial distribution of SWAN simulation results for the hindcast and RCP8.5 case at Oct-29 04:00 UTC, during the occurrence of highest simulated significant wave heights. Left figure is for hindcast and right figure is for RCP8.5 scenario calculations.

5.4 Wind according to the 2010 storm Xynthia (no surge)

The 2010 storm had the potential to elevate sea levels to a certain degree, however, in the late February the Estonian archipelago was locked by sea ice. Furthermore, the storm was considerably weakened once it arrived in the Baltic Sea region and therefore the main interest for that storm was to investigate wind and precipitation changes. The hindcast simulations at four weather stations showed reasonably good results (Fig. 41), considering that modelling in general tends to have some difficulty in capturing weak synoptic patterns and winds. Overestimation of weaker winds occurred at the beginning and at the end phases of the simulations, whereas peak winds were well captured. Moreover, local natural or man-made obstructions (e.g. lighthouse at Vilsandi) in the vicinity of the stations can affect the actual measurements, while numerical models are not supposed to capture those local factors. Similarly, most stations, at times, showed model wind direction deviations as high as 50 degrees (Fig. 41; Kihnu and Pärnu-Sauga). Also, the friction due to local dampening objects may easily turn the observed (weak) wind directions.

The future simulations aimed to study whether ETCs, travelling from far SW section of Europe, would reach north Europe as stronger systems. According to current study results, the "future storm Xynthia" would not. The 2010 storm started out as a subtropical cyclone (Liberato et al. 2013) and transitioned into ETC soon after its formation. The results on atmospheric pressure and winds, however, were not much different from the 2005 and 2013 cases. The RCP4.5 scenarios showed little to no change, whereas simulations with the RCP8.5 initially showed increased wind speeds over the Ruhnu and Kihnu stations (Fig. 41), although after 18 hours the effect decreased.

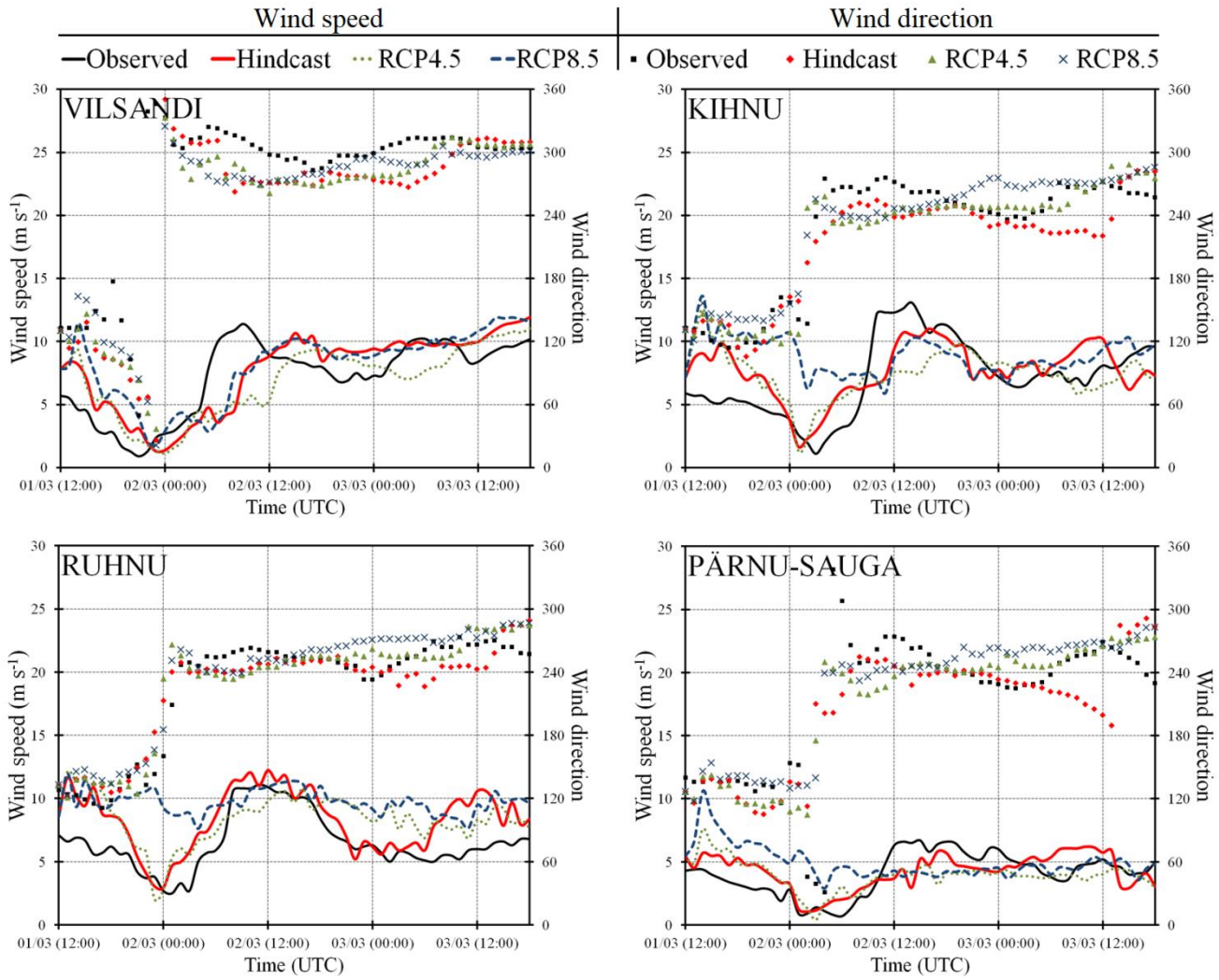

Figure 41. Simulation results for the 2010 storm Xynthia.

5.5 Precipitation changes (all North Atlantic cases)

Firstly, the 2008 storm featured by low minimum sea level pressure and high precipitation. The comparison of minimum observed and modelled atmospheric pressures above Estonia yielded good results. The minimum pressure (both measured and modelled) was approximately 951 hPa and the corresponding differences were rather small (average 1.1 hPa) at the mainland stations. Higher deviations occurred at the western Estonian coastline and island stations (average 7.6 hPa). Over the period of 96 hours (22-25 November 2008), the accumulated precipitation amount in different Estonian weather stations varied between 15-37 mm in water equivalence. The average above the mainland was 29 mm, and the average considering also the islands (altogether 23 stations) was 25 mm. Despite "patchy" nature in precipitation distribution, the WRF modelled, area-weighted average precipitation amounted for 25.1 mm over the similar area.

As about the four storm cases, the future changes remained rather modest and unclear under the RCP4.5 scenario. The RCP8.5 simulations exhibited more clear tendencies. The three Atlantic storms (I-III, Fig. 6) showed steady precipitation increase from d01 to d03, while for the southerly 2008 storm it was the other way around (d01 highest and d03 the least). Furthermore, the homogeneous domains used for the Atlantic storms showed that over parent domain the increase for these storms were roughly the same, with average increase of 7.5 %, regardless of the precipitation potential for these storms. The second domain, that encompasses Baltic Sea and its surrounding countries, showed 12–18% increase in total precipitation values (Table 6; Fig. 42). For the Estonian west coast (d03) the increase was between 13–23%. Among the three storms approaching from the Atlantic, the highest increase for the study area was for the 2013 October storm. However, the 2010 storm was already considerably weakened when it approached the domain 2, whereas the 2005 storm was at its strongest and the almost 12% precipitation increase for an already strong cyclonic system could potentially cause far more serious outcomes. For the 2005 and 2013 storms (both approaching from W-SW) a clear orographic enhancement of precipitation occurred over the Scandinavian mountains (Fig. 42).

Table 6. Future scenario (year ~2090) area-total precipitation averages and corresponding changes (values in brackets) relative to hindcast.

	Av. (mm)		%	Av. (mm)		%
		2005			2008	
d01 RCP4.5	14.65	(+0.79)	5.4	17.52	(+0.61)	3.5
d02 RCP4.5	26.65	(+1.45)	5.2	16.72	(+0.71)	4.3
d03 RCP4.5	15.4	(+0.54)	3.5	24.46	(-1.49)	-6.1
d01 RCP8.5	15.01	(+1.14)	7.6	22.88	(+5.96)	27.3
d02 RCP8.5	28.61	(+3.40)	11.9	19.09	(+3.08)	16.1
d03 RCP8.5	18.6	(+3.74)	20.1	25.08	(-0.87)	-3.5
		2010			2013	
d01 RCP4.5	19.52	(+0.72)	3.7	15.97	(+0.59)	3.7
d02 RCP4.5	18.25	(+0.77)	4.2	23.14	(+2.33)	10.1
d03 RCP4.5	17.88	(+0.35)	1.9	21.8	(+0.85)	3.9
d01 RCP8.5	20.31	(+1.50)	7.4	16.61	(+1.23)	7.4
d02 RCP8.5	19.86	(+2.38)	11.9	25.38	(+4.57)	18
d03 RCP8.5	20.21	(+2.67)	13.2	27.11	(+6.16)	22.7

Thus, according to the projections, westerly storms will all bring more precipitation to the study area, while the southerly storm case showed somewhat mixed results. In 2008 storm case, more precipitation occurred within the larger domains, and less in the smallest domain, covering a slightly larger area than Estonian territory (Table 6). As the atmospheric

temperature will increase by 2-3 degrees by that time (~2090; Fig. 28 and 29), the majority of precipitation would be in liquid form, not in snow.

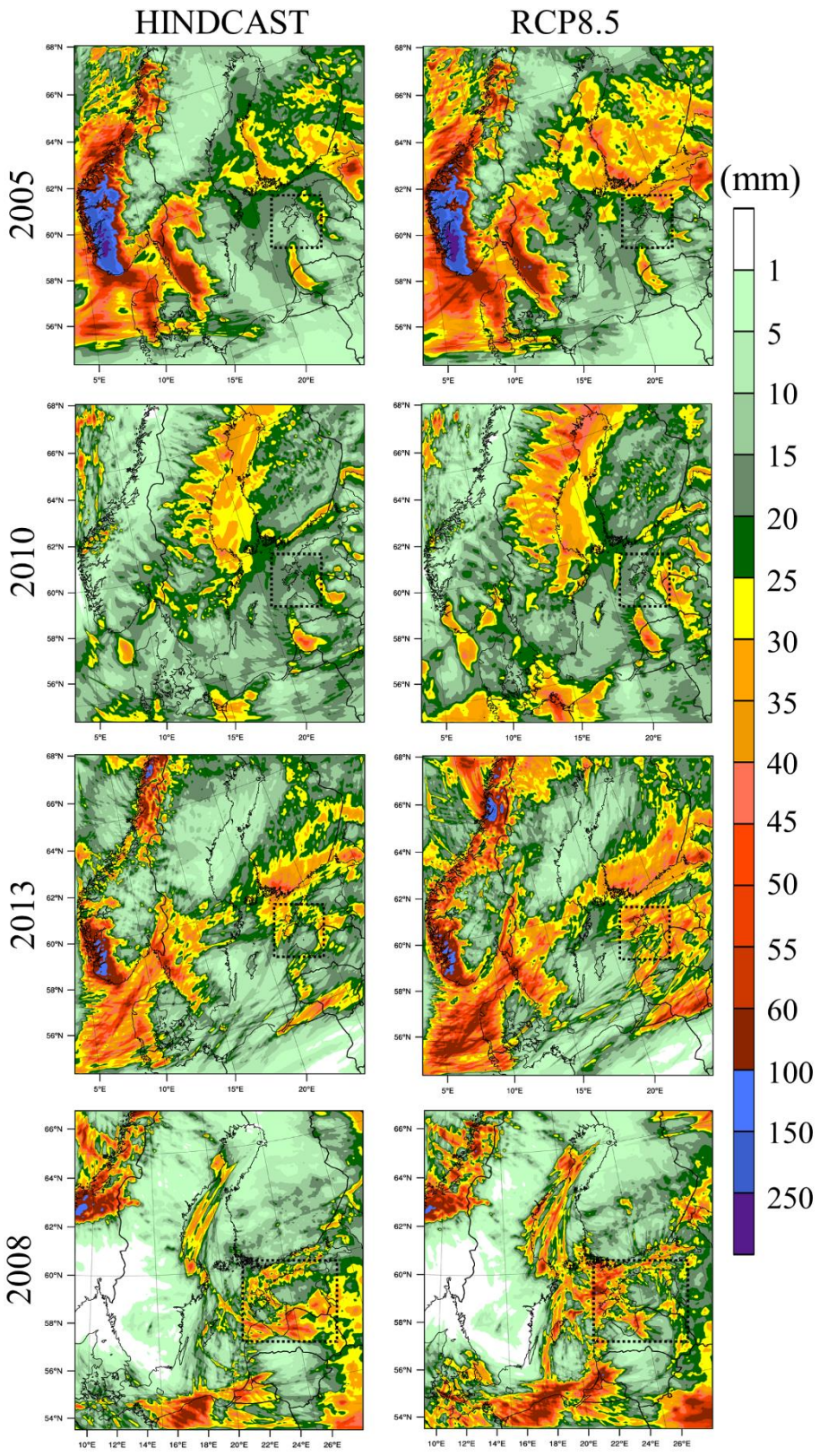

Figure 42. Total precipitations spatial distribution comparisons of hindcast and RCP8.5 scenarios over WRF domain 2. The dashed bounding boxes show the location of WRF d03.

5.6 Metocean results for Arctic Storm

5.6.1 Arctic Ocean

In the Arctic Ocean, the sea state climate is rapidly changing due to fast yearly decrease of seasonal sea ice extent. September months have the lowest extent, and according to data provided by the NSDIC (Fetterer et al. 2017), the September ice retreat is 82 300 km^2 / year. Much of the Beaufort Sea is open to relatively large fetch (up to 1000 km) at the end of summer. And by 2050 the entire is projected to show ice-free summer months (or at very least, September month). However, this massive decrease of seasonally land locked sea ice coverage will likely reshape the coastal areas of Arctic basin. The relatively fetch limited wind sea could in the future also exhibit changes not only from local wind, but also wind swell generated far away in the Arctic Ocean. Arctic region is mostly dominated by diverse climatic conditions, where clusters of high pressure systems dominate the region and low pressure systems fill the in-betweens (Fig. 33).

Under future climate conditions however no notable change is observed under any RCP scenario (Fig. 43). Slight changes in wind pattern and pressure fields can be seen, however not that could potentially invoke more extreme climate conditions. It could be that the thermal dynamics changed under the 2050 conditions and lack of sea ice is not enough to invoke more applicable shifts and departures from the hindcast study. Furthermore, it is highly likely that polar system in the future could be more affected by the various teleconnections that are currently out of the scope of this study.

As for significant wave height fields, it can be seen that by using the 1999 September storm as a study period, relatively high wave fields occur along the Canadian Beaufort coastline. The coastal water depths in the area are relatively shallow (5-50 m), however around ~4 m waves are generated. One of the main reasons for this is suitable wind direction and long fetch (especially for the Hindcast study with the presence of sea ice, forming almost like a funnel type of conditions). In contrast however, the rest of the Arctic Ocean under future scenarios are relatively calm, which can be well explained by the wind a pressure fields of the area (Fig. 44). The relatively calm wind fields and various opposing direction, and throughs do not enable for the creation of any high wave fields. However, if a strong storm system was to cross the central Arctic Ocean or follow any of the coastlines where seaward wind fields would dominate, the high wave fields could possibly occur over a large area in the Arctic Ocean and create high energy swell waves along the opposing coastlines.

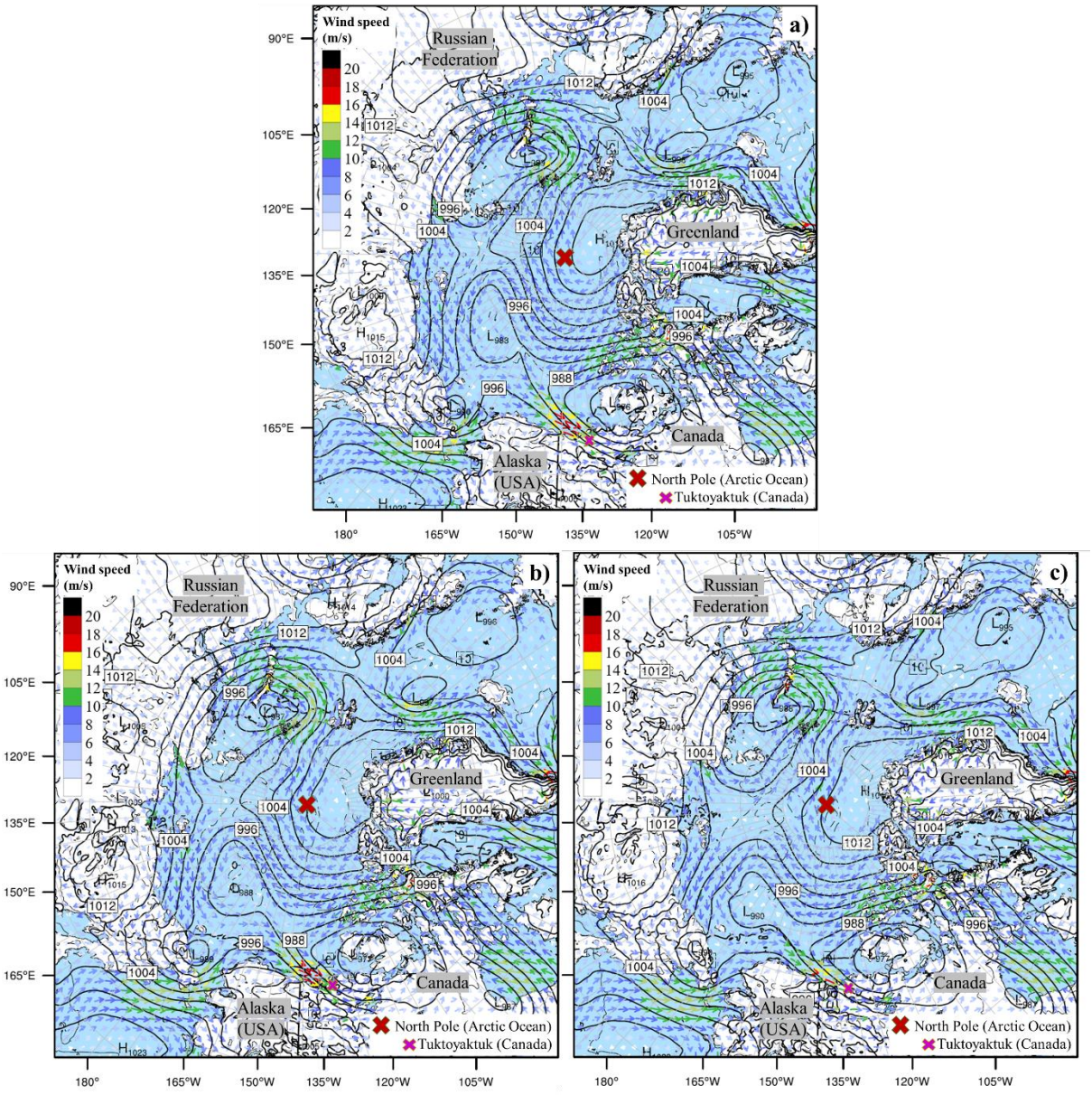

Figure 43. Regional look at Polar WRF wind and pressure field modelling results over the modelling domain 1 (parent domain; 20 km resolution) for hindcast (a) and future (b is RCP4.5; c is RCP8.5) scenarios at 25 September 10:00 UTC.

The currently main limitation of the wide area study is the lack of observational data to confirm or reject the accuracy of the simulation results. While the models used themselves are validated by numerous studies in the past, it is still highly necessary to confirm modelling results with observational data. In future studies however, it would be desirable to investigate a number of storm system that cross the central Arctic Ocean and/or the storm winds would follow the seaward direction from nearshore systems. However, currently the main issue in determining the occurrence of such storms is restricted to the afore mentioned lack of observational data. A plausible workaround would be to employ other modelled hindcast

studies, however in that case looking at thermal changes could be more difficult since the vertical structure of such datasets might be too limiting for proper dynamical changes and development of future storm studies.

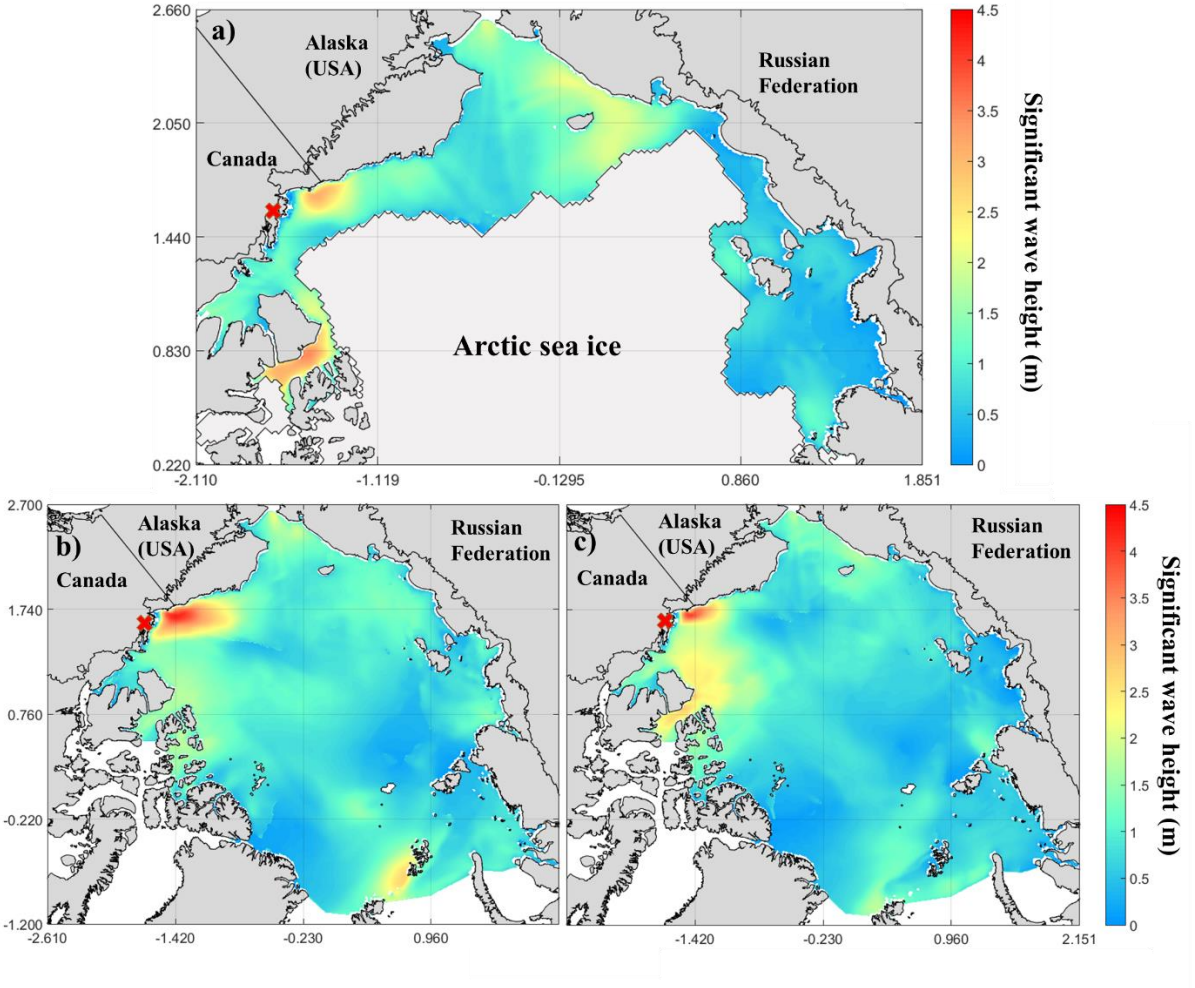

Figure 44. Hindcast (a) and future 2050 RCP (b is RCP4.5; c is RCP8.5) significant wave height spatial distributions in the Arctic Ocean at 25 September 10:00 UTC. Hindcast results were conducted with the consideration of Arctic sea ice. The red X marks the location of Canadian port hamlet Tuktoyaktuk. The scalebar is in meters "x 10^6", where the reference longitude is at 0° and latitude at 90° (North Pole).

5.6.2 Canadian Beaufort

In the 1999 Arctic storm, the weather station data from Tuktoyaktuk showed that the wind speed values stayed rather streamlined at 13 ms^{-1}, instead of forming a specific peak as was seen for the stronger North Atlantic storms (Gudrun and St. Jude). The wind direction was dominantly from 270-300 degree sector, which considering the Kugmallit Bay configuration is suitable for potential surge in the bay and thus in Tuktoyaktuk. The PWRF modelling results showed a good fit with the Tuktoyaktuk measurements, however more significant deviations can be seen at the early stages of the simulation results (Fig. 45) for wind direction and speed. As for future scenario simulations, no increase in the local wind speed was observed, in general these results seem to exhibit same randomness as for the 2010 Xynthia case, where it the weaker fields are not as streamlined as the strongest ETC cases, and deviations especially near the land-sea interface are more easily to occur.

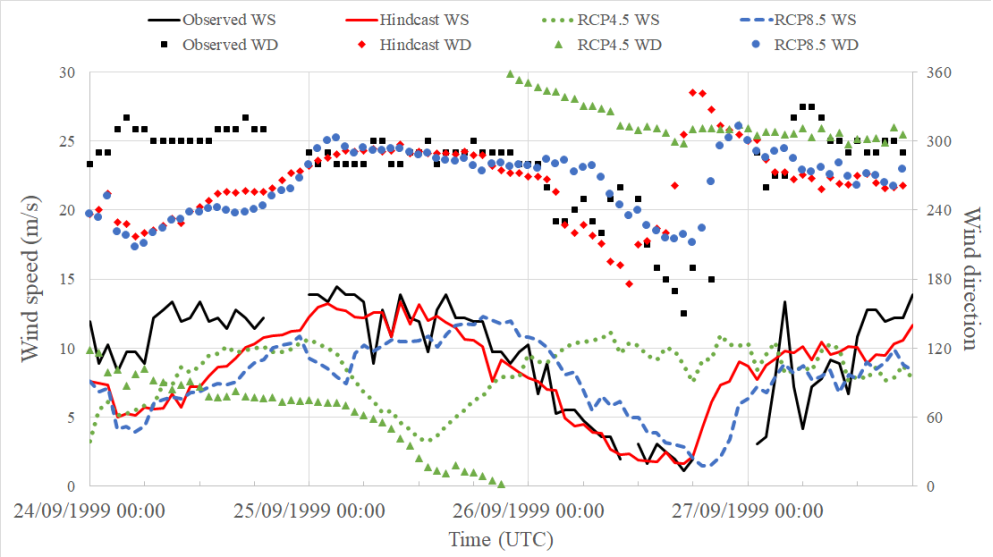

Figure 45. Wind speed and direction modelling results for the 1999 Arctic storms, including hindcast and future scenarios.

The FVCOM-SWAVE simulations were conducted for both hindcast and RCP scenarios. In the vicinity of Tuktoyaktuk the surge and significant wave height were rather modest compared to that of MSBC hindcast results (which suggested 2.13m surge and 1.9 m Hs). The maximum modelled surges were 0.47, 0.47 and 0.48 for hindcast, RCP4.5 and RCP8.5, respectively (Fig. 46). Even when considering the recent years tidal effect (0.2-0.7 m; no historical 1999 data available) as an assumption, then the current simulations would not reach the 2.13m mark set by the MSBC hindcast. Similar to surge results, the significant wave height peaks are severely underestimated against the MSBC hindcast. The modelled

values near Tuktoyaktuk are 0.89, 0.63 and 0.57 m for hindcast, RCP4.5 and RCP8.5, respectively. However, since MSBC is a model product, these results are not desirable to compare current modelling results against, but in this study served more as guidelines to determine extreme events in Tuktoyaktuk. Furthermore, Tuktoyaktuk and Canadian Beaufort in general exhibits highly complex coastal features (peninsulas, small islands), therefore it is presumed that by using high resolution bathymetry and coastline data, the results could improve. But even so, it would be impossible to truly verify any simulation results in Tuktoyaktuk for this particular case study.

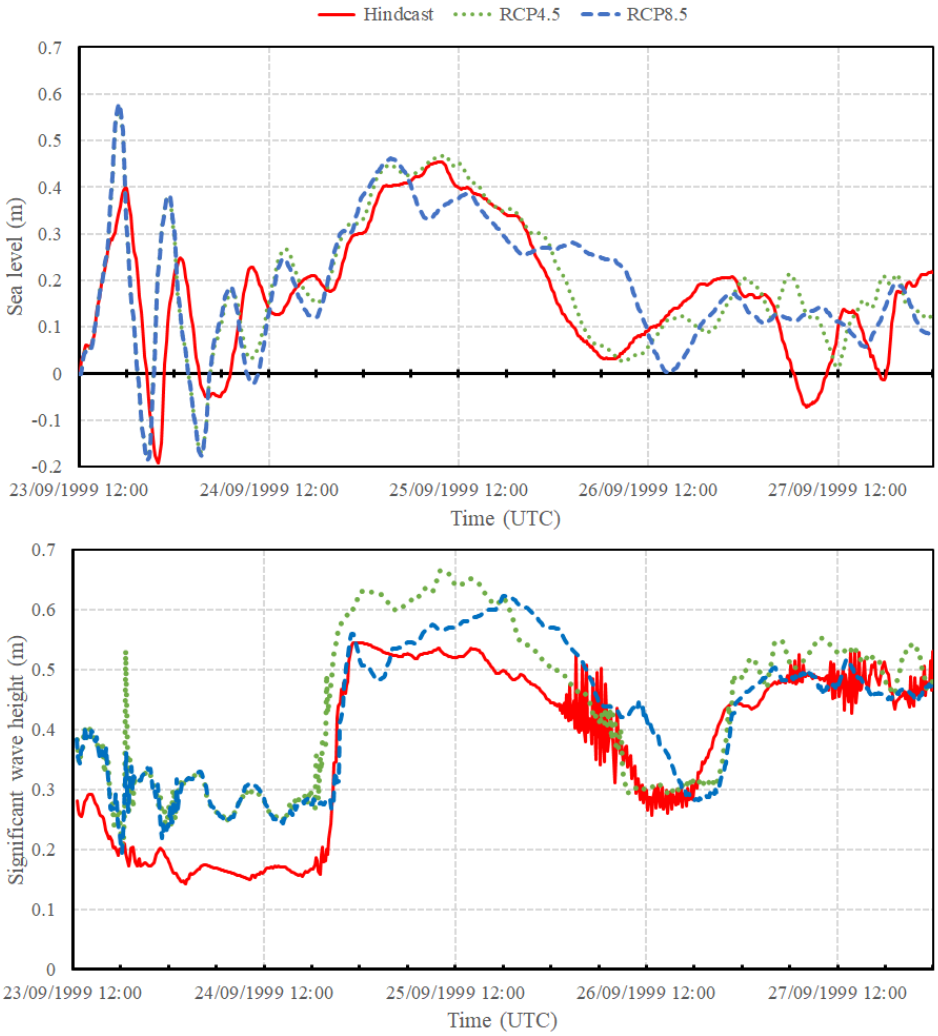

Figure 46. Storm surge and significant wave height simulation results in the vicinity of Tuktoyaktuk. Both surge and Hs values were picked from the same node.

In addition to local simulation results, results were analysed for the Canadian Beaufort as well (Figs. 47, 48). All the simulated storms followed the same route and minimum pressure levels at the cyclone core (975 hPa) did not change either. However, there

are temporal shifts in the wind field intensity, where the RCP4.5 stands out the most in contrast to hindcast and RCP8.5 timestamps. The storms followed the same path, however did not get any stronger and it is difficult to quantify whether they stayed the same or actually weakened. Based on the Tuktoyaktuk data and statistical analysis (Fig. 45, Appendix 6), it can be said that significant changes between hindcast and future scenarios occurred. By visual comparison, the largest change was RCP4.5, which did not follow the same wind pattern as hindcast and RCP8.5

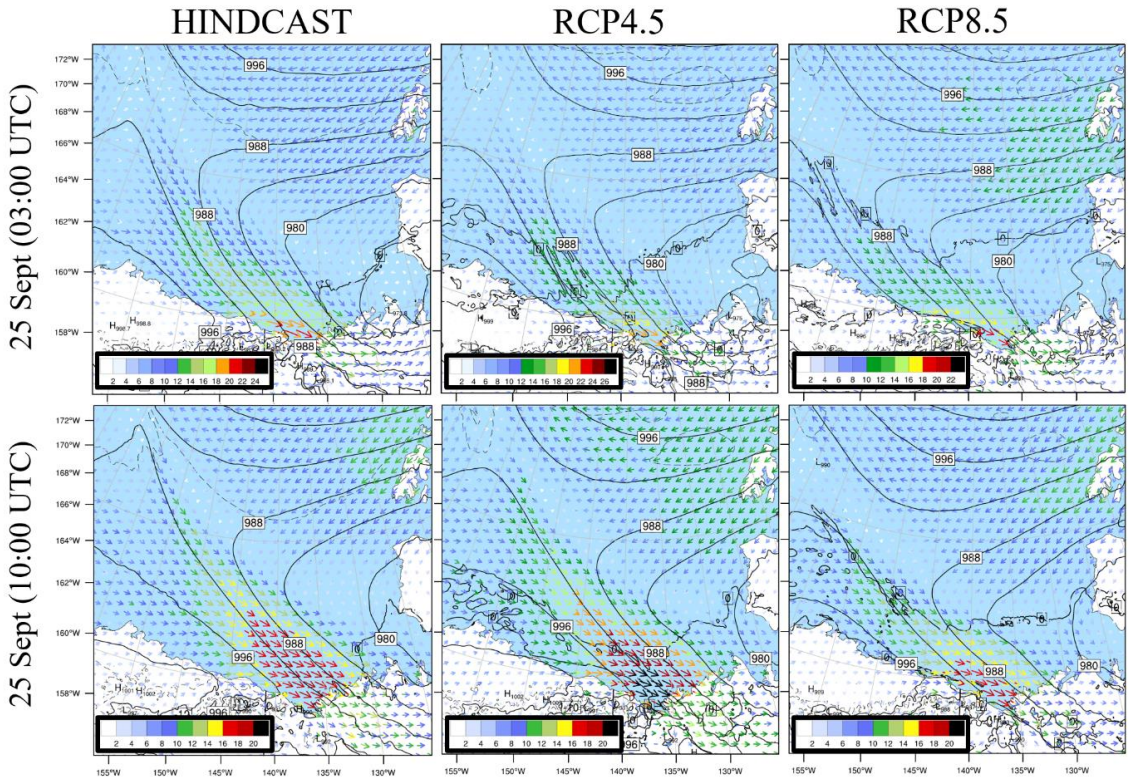

Figure 47. Wind and MSLP fields over PWRF d02 for hindcast and RCP simulations.

These spatial wind field differences also translated into the significant wave height simulation (Fig. 48), where the highest wave heights are at the Mackenzie Delta area. However surprisingly, during the same investigated timesteps the highest wave fields occurred under hindcast simulation with the presence of sea ice. This is mainly explained by the direction of the wind, comes from the open waters between the sea ice edge and land. Since during this storm the prevailing winds are from NW and concentrated near the land boundary then these results are expected.

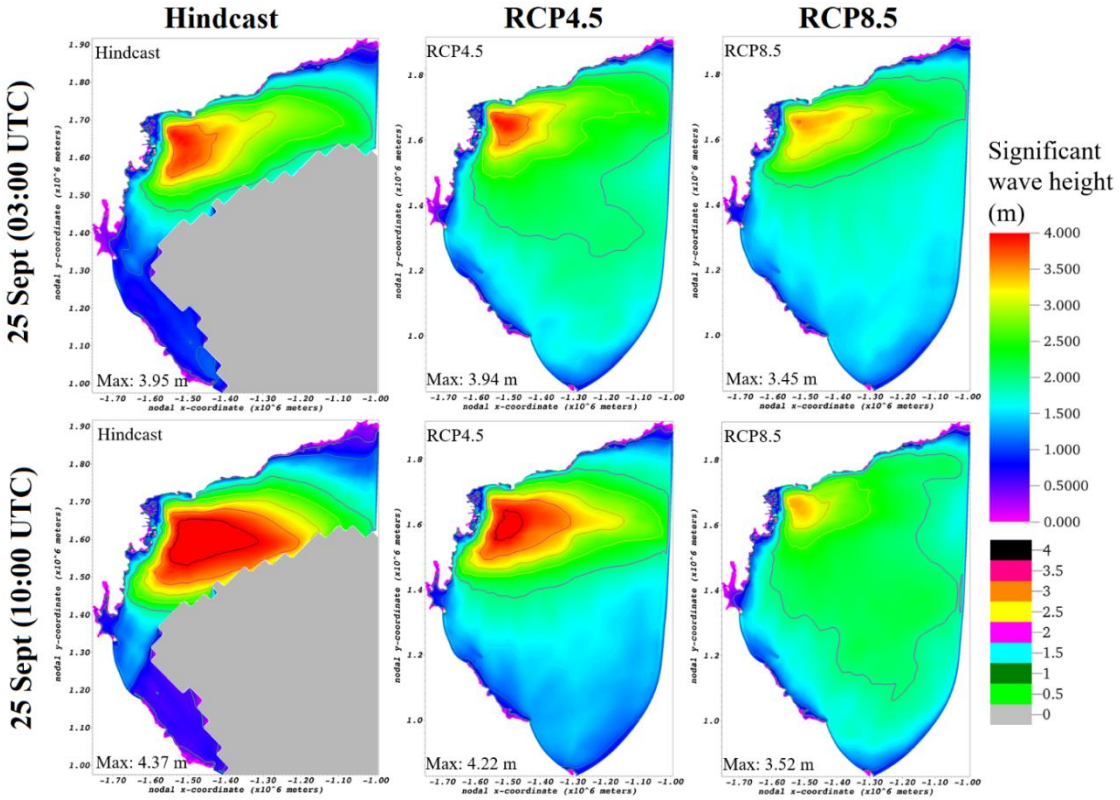

Figure 48. Significant wave height simulation results for hindcast and RCP simulations. In the hindcast simulations, the grey area marks the extent of the sea ice.

6 Discussion

6.1 Modelling accuracy

The current study highlighted the importance of the initial and boundary conditions quality used for such modelling approach. The study by Mäll et al. (2017) employed quite similar calculation conditions as Nakamura et al. (2016) used for the 2013 tropical cyclone Haiyan. There, the results showed notable increase in storm intensity, whereas for a strong ETC (2005 Gudrun), no changes were captured. This indicated that one course calculation setup might be sufficient for capturing changes in tropical cyclones, but more resolved atmospheric calculation conditions are necessary to capture changes in ETCs. The most notable improvements in this study, compared to the previous one, which led to the different results, were: 1) higher resolution meteorological data (CFSR vs. FNL), 2) larger simulation domains, 3) more meteorological grid levels (38 vs 27), 4) more vertical layers (61 vs 30 layers), 5) increased pressure top (1 hPa vs 50 hPa), 6) increased horizontal resolutions (20 vs 22.5 km; parent grid/time-step ratio: 5), 7) number of CMIP5 GCMs (14 vs 1), 8) surge model (FVCOM-SWAVE vs FVCOM) and 9) inclusion of wave model SWAN for the entire Baltic Sea.

For many stations and parameters, the hindcast seems to require improvement to more accurately reflect observations. However, it also seems that for several events (St. Jude, Gudrun) a re-analysis of hindcast peak data against observations may be useful, as the storm signal is strongest in this sample segment. For both strong (Gudrun, St. Jude) and weaker (Xynthia) storm events it can be observed that Ruhnu and Kihnu tend to experience wind fields in terms of wind speed and direction similarly, both in hindcasts, as well as the RCP scenarios. This is likely due to the physical proximity between the stations.

For Arctic simulation the largest concern is still the data availability. Whether in the form of in-situ measurements from the stations or topography and bathymetry high resolution data for accurate numerical modelling. Even though, for example, the Beaufort MSC hindcast data has been thoroughly validated against all the available measurements, it still a secondary source data (i.e. computed). In case there is a real concern or need for extremely localized model validation, it would be then beneficial to conduct on-site measurements to collect such data. However, it should be also noted that it might be possible to gather such data, or at very least more precise measurement (especially bathymetry/topography and coastline profiles) through some other institutions (e.g. Geological Survey of Canada).

6.2 Limitations

Storm surges and significant wave heights under future climates relative to present time mean sea level were studied. However, it is necessary to assess the likely global scenarios for mean sea level rise (SLR) and acceleration (SLA), and their combined effect on sea level during an ETC. Although both SLR and SLA in the Baltic Sea may deviate from the global ones as a result of meteorological factors (Jaagus and Suursaar, 2013; Johansson and Kahma 2016), steric effects and spatially varying influence of land uplift (Kall et al. 2016), their influence is much smaller than that of the expected global SLR. Combining the median values of the IPCC AR5 proposed global SLR by 2100 (0.48 m for RCP4.5 and 0.63 m for RCP8.5) with the Gudrun-time surge heights, we obtain 3.12 and 3.27 m for 2100RCP4.5 and 2100RCP8.5, respectively. These estimates are indicative only for several reasons. As a result of sea level rise, also morphometric features of the basin (depth, coastline) and thus, hydrodynamic conditions will change, which would lead to certain (presumably small) differences in storm surge calculations.

The present study did not try to find out what the physically possible highest sea levels at Pärnu are. Quite often, recurrence statistics of high sea level are computed and extrapolated to certain longer periods. Maximum value analysis of such events is of crucial importance for Pärnu, as is vulnerability analysis. However, as it was shown earlier (Fig. 8; Suursaar and Sooäär 2007), the approach is problematic in the Pärnu case. One problem is that the existing bulk of the sea level measurement data does not carry sufficient statistical information about possible extreme sea level values at Pärnu, where the return-graph (Fig. 8) is similar to a graph for sea level data that includes abnormal tsunami events. High sea levels in Pärnu for 1:5, 1:10, 1:50 and 1:100 year return periods can be estimated to be 1.65, 1.77, 1.9 and 2.0 m, respectively, if the two highest events in the record (storms in 1967 and 2005) are excluded. Thus, while return statistics of moderately high events can be estimated from the corresponding graphs, and even extrapolation to e.g. 100 or 200 years is possible, then the parameters of the truly highest events are still statistically unpredictable. Probability for an outstanding Pärnu storm surge therefore appears as a product of probabilities of the two events: a strong cyclone with a suitable track, and a high background sea level. Soomere et al. (2015) separated the Pärnu sea level record into two components, describing slowly changing variations of the Baltic water volume surplus, and meteorologically forced fast movements. Still, the statistical prediction of such combined events seemed to be problematic and these must be evaluated using numerical modelling.

The capacity of changes in individual, possibly the strongest storms was studied. The work did not deal with general storminess and with the question of whether there will be a larger number of ordinary storms in Northern Europe? Several parameters of storm track activity and wind statistics have changed over the last decades, and will change in the future (Christensen et al. 2015). Separately from developments in the most extreme events, the storms of moderate strengths may get more frequent or even more powerful in the moderate and high latitudes (Lambert and Fyfe 2006). According to a literature review conducted by Bader et al. (2011) the most agreed upon result is that observations and future projections of the mid-latitude storms are exhibiting a poleward shift, especially in Southern Hemisphere. With lesser certainty the same extent in shift applies in the Northern Hemisphere (Christensen et al. 2015).

6.3 Potential implications and future outlook

The results of the present study indicate that under applied conditions and methodology (which inevitably includes some modelling simplifications and omissions), the ETCs of future climates might not get much stronger in Northern Europe. The reason may lay behind the formation and development mechanisms of ETCs. Interestingly, studies applying the same methodology for tropical cyclones (Tasnim et al. 2015; Nakamura et al. 2016) have shown clear intensification of future storms (tropical cyclones, hurricanes). These tropical low pressure systems derive their energy from warm water evaporation and increased SST enhances their strength. However, ETCs usually form as perturbations of the polar front and harvest their energy from temperature gradient at the front where cold and warm air masses interact (e.g. Mizuta et al. 2011). According to a number of projections, the differences on the sides of the polar front may decrease as the Arctic warms up (Lambert and Fyfe 2006; Pinto et al. 2007). As the difference in atmospheric air temperatures between poles and tropics decrease, the energy available for the ETCs decreases.

The current study showed that although no notable changes took place in minimum atmospheric pressure values within the ETCs of the future, the low pressure area was somewhat larger and the strong wind zone was extending further south with slightly higher peak wind speeds, especially in the case of RCP8.5. This, in turn, yielded a slight (3-18 cm) surge height increase at Pärnu under RCP4.5 scenario, and a more pronounced (22-59 cm) surge increase under RCP8.5 scenario. The different results this time (compared to Mäll et al., 2017) were obtained due to a more advanced modelling system, and due to use of multi-

model ensemble of 14 GCMs as opposed to a single GCM model in the previous study. It is difficult to estimate the uncertainty degree in one model simulation. In multi-model approach it is virtually impossible to decide which one of the models is the "right one", either. However, some guidance can be gained considering the scatter within the applied GCMs (Fig. 22 and Table 3).

Surge height increase occurred already in RCP4.5, but it was small, and against model scatter (Table 4), insignificant. The surge increase under RCP8.5, however, was more substantial (Table 4). A small increase in wave heights was also projected. Although the RCP8.5 future scenario is usually considered rather steep (i.e. pessimistic), it still shows that ETC-related storm surges can increase under warmer climates just like in the case of tropical cyclones (e.g. Nakamura et al. 2016). Perhaps, even if the pressure gradients at the polar front will not increase in the future due to warm-up of the polar regions (as suggested e.g. by Harvey et al. 2014), the increased global temperature (IPCC 2014) may still give growth to ETCs. However, this study presented the simulation results, but is not able to point on exact underlying processes in atmosphere physics.

Precipitation changes showed that westerly approaching storms will bring more precipitation to the Baltic Sea area in the (warmer) future (Table 6). In case of southerly cyclones the results were more mixed, but some increase could be expected there, too. Considering the results of four different storm cases, it is plausible that the extreme ETCs, could become more severe and dangerous, at least under the most extreme emission scenario RCP8.5. Storms passing the Scandinavian mountains leave more precipitation there through orographic enhancement. Storm surge and increased fluvial risks as a result of increased precipitation can magnify each other impact on low-lying coastal communities locating in the river mouth areas (e.g. in the Pärnu city; Tõnisson et al. 2019).

Overall, it can be observed that larger storms are experienced similarly across the whole measurement area and also change similarly over the measurement area under different RCP scenario conditions (St. Jude and Gudrun). Weaker storms such as Xynthia however display more spatially varied changes in storm parameter behaviour over their impact area as conditions change. From an engineering perspective, this may suggest that for strong storm events, we can expect changes in protection requirements to change similarly across Baltic communities in future conditions. For weaker storms however, it may be necessary to assess various areas individually for how they will react to changed future conditions of the storm

event occurring. For local response to potentially more extreme storm surge events at Pärnu Bay and city, the strategies can vary and as of the time of writing this work (2019), it seems that long-term soft measures are preferred over hard measure defences. A study by Tõnission et al. (2019) compiled the current responses and adaptation strategies more preferred (Fig. 49). While Pärnu city in Estonia, is one of the most vulnerable locations to storm surges, the future preparedness for extreme surge events seems to rely more on the spatial planning of new buildings and changing regulations. If these are however expected not to be sufficient prior to an impactful event, evacuation alarms and managed retreat during such an event seem to be next step in management and subsequent response during such an event. While hard measures offer more reassurance for local citizens, they also come with heavy financial and aesthetical considerations. The Pärnu city is relatively spread out and population density is not that high, especially during winter months when the winterstorms are the most intense and frequent, while during summer the coastal city acts a resort area with considerable increase in tourism. In that regard, having high concrete coastal defences could potentially have a negative impact for the area. Furthermore, as seen for the historical storm surge measurement in the area, the water levels rarely breach the 160 cm critical mark. The 2005 Gudrun with 275 cm surge was truly and outlier, however such event, in theory, could still occur at any time (however improbable). The current study found that such an event under future conditions could reach surges as high as 300 cm (the study did not consider the precipitation effect on local surge levels, which further increase the inundation height). While extremely high surge could feasible occur in the future, from the socio-economic impact it still worthwhile pursuing and developing city specific smart solutions, by raising the elevations of building ground floors in consideration to geospatial hazard potential, updating warning systems and have localized evacuation plans set with possible including a number of high ground evacuation spots (either public spaces or dedicated buildings; especially necessary for areas with older building that do not meet new construction regulations.

In the Arctic the threats are however more immediate. During summer period, the Arctic storms are not particularly strong, however if the coastal waters will have gradually longer periods of sea ice free months, then that will further increase the open water season in spring and autumn. In return this would leave the areas open for potential storm waves and surges, that will further accelerate erosion processes and cause irreversible damage to ecosystems in the coastal regions. Currently the hamlet of Tuktoyaktuk is already experiencing heavy erosions every year. While various makeshift protective measure have

been implemented over the years, they tend be destroyed with the next larger storm event. Currently it seems that it is economically too expensive to bolster the Tuktoyaktuk coastline with hard defences (mainly because of the remote area and long coastline that would need to be covered). Managed retreat is currently already happening, where the near coast homes need to be abandoned and people need to more towards inland. From coastal engineering and management perspective, Tuktoyaktuk is truly a challenging case. In this area, smart solutions are not truly viable solutions as surge itself is not the largest issue, but rather the gradual loss of coastline. Simply put, Tuktoyaktuk has two options: 1) get substantial government or other funding to build coastal defences or 2) retreat towards higher ground inland (this is currently already happening). However even if wide range of coastal defences against waves are implemented, the area is still experiencing relative sea level rise. For a low-lying area, this is will present future engineering complications and funding necessities in the area. A specific study is necessary for Tuktoyaktuk that looks various combinations of adaption measures and their potential lifetime, project costs, maintenance costs with on-site feasibility, and what range of future emerging threats would be covered.

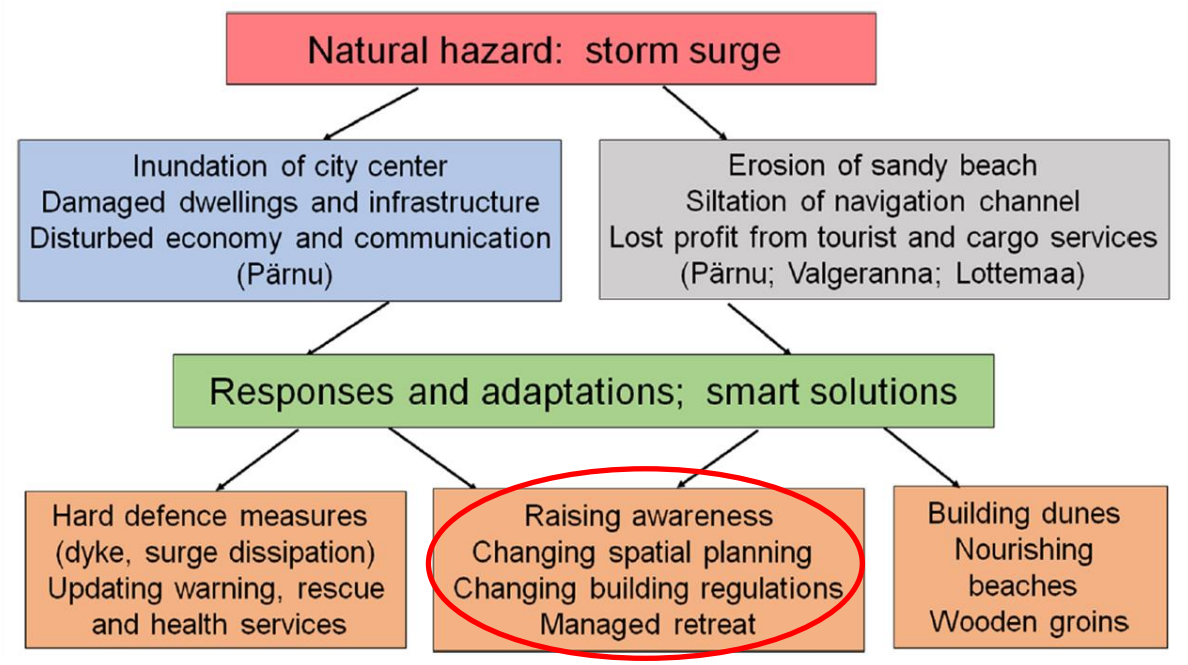

Figure 49. Conceptual model of Pärnu Bay study area. Grey boxes – problems related to erosion and siltation, Blue boxes – inundation problems, Brown boxes – the most suitable response (after Tõnisson et al. 2018).

7 Conclusion

In order to estimate the possible parameters of future ETCs, a pseudo climate modelling study of four historic storms was performed using multi-model approach and considering the 21st centuries RCP4.5 and RCP8.5 emissions scenarios. The changes in cyclone parameters under future (2081-2100 avg. minus 2006-2015 avg. interpolated to reanalysis data) conditions in relation to hindcasted (present; NCEP CFSR/v2) conditions were calculated using WRF model, whereas FVCOM-SWAVE and SWAN models were used for estimating future storm surges at Pärnu (Estonia) and wave fields within the Baltic Sea, respectively. Furthermore, polar-optimized WRF (PWRF) and FVCOM-SWAVE model were applied for Arctic extreme storm studies, within the Canadian Beaufort Sea and Tuktoyaktuk.

Although all the studied storms occurred during different thermal conditions (months) and responses somewhat varied, depending on the storm and the scenario, it was possible to draw some general conclusions. As there was a high variability among the individual GCM models (14 CMIP5 models), it was necessary to use multi-model ensemble approach and not to rely on a single model. Compared to RCP4.5, the RCP8.5 scenario yielded much more pronounced future changes in virtually every aspect. The increase in domain-average weighed RCP4.5 and RCP8.5 were roughly 2°K vs. 4°K correspondingly (with mixed results in terms of humidity). Regarding precipitation changes during cyclonic storms, the RCP4.5 scenario showed mostly increasing but small tendencies, ranging between -6 and +10% and depending on storm case and studied domain tier. Under RCP8.5, the total precipitation during the Atlantic storms increased ~7% over the wider domain. The precipitation amount increased 12-18% over the Baltic Sea domain and 13-23% over western Estonia. Although during the 2008 (southerly) storm the results were somewhat mixed, some overall increase in precipitation could be still expected there, whereas the westerly approaching ETCs will very likely bring much more precipitation to the Baltic Sea area in the (warmer) future.

No notable changes took place in minimum atmospheric pressure values within the ETCs of the future, but the low pressure area was somewhat larger and the strong wind zone was extending further south with slightly elevated peak wind speeds. There were little to no changes in peak wind speeds under the RCP4.5 scenario, however changes occurred under RCP8.5 scenario. This, in turn, yielded a small surge height increase at Pärnu under RCP4.5, but significant, up to 22-59 cm surge increase under RCP8.5 simulations. Besides wind speed increment, this large surge increase could occur due to peak wind zone shift to better satisfy

the optimum exposure conditions of Pärnu Bay. Under RCP8.5 scenario, an (insignificant) increase in maximum wave heights during extreme storms occurred. Along with the strong wind area spread from the cyclone core, also the higher wave areas extended further south and over larger sea areas. This, in turn, can also lead to increased hazards through wind damage and wave attacks along more extensive coastal stretches in the Baltic Proper.

In the Arctic study domain the hindcast results showed relatively good results for wind. However, based on only available surge and wave (MSCB hindcast model) data in the area, the current studies results were severely different (underestimated). However, since no observational data during the simulation period was available for sea state parameters, then it difficult to assess how much the current results underestimated the results. The future simulations (2050 RCP4.5/RCP8.5) showed highly mixed results compared to hindcast, especially for the RCP4.5 which did not follow the expected wind patterns. No future scenario caused any higher notable surge or significant wave height conditions in the Kugmallit Bay (where Tuktoyaktuk is situated). Canadian Beaufort Sea simulations with or without sea ice presence did not yield in any significant wave height changes either. Likely because of prevailing storm wind during sea-ice-present hindcast were from NW direction, which was open water between and land sea ice, allowing the development of a long fetch for generation of constant high waves. As for the entire Arctic Ocean results, the maximum wave fields were still near the vicinity of Tuktoyaktuk, due to the storm driven wave fields. However, the effective fetch under ice-free Arctic Ocean is many times larger than with the ice. Therefore, if storm systems were to pass over the ocean or coastal areas seaward prevailing winds, they could generate larger higher wave fields and energy dense swell waves. Potentially accelerating coastal erosion and/or influencing the people trying to operate in the future Arctic. For adaptation strategies soft and smart solutions are preferred in Pärnu (Estonia), whereas hard measures would likely be more effective in Tuktoyaktuk (Canada).

In general, for hindcasting, as well as for future scenarios (RCP8.5 mainly) the wind fields seem to be better captured and noticeable change in peak wind could be observed for the strongest storm cases (e.g. 2005 Gudrun, 2013 St. Jude). Weaker storms exhibited little response in terms of intensity under all scenarios. Furthermore, the hindcast for these weaker synoptic flows were also mixed results. However, even if the steep RCP8.5 future scenario is usually considered as unrealistic, it still shows that the extreme ETCs could become more dangerous in case of substantial climate warming, and the related storm surges can increase similar to tropical cyclones, however with higher uncertainty.

8 References

Akpınar, A., Van Vledder, G., Kömürcü, M. İ., & Özger, M. (2012). Evaluation of the numerical wave model (SWAN) for wave simulation in the Black Sea. Continental Shelf Research, 50–51, 80–99.

Alexandersson, H., Schmith, T., Iden, K., Tuomenvirta, H. (1998). Long-term variations of the storm climate over NW Europe. The Global Atmosphere and Ocean System, 6(2), 97–120.

Arkhipkin V.S., Gippius F.N., Koltermann K.P., & Surkova G.V. (2014). Wind waves in the Black Sea: results of a hindcast study. Natural Hazards and Earth System Science, Copernicus Gesellschaften (Germany), T. 14, № 11, pp. 2883-2897.

Averkiev, A.S. & Klevannyy K.A. (2010). A case study of the impact of cyclonic trajectories on sea-level extremes in the Gulf of Finland. Continental Shelf Research, 30(6), 707–714. https://doi.org/10.1016/j.csr.2009.10.010.

BACC (2015) In: The BACC II Author Team (ed) Second assessment of climate change for the Baltic Sea Basin. Reg Clim St. Springer, p 501.

Bader, J., Mesquita, M.D.S., Hodges, K.I., Keenlyside, N., Østerhus, S., & Miles, M. (2011). A review on Northern Hemisphere sea-ice, storminess and the North Atlantic Oscillation: Observations and projected changes. Atmospheric Research, 101(4), 809–834. https://doi.org/10.1016/j.atmosres.2011.04.007.

Barnston, A.G., & Livezey, R.E. (1987). Classification, seasonality and persistence of low-frequency atmospheric circulation patterns. Monthly Weather Review, 115, 1083–1126. https://doi.org/10.1175/1520-0493(1987)115<1083:CSAPOL>2.0.CO;2.

Berkman, P.A., & Young, O.R. (2009). Governance and Environmental Change in the Arctic Ocean. Science, 324(5925), 339 LP – 340.

Bertin, X., Bruneau, N., Breilh, J.F., Fortunato, A.B., & Karpytchev, M. (2012). Importance of wave age and resonance in storm surges: the case Xynthia, Bay of Biscay. Ocean Model 42, 16-30.

Björkqvist, J.-V., Lukas, I., Alari, V., van Vledder, G., Hulst, S., Pettersson, H., Behrens, A., & Männik, A. (2018). Comparing a 41-year model hindcast with decades of wave measurements from the Baltic Sea. Ocean Engineering, 152, 57−71.

Booij, N., Ris, R.C., & Holthuijsen, L.H. (1999). A third-generation wave model for coastal regions: 1. Model description and validation. Journal of Geophysical Research, 104 (C4), 7649-7666. https://doi.org/10.1029/98JC02622.

Booij, N., Haagsma, I.J.G., Holthuijsen, L.H., Kieftenburg, A.T.M.M., Ris, R.C., van der Westhuysen, A.J., & Zijlema, M. (2004). SWAN Cycle III version 40.51 User Manual. Delft University of Technology. http://fluidmechanics. tudelft.nl/swan/index.htm.

Britannica. (2017). Tuktoyaktuk. https://www.britannica.com/place/Tuktoyaktuk (Accessed 10 September 2019).

Britannica. (2019). Beaufort Sea. https://www.britannica.com/place/Beaufort-Sea (Accessed 10 September 2019).

Barnes C.A., LaMourie M.J, and Others. (2019). Atlantic Ocean. Encyclopaedia Britannica. Internet link: https://www.britannica.com/place/Atlantic-Ocean/Climate (Accessed 09 September 2019).

Bromwich, D.H., Hines K.M., & Bai, L.-S. (2009). Developments and testing of Polar Weather Research and Forecasting model: 2. Arctic Ocean. Journal of Geophysical Research, 114, D08122, doi:10.1029/2008JD010300.

Campos, C., & Horn, M. (2018). YOUMARES 8 – Oceans Across Boundaries: Learning from each other. YOUMARES 8 – Oceans Across Boundaries: Learning from Each Other. https://doi.org/10.1007/978-3-319-93284-2.

Carpenter, G. (2005). Windstorm Erwin/ Gudrun – January 2005. Specialty Practice Briefing 2. http://www.dmi.dk/fileadmin/user_upload/2005-nyheder/8januarstormguycarprapport.pdf.

Cayan, D.R. (1992). Latent and sensible heat-flux anomalies over the northern oceans — the connection to monthly atmospheric circulation. Journal of Climate, 17, 354–369.

Chen, C., Liu, H., & Beardsley, R.C. (2003). An unstructured grid, finite-volume, three-dimensional, primitive equations ocean model: application to coastal ocean and estuaries. Journal of Atmospheric and Oceanic Technology, 20 (1),159–186.

Christensen, O.B., Kjellström, E., & Zorita, E. (2015). Projected change – atmosphere. In: The BACC II Author Team (ed) Second assessment of climate change for the Baltic Sea Basin. Springer, Cham, pp. 217–233.

Church, J.A., P.U. Clark, A. Cazenave, J.M. Gregory, S. Jevrejeva, A. Levermann, M.A. Merrifield, G.A. Milne, R.S. Nerem, P.D. Nunn, A.J. Payne, W.T. Pfeffer, D. Stammer and A.S. Unnikrishnan, 2013a. Sea Level Change. In: Climate Change 2013: The Physical Science Basis. Contribution of Working Group I to the Fifth Assessment Report of the Intergovernmental Panel on Climate Change [Stocker, T.F., D. Qin, G.-K. Plattner, M. Tignor, S.K. Allen, J. Boschung, A. Nauels, Y. Xia, V. Bex and P.M. Midgley (eds.)]. Cambridge University Press, Cambridge, United Kingdom and New York, NY, USA.

Church, J.A., P.U. Clark, A. Cazenave, J.M. Gregory, S. Jevrejeva, A. Levermann, M.A. Merrifield, G.A. Milne, R.S. Nerem, P.D. Nunn, A.J. Payne, W.T. Pfeffer, D. Stammer and A.S. Unnikrishnan, 2013b. Sea Level Change Supplementary Material. In: Climate Change 2013: The Physical Science Basis. Contribution of Working Group I to the Fifth Assessment Report of the Intergovernmental Panel on Climate Change [Stocker, T.F., D. Qin, G.-K. Plattner, M. Tignor, S.K. Allen, J. Boschung, A. Nauels, Y. Xia, V. Bex and P.M. Midgley (eds.)].

Colle, B.A., Booth, J.F., & Chang, E.K.M. (2015). A Review of Historical and Future Changes of Extratropical Cyclones and Associated Impacts Along the US East Coast. Current Climate Change Reports, 1, 125-143.

Deser, C., Walsh, J.E., & Timlin, M.S., (2000). Arctic sea ice variability in the context of recent atmospheric circulation trends. Journal of Climate, 13, 617–633.

Dobrynin M, Murawsky J, Yang S. (2012). Evolution of the global wind wave climate in CMIP5 experiments. Geophysical Research Letters, 39(18), L18606, doi:10.1029/2012GL052843.

Eady, E. (1949). Long waves and cyclone waves. Tellus, 1, 33-52.

Emanuel, K. (2005). Increasing destructiveness of tropical cyclones over the past 30 years. Nature, 436, 686–688.

ENR. Environment and Natural Resources. (2015). 1.7 Projected trends in Beaufort Sea levels. https://www.enr.gov.nt.ca/en/state-environment/17-projected-trends-beaufort-sea-levels (Accessed 10 October 2019).

Feser, F., Barcikowska, M., Krueger, O., Schenk, F., Weisse, R., & Xia, L. (2015). Storminess over the North Atlantic and northwestern Europe – A review. Quarterly Journal of the Royal Meteorological Society, 141,350–382. https://doi.org/10.1002/qj.2364.

Fisheries and Oceans Canada. (2019). Canadian Tides and Water Levels Data Archive. http://www.isdm-gdsi.gc.ca/isdm-gdsi/twl-mne/index-eng.htm (Accessed 21 November 2018).

Forbes, C., Rhome, J., Mattocks, C., & Taylor, A. (2014). Predicting the storm surge threat of hurricane sandy with the National Weather Service SLOSH model. Journal of Marine Science and Engineering, 2(2), 437–476. https://doi.org/10.3390/jmse2020437.

Francis, O.P., Panteleev, G.G., & Atkinson, D.E. (2011). Ocean wave conditions in the Chukchi Sea from satellite and in situ observations. Geophysical Research Letters, 38(24), n/a-n/a. https://doi.org/10.1029/2011GL049839

Frankcombe, L.M., von der Heydt, A., & Dijkstra, H.A. (2010). North Atlantic multidecadal climate variability: an investigation of dominant time scales and processes. Journal of Climate, 23, 3626-3638. doi:10.1175/2010JCLI3471.1, 3626-3638.

Fetterer, F., Knowles K., Meier, W.N., Savoie, M., & Windnagel, A.K. (2017). updated daily. *Sea Ice Index, Version 3*. [Monthly sea ice extent]. Boulder, Colorado USA. NSIDC: National Snow and Ice Data Center. doi: https://doi.org/10.7265/N5K072F8. [17 August 2019].

Gibbs A.E. & Richmond B.M. (2015). National assessment of shoreline change—historical shoreline change along the north coast of Alaska U.S.–Canadian border to Icy Cape *Geological Survey Open-File Report 2015–1048*. https://doi.org/10.3133/ofr20151048.

Gregow, H., Ruosteenoja, K., Pimenoff, N., & Jylhä, K. (2012). Changes in the mean and extreme geostrophic wind speeds in Northern Europe until 2100 based on nine global climate models. International Journal of Climatology 32(12), 1834–1846. https://doi.org/10.1002/joc.2398.

Grell, G.A., & Freitas, S.R. (2014). A scale and aerosol aware stochastic convective parameterization for weather and air quality modelling. Atmospheric Chemistry and Physics, 14, 5233-5250. https://doi.org/10.5194/acp-14-5233-2014.

Hakkinen, S., Proshutinsky, A., & Ashik, I. (2008). Sea ice drift in the Arctic since the 1950s. Geophysical Research Letters, *35*(19), L19704. https://doi.org/10.1029/2008GL034791

Hansen, J., Sato, M., Hearty, P., Ruedy, R., Kelley, M., Masson-Delmotte, V., Russell, G., Tselioudis, G., Cao, J., Rignot, E., Velicogna, I., Tormey, B., Donovan, B., Kandiano, E., von Schuckmann, K., Kharecha, P., Legrande, A.N., Bauer, M., & Lo, K.W. (2016). Ice melt, sea level rise and superstorms: evidence from paleoclimate data, climate modeling, and modern observations that 2°C global warming could be dangerous. Atmos Chem Phys 16:3761–3812.

Hartmann, D.L., & Co-authors. (2013). Observations: Atmo- sphere and surface. Climate Change 2013: The Physical Science Basis, T. F. Stocker et al., Eds., Cambridge University Press, 159–254.

Harvey, B.J., Shaffrey, L.C., & Woollings, T.J. (2014). Equator-to-pole temperature differences and the extratropical storm track responses of the CMIP5 climate models. Climate Dynamics, 43, 1171–1182.

Hines, K.M., & Bromwich, D.H. (2008). Development and testing of Polar WRF. Part I. Greenland ice sheet meteorology. Monthly Weather Review, 136, 1971-1989. https://doi.org/10.1175/2007MWR2112.1

Hines, K.M., Bromwich, D.H., Bai, L., Bitz, C.M., Powers, J.G., & Manning, K.W. (2015). Sea ice enhancements to Polar WRF. Monthly Weather Review, 143, 2363-2385. doi: 10.1175/MWR-D-14-00344.1.

Hynes, S., Solomon, S.M., & Whalen, D. Geological Survey of Canada, Open File 7685, 2014, 7 pages, https://doi.org/10.4095/295579.

Hoegh-Guldberg, O., & Bruno, J.F. (2010). The impact of climate change on the World's marine ecosystems. Science, 328, 1523-1528.

Honda, C., & Mitsuyasu, K. (1980). Laboratory study on wind effect to ocean surface. Journal of Coastal Engineering (JSCE), 27, 90-93. [in Japanese]

Hong, S.Y., & Lim, J.O.J. (2006a). The WRF single–moment 6–class microphysics scheme (WSM6). Journal of the Korean Meteorological Society, 42,129–151.

Hong, S.Y., Noh, Y., & Dudhia, J. (2006b). A new vertical diffusion package with an explicit treatment of entrainment processes. Monthly Weather Review, 134, 2318–2341.

Hoskins, B.J., & Hodges K.I. (2002). New Perspectives on the Northern Hemisphere Winter Storm Tracks. Journal of Atmospheric Sciences, V59, 1041-1061. https://doi.org/10.1175/1520-0469(2002)059<1041:NPOTNH>2.0.CO;2.

Hurrell, J.W., & Deser, C. (2009). North Atlantic climate variability: the role of the North Atlantic Oscillation. Journal of Marine Systems, 78, 28-41. doi:10.1016/j.jmarsys. 2008.11.026.

Hurrell, J.W., & van Loon, H. (1997). Decadal variations in climate associated with the North Atlantic Oscillation. Climatic Change, 36, 301–326.

Hurrell, J.W., Kushnir, Y., Ottersen, G., Visbeck, M. (2003). An overview of the North Atlantic Oscillation. In: Hurrell, J.W., Kushnir, Y., Ottersen, G., Visbeck, M. (Eds.), 2003: The North Atlantic Oscillation: Climatic Significance and Environmental Impact. American Geophysical Union, Washington DC. 279 pp.

IPCC. (2013). Summary for policymakers. Climate Change 2013: The Physical Science Basis. T. F. Stocker et al., Eds., Cambridge University Press, 3–29.

IPCC. (2014). IPCC Fifth Assessment Report (AR5). https://www.ipcc.ch/report/ar5/

Iacano, M., Delamere, J., Mlawer, E., Shephard, M., Clough, S., & Collins, W. (2008). Radiative forcing by long-lived greenhouse gases: Calculations with the AER radiative transfer models. Journal of Geophysical Research, 113(D13), 103. https://doi.org/10.1029/2008JD009944.

Jaagus, J., & Suursaar, Ü. (2013). Long-term storminess and sea level variations on the Estonian coast of the Baltic Sea in relation to large-scale atmospheric circulation Estonian Journal of Earth Sciences, 62(2), 73–92. doi: 10.3176/earth.2013.07.

Jacob, D., Elizalde, A., Haensler, A., Hagemann, S., Kumar, P., Podzun, R., Rechid, D., Remedio, A.R., Saeed, F., Sieck, K., Teichmann, C., & Wilhelm, C. (2012). Assessing the transferability of the regional climate model REMO to different coordinated regional climate downscaling experiment (CORDEX) regions. Atmosphere 3, 181–199.

Jakobsson, M., Mayer, L.A., Coakley, B., Dowdeswell, J.A., Forbes, S., Fridman, B., Hodnesdal, H., Noormets, R., Pedersen, R., Rebesco, M., Schenke, H.-W., Zarayskaya, Y., Accettella, A.D., Armstrong, A., Anderson, R.M., Bienhoff, P., Camerlenghi, A., Church, I.,

Edwards, M., Gardner, J.V., Hall, J.K., Hell, B., Hestvik, O.B., Kristoffersen, Y., Marcussen, C., Mohammad, R., Mosher, D., Nghiem, S.V., Pedrosa, M.T., Travaglini, P.G. & Weatherall, P. (2012). The International Bathymetric Chart of the Arctic Ocean (IBCAO) Version 3.0, Geophysical Research Letters, doi: 10.1029/2012GL052219.

James, T.S., Henton, J.A., Leonard, L.J., Darlington, A., Forbes, D., & Craymer M. (2014). Relative Sea-level Projections in Canada and the Adjacent Mainland United States; Geological Survey of Canada, Open File 7737, 72 p. doi:10.4095/295574.

Jimenez, P.A., Dudhia, J., Gonzalez-Rouco, J.F., Navarro, J., Montavez, J.P., & García-Bustamante, E. (2012). A revised scheme for the WRF surface layer formulation. Monthly Weather Review, 140, 898-918.

Khon, V.C., Mokhov, I.I., Pogarskiy, F.A., Babanin, A., Dethloff, K., Rinke, A., & Matthes, H. (2014). Wave heights in the 21 century Arctic Ocean simulated with a regional climate model, Geophysical Research. Letters, 41, 2956–2961. doi:10.1002/ 2014GL059847.

Kirkpatrick, N. (2018). MNN. What are extratropical cyclones? https://www.mnn.com/earth-matters/climate-weather/stories/extratropical-cyclones-arctic/; (Accessed 11 September 2019).

Knutson, T.R., & Tuleya, R.E. (2004). Impact of CO2-induced warming on simulated hurricane intensity and precipitation: Sensitivity to the choice of climate model and convective parameterization. Journal of Climate, 17, 3477–3495.

Komen, G.J., Cavaleri, L., Donelan, M., Hasselmann, K., Hasselmann, S. & Janssen, P.A.E.M. (1994). Dynamics and Modelling of Ocean Waves, Cambridge University Press, 532 p.

Liberato, M.L.R., Pinto, J.G., Trigo, R.M., Ludwig, P., Ordóñez, P., Yuen, D., & Trigo, I.F. (2013). Explosive development of winter storm Xynthia over the subtropical North Atlantic Ocean. Natural Hazards and Earth System Sciences, 13, 2239–2251.

Madsen, O., Poon, Y., & Graber, Y. (1988). Spectral wave attenuation by bottom friction: Theory. Coastal Engineering Proceedings, 1, 492-504.

Martin, J.E. (2006). Mid-latitude atmospheric dynamics. Wiley, 324 pp.

Matulla, C., Schöner, W., Alexandersson, H., von Storch, H., & Wang, X.L. (2008). European storminess: late nineteenth century to present. Climate Dynamics 31:125–130.

McClearn, M. (2018). The Globe and Mail. In Tuktoyaktuk, residents take a stand on shaky ground against the Beaufort Sea's advance. https://www.theglobeandmail.com/canada/article-in-tuktoyaktuk-residents-take-a-stand-on-shaky-ground-against-the/ (Accessed 20 March 2019).

Mei, W., & Xie, S.-P. (2016). Intensification of landfalling typhoons over the northwest Pacific since the late 1970s. Nature Geoscience, 9, 753-757.

Mizuta, R., Matsueda, M., Endo, H., Yukimoto, S. (2011). Future change in extratropical cyclones associated with change in the upper troposphere. Journal of Climate, 24, 6456–6470.

Mizuta, R. (2012). Intensification of extratropical cyclones associated with the polar jet change in the CMIP5 global warming projections. Geophysical Research Letters, 39(L19), 19707-

Mäll, M., Suursaar, Ü., Nakamura, R., & Shibayama, T. (2017). Modelling a storm surge under future climate scenarios: case study of extratropical cyclone Gudrun (2005). Natural Hazards, 89(3), 1119-1144.

Mändla, K., Jaagus, J., & Sepp, M. (2015). Climatology of cyclones with southern origin in northern Europe during 1948–2010. Theoretical and Applied Climatology, 120, 75−86.

Nakamura, R., Shibayama, T., Esteban, M., & Iwamoto, T. (2016). Future typhoon and storm surges under different global warming scenarios: case study of typhoon Haiyan (2013). Natural Hazards 82, 1645–1681.

Nakanishi, M., & Niino, H. (2006). An improved Mellor–Yamada level 3 model: its numerical stability and application to a regional prediction of advecting fog. Boundary-Layer Meteorology, 119(2), 397–407. doi:10.1007/s10546-005-9030-8.

Nakanishi, M., & Niino, H. (2009). Development of an improved turbulence closure model for the atmospheric boundary layer. Journal of the Meteorological Society of Japan, 87(5), 895–912. doi:10.2151/jmsj.87.895

Nelson, M. YachtingWorld. How the North Atlantic Oscillation affects European and Atlantic weather. https://www.yachtingworld.com/weather/how-the-north-atlantic-oscillation-affects-european-and-atlantic-weather-105954 2017 (Accessed 07 September 2019).

Nevalainen, K. (2012). A case study of a snowstorm with multiple snowbands in southern Finland 23 November 2008 (Master's thesis). University of Helsinki, Faculty of Science, Department of Physics, Retrieved from http://urn.fi/URN:NBN:fi-fe2017112251920.

NOAA. (2019). Arctic Oscillation (AO). https://www.ncdc.noaa.gov/teleconnections/ao/ (accessed 10 October 2019).

NSIDC. (2019). National Snow & Ice Data Center. Sea Ice Index, Version 3. https://nsidc.org/data/G02135 (Accessed 08 September 2019)

Olson, Joseph B., Jaymes S. Kenyon, Wayne M. Angevine, John M . Brown, Mariusz Pagowski, and Kay Sušelj, 2019: A Description of the MYNN-EDMF Scheme and the Coupling to Other Components in WRF–ARW. NOAA Technical Memorandum OAR GSD, **61**, pp. 37. doi:10.25923/n9wm-be49.

Ostenso NA. (2018). Encyclopaedia Britannica. Arctic Ocean. https://www.britannica.com/place/Arctic-Ocean 2018 (Accessed 09 September 2019).

Patricola, C.M., & Wehner, M.F. (2018). Anthropogenic influences on major tropical cyclone events. Nature 563, 339-346.

Pinto, J.G., Ulbrich, U., Leckebusch, G.C., Spangehl, T., Reyers, M., Zacharias Kjellström, E., Nikulin, G., Hansson, U., Strandberg, G., & Ullerstig, A. (2011). 21st century changes in the European climate: uncertainties derived from an ensemble of regional climate model simulations. Tellus A 63, 24–40.

Pisaric, M.F., Thienpont, J.R., Kokelj, S.V., Nesbitt, H., Lantz, T.C., Solomon, S., & Smol, J.P. (2011). Impacts of a recent storm surge on an Arctic delta ecosystem examined in the context of the last millennium. Proceedings of the National Academy of Sciences of the United States of America, 108(22), 8960–8965. doi:10.1073/pnas.1018527108

Proshutinsky, A., & Johnson, M. (1997). Two circulation regimes of the wind-driven Arctic Ocean. Journal of Geophysical Research, 102(12), 493–12,514.

Proshutinsky, A., Polyakov, I., & Johnson, M. (1999). Climate states and variability of Arctic ice and water dynamics during 1946-1997. Polar Research, 18(2), 135–142. https://doi.org/10.1111/j.1751-8369.1999.tb00285.x

Proshutinsky, A., Dukhovskoy, D., Timmermans, M.-L., Krishfield, R., & Bamber, J.L. (2015). Arctic circulation regimes. Philosophical Transaction A, Royal Society, 373: 20140160. http://dx.doi.org/10.1098/rsta.2014.0160.

Polar Meteorology Group. (2019). The Polar WRF. http://polarmet.osu.edu/PWRF/ (Accessed 20 September 2019).

Post P, & Kõuts, T. (2014) Characteristics of cyclones causing extreme sea levels in the northern Baltic Sea. Oceanologia, 56, 241–258.

Rasmussen, E.A. & Turner J. (Eds). (2003). Polar Lows: Mesoscale Weather Systems in the Polar Regions. Cambridge University Press, 602 pp.

Rauhala, J., & Juga, I. (2010). Wind and snow storm impacts on society. 15th International Road Weather Conference, Quebec City, Canada, 5-7 February 2010. 8 pp.

Roberts, J.F., Champion, A.J., Dawkins, L.C., Hodges, K.I., Shaffrey, L.C., Stephenson, D.B., Stringer, M.A., Thornton, H.E., & Youngman, B.D. (2014). The XWS open access catalogue of extreme European windstorms from 1979 to 2012. Natural Hazards and Earth System Sciences, 14, 2487–2501.

Roelvink, D., Reniers, A., Van Dongeren, A., Van Thiel De Vries, J., Lescinski, J., & McCall, R. (2009). Modeling storm impacts on beaches, dunes and barrier islands. Proceedings of the Coastal Engineering Conference, 56(11–12), 1684–1696.
https://doi.org/10.1016/j.coastaleng.2009.08.006

Rusu E. (2011). Strategies in using numerical wave models in ocean/coastal applications, Journal of Marine Science and Technology, 19, 58–75.

Qi, J., Chen, C., Beardsley, R.C., Perrie, W., Cowles, G.W., & Lai, Z. (2009). An unstructured-grid finite-volume surface wave model (FVCOM-SWAVE): Implementation, validations and applications. Ocean Model, 28, 153-166.

Sanders, F., & Gyakum, J.R. (1980). Synoptic-Dynamic Climatology of the "Bomb". Monthly Weather Review, 108, 1589–1606.

Schär, C., Christoph, F., Lutthi, D., & Davies, H.C. (1996) Surrogate Climate-Change Scenarios for Regional Climate Models. Geophysical Research Letters, 23, 669-672.

Screen, J.A., & Deser, C. (2019). Pacific Ocean variability influences the time of emergence of a seasonally ice‐free Arctic Ocean. Geophysical Research Letters, 46, 2222‐2231. https://doi.org/ 10.1029/2018GL081393.

Semedo, A, Vettor, R., Breivik, O., Sterl, A., Reistad, M., Soares, C.G., & Lima, D. (2014). The wind sea and swell waves climate in the Nordic seas. Ocean Dynamics, 65, 223–240, doi:10.1007/s10236- 014-0788-4.

Serreze, M.C., Barry, R.G., & Rogers, J.C. (1997). Icelandic low activity: climatological features, linkages with the NAO, and relationships with recent changes in the Northern Hemisphere circulation. Journal of Climate, 10, 453–464.

Shapiro, M.A., & Keyser, D. (1990). Fronts, jet streams and the tropopause. Extratropical Cyclones, The Erik Palm en Memorial Volume, C. W. Newton and E. O. Holopainen, Eds., American Meteorological Society, Boston, USA, 167191.

Simmonds, I. & Rudeva, I. (2012). The great Arctic cyclone of August 2012, Geophysical. Research. Letters, 39(23), L23709. doi:10.1029/2012gl054259.

Skamarock, W.C., Klemp, J.B., Duddhia, J., Gill, D.O., Barker, D.M., Duda, M.G., Huang, X.Y., Wang, W., & Powers, J.G. (2008). A Description of the Advanced Research WRF Version 3, NCAR Technical Note.

Stainforth, D.A., Alna, T., Christensen, C., et al. (2005). Uncertainty in the predictions of the climate response to rising levels of greenhouse gases. Nature 433, 403–406.

Soomere, T., Behrens, A., Tuomi, L., & Nielsen, J.W. (2008). Wave conditions in the Baltic Proper and in the Gulf of Finland during windstorm Gudrun. Natural Hazards and Earth System Sciences, 8, 37-46.

Stopa, J.E., Ardhuin, F., & Girard-Ardhuin, F. (2016). Wave climate in the Arctic 1992–2014: seasonality and trends. The Cryosphere, 10, 1605–1629. doi:10.5194/tc-10-1605-2016.

Sun, Y., Chen, C., Beardsley, R.C., Xu, Q., Qi, J., & Lin, H. (2013). Impact of current-wave interaction on storm surge simulation: A case study for Hurricane Bob. Journal of Geophysical Research: Oceans, 118, 2685-2701.

Suursaar, Ü., & Kall, T. (2018). Decomposition of Relative Sea Level Variations at Tide Gauges Using Results From Four Estonian Precise Levelings and Uplift Models. IEEE J-STARS 11, 1966−1974.

Suursaar, Ü., Kullas, T., & Otsmann, M. (2002). A model study of sea level variations in the Gulf of Riga and the Väinameri Sea. Continental Shelf Research, 22, 2001–2019.

Suursaar, Ü., Sepp, M., Post, P., & Mäll, M. (2018). An Inventory of Historic Storms and Cyclone Tracks That Have Caused Met-Ocean and Coastal Risks in the Eastern Baltic Sea. Journal of Coastal Research, Special Issue 85, 531−535. Doi:10.2112/SI85-107.1.

Suursaar, Ü., Jaagus, J., & Tõnisson, H. (2015). How to quantify long-term changes in coastal sea storminess? Estuarine, Coastal and Shelf Science, 156, 31–41.

Suursaar, Ü., Kullas, T., Otsmann, M., Saaremäe, I., Kuik, J., & Merilain, M. (2006). Hurricane Gudrun and modelling its hydrodynamic consequences in the Estonian coastal waters. Boreal Environment Research, 11, 143–159.

Swail, V.R., Cardone, V.J., Ferguson, M., Gummer, D.J., Harris, E.L., Orelup, E.A., & Cox, A.T. (2006). The MSC50 Wind and Wave Reanalysis. 9th International Wind and Wave Workshop, September 25-29, 2006, Victoria, B.C.

SWAN. (2019). SWAN Scientific and Technical Documentation. http://swanmodel.sourceforge.net/download/zip/swantech.pdf (accessed 27 September 2019)

Tasnim, K.M., Shibayama, T., Esteban, M., Takagi, H., Ohira, K., & Nakamura, R. (2015). Field observation and numerical simulation of past and future storm surges in the Bay of Bengal: case study of cyclone Nargis. Natural Hazards 75, 1619–1647

Tewari, M., Chen, F., Wang, W., Dudhia, J., LeMone, M.A., Mitchell, K., Ek, M., Gayno, G., Wegiel, J., & Cuenca, R.H. (2004). Implementation and verification of the unified NOAH land surface 677 model in the WRF model. 678 20th conference on weather analysis and forecasting/16th conference on numerical weather prediction (679), pp. 1–15.

Trenberth, K. (2005). Uncertainty in hurricanes and global warming. Science 308, 1753–1754.

Turner, J., & Bracegirdle, T. (2006). Polar Lows and Other High Latitude Weather Systems. ECMWF Seminar on Polar Meteorology, 4-8 September 2006. Internet link (PDF):

https://www.ecmwf.int/sites/default/files/elibrary/2007/12857-polar-lows-and-other-high-latitude-weather-systems.pdf (Accessed on 10 September 2019).

Tõnisson, H., Kont, A., Orviku, K., Suursaar, Ü., Rivis, R., & Palginõmm, V. (2019). Application of System Approach Framework for Coastal Zone Management in Pärnu, SW Estonia. Journal of Coastal Conservation, 23(5), 931-942. doi.org/10.1007/s11852-018-0637-6.

Tõnisson, H., Orviku, K., Jaagus, J., Suursaar, Ü., Kont, A., & Rivis, R. (2008). Coastal damages on Saaremaa Island, Estonia, caused by the extreme storm and flooding on January 9, 2005. Journal of Coastal Research, 24(3), 602–614. DOI: 10.2112/06-0631.1.

Tõnisson H, Suursaar Ü, Alari V, Muru M, Rivis R, Kont A, Viitak M (2016) Measurement and Model Simulations of Hydrodynamic Parameters, Observations of Coastal Changes and Experiments with Indicator Sediments to Analyse the Impact of Storm St. Jude in October, 2013. Journal of Coastal Research, 75 (sp1), 1257-1261. https://doi.org/10.2112/SI75-252.1.

Ulbrich, U., Leckebusch, G.C., & Pinto, J.G. (2009). Extra-tropical cyclones in the present and future climate: A review. Theoretical and Applied Climatology, 96, 117–131.

Van Gelder, P.H.A.J.M., Mai, C.V., Wang, W., Shams, G., Rajabalinejad, M., & Burgmeijer, M. (2008). Data management of extreme marine and coastal hydro-meteorological events. Journal of Hydraulic Research, 46 (Suppl. 2), 191–210.
https://doi.org/10.1080/00221686.2008.9521954.

Viitak, M., Maljutenko, I., Alari, V., Suursaar, Ü., Rikka, S., & Lagemaa, P. (2016). The impact of surface currents and sea level on the wave field evolution during St. Jude storm in the eastern Baltic Sea. Oceanologia 58, 176−186.

Vousdoukas, M.I., Voukouvalas, E., Annunziato, A., Giardino, A., & Feyen, L. (2016). Projections of extreme storm surge levels along Europe. Climate Dynamics, 47(9-10), 3170-3190. doi:10.1007/s00382-016-3019-5.

Weisse, R., von Storch, H., Callies, U., Chrastansky, A., Feser, F., Grabemann, I., Günther, H., Pluess, A., Stoye, T., Tellkamp, J., Winterfeldt, J., & Woth, K. (2009). Regional Meteorological–Marine Reanalyses and Climate Change Projections. Bulletin of the American Meteorological Society, 90, 849–860. https://doi.org/10.1175/2008BAMS2713.1

Wood Hole Oceanographic Institute (WHOI). (2019). Arctic Ocean Oscillation Index (AOO). Internet link: https://www.whoi.edu/page.do?pid=66578 (Accessed 27 December 2019).

Wolski, T., Wiśniewski, B., Giza, A., Kowalewska-Kalkowska, H., Boman, H., Grabbi-Kaiv, S., Hammarklint, T., Holfort, J., & Lydeikaite, Ž. (2014). Extreme sea levels at selected stations on the Baltic Sea coast. Oceanologia 56(2), 259–290. DOI: 10.5697/oc.56-S.000.

Wu, J. (1982). Wind-Stress Coefficients Over Sea Surface From Breeze to Hurricane. Journal of Geophysical Research, 87(C12), 9704-9706. https://doi.org/10.1029/JC087iC12p09704.

Wu, L., Chen, C., Guo, P., Shi, M., Qi, J., & Ge, J. (2010). A FVCOM-based unstructured grid wave, current, sediment transport model, I. Model description and validation. Journal of Ocean University of China, 10(1), 1-8.

Wood, K.R., Overland, J.E., Salo, S.A., Bond, N.A., Williams, W.J., & Dong, X. (2013). Is there a "new normal" climate in the Beaufort Sea? Polar Research, 32(1), 19552. https://doi.org/10.3402/polar.v32i0.19552.

Woollings, T., 2010. Dynamical influences on European climate: an uncertain future. Philosophical Transactions of The Royal Society A, 368(1924), 3733-3756. doi:10.1098/rsta.2010.0040.

Woollings, T., Hoskins, B., Blackburn, M., Hasssell, D., & Hodges, K. (2010). Storm track sensitivity to sea surface temperatures resolution in a regional atmosphere model. Climate Dynamics, 35, 343–353.

Zappa, G., Shaffrey, L.C., & Hodges, K.I. (2013a). The ability of CMIP5 models to simulate North Atlantic extratropical cyclones. Journal of Climate, 26:5379-5396. https://doi.org/10.1175/JCLI-D-12-00501.1.

Zappa, G., Shaffrey, L.C., Hodges, K.I., Sansom, P.G., & Stephenson, D.B. (2013b). A multi-model assessment of future projections of north atlantic and european extratropical cyclones in the CMIP5 climate models. Journal of Climate, 26, 5846–5862.

Zhang, J.L., & Rothrock D.A. (2003). Modeling global sea ice with a thickness and enthalpy distribution model in generalized curvilinear coordinates. Monthly Weather Review, 131, 845-861.

Zhang, J., Lindsay, R., Schweiger, A., & Steele, M. (2013). The impact of an intense summer cyclone on 2012 Arctic sea ice retreat. Geophysical Research Letters, 40, 720–726. doi:10.1002/grl.50190.

Zijlema, M. (2010). Computation of wind-wave spectra in coastal waters with SWAN on unstructured grids. Coastal Engineering, 57(3), 267–277.
doi:10.1016/j.coastaleng.2009.10.011, 2010.

Appendix

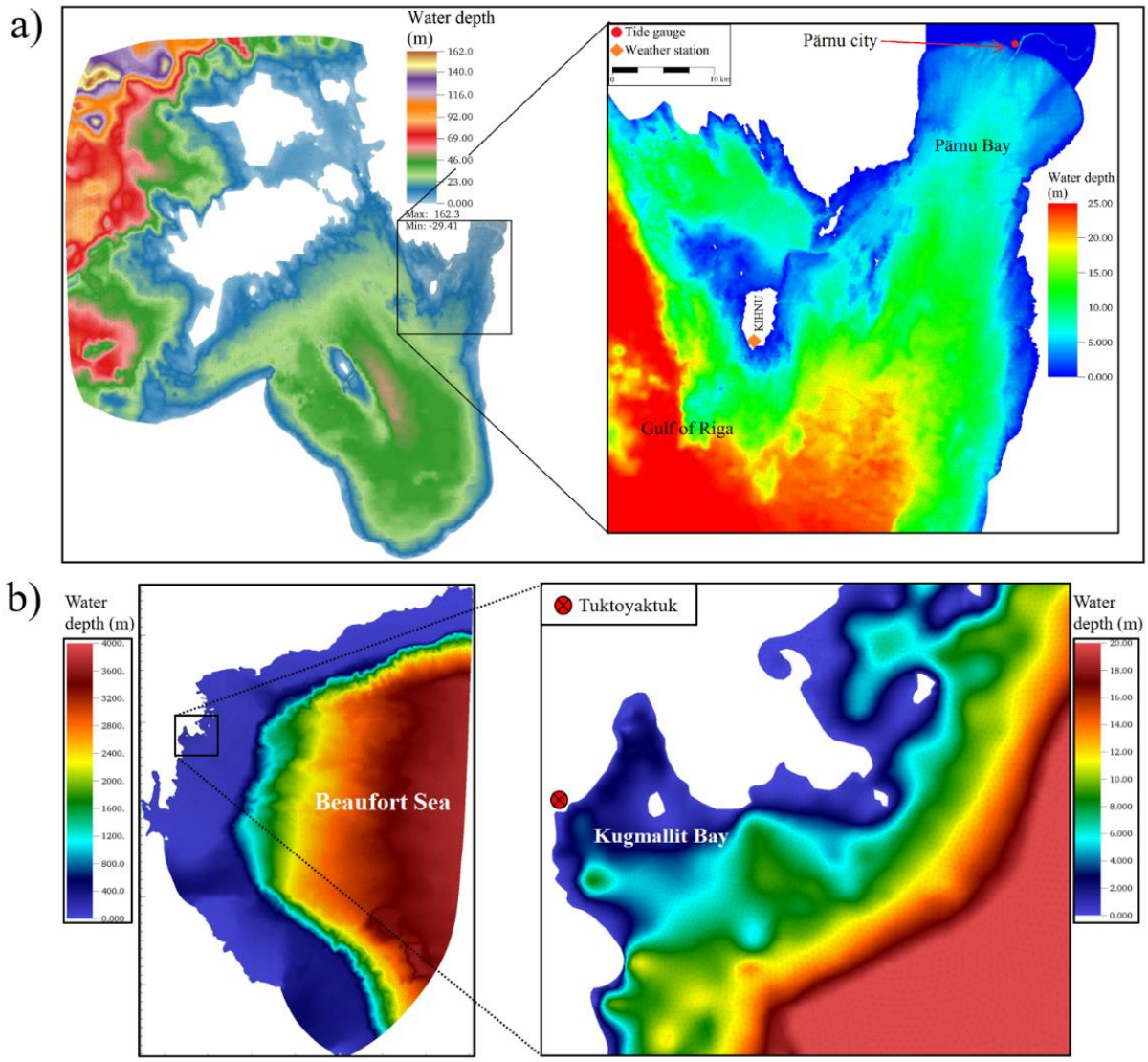

Appendix 1. Bathymetry output from FVCOM-SWAVE simulations, for a) Estonian coastal waters + Pärnu, and b) For Canadian Beaufort Sea + Tuktoyaktuk.

Appendix 2. WRF and PWRF physics schemes used in the study and their short descriptions. Left table is for North Atlantic case studies, and table on the right of for the Arctic study area.

Physics options	Description
Microphysics (WRF Single-Moment 6-class scheme)	A scheme with ice, snow and graupel processes suitable for high-resolution simulations
Cumulus parameterizations (Grell Freitas ensemble scheme)	The scheme is distinguished from other cumulus schemes by allowing subsidence effects to be spread to neighboring grid columns, making the method more suitable to grid sizes less than 10 km
Surface physics (Noah Land Surface Model)	Unified NCEP/NCAR/AFWA scheme with soil temperature and moisture in four layers, fractional snow cover and frozen soil physics
Planetary boundary layer physics (Yonsei University scheme)	Non-local-K scheme with explicit entrainment layer and parabolic K profile in unstable mixed layer
Atmospheric radiation physics (RRTMG)	Most complex radiative tranfer treatment among all schemes available in WRF-ARW (interaction with microphysics through Qc Qr Qi Qs)

Physics options	Description
Microphysics (WRF Single-Moment 6-class scheme)	A scheme with ice, snow and graupel processes suitable for high-resolution simulations
Cumulus parameterizations (Grell Freitas ensemble scheme)	The scheme is distinguished from other cumulus schemes by allowing subsidence effects to be spread to neighboring grid columns, making the method more suitable to grid sizes less than 10 km
Surface physics (Noah Land Surface Model)	Unified NCEP/NCAR/AFWA scheme with soil temperature and moisture in four layers, fractional snow cover and frozen soil physics
Planetary boundary layer physics (Mellor-Yamada-Janjic scheme)	Eta operational scheme. One-dimensional prognostic turbulent kinetic energy scheme with local vertical mixing
Atmospheric radiation physics (RRTMG)	Most complex radiative tranfer treatment among all schemes available in WRF-ARW (interaction with microphysics through Qc Qr Qi Qs)

Appendix 3. Parametricity test using the Shapiro-Wilk test for each of the storm and their respective stations, where ID 1) is Gudrun, 2) is St. Jude 3) Xynthia and 4) is Arctic storm. See chapter 4.5 for more details.

ID	Station	Wind_speed				Wind_direction				Storm_surge				sig_wave_height			
		obs	hind	RCP_4.5	RCP_8.5	obs	hind	RCP_4.5	RCP_8.5	obs	hind	RCP_4.5	RCP_8.5	obs	hind	RCP_4.5	RCP_8.5
1	Kihnu	1.04E-05	0.196834	0.4043741	0.1798647	0.00284892	0.00070801	0.00999355	0.00217764								
	Ruhnu	3.05E-05	0.2980372	0.03415443	0.03523355	0.01967851	0.00113086	0.0058296	0.00157392								
	Vilsandi	0.26814	0.5474319	0.3063377	0.09656831	0.00020603	0.00028477	0.00060693	0.0023481								
	Parnu-Sauga	0.01285755	0.1820926	0.5047274	0.100015	0.02374126	0.0005099	0.0935326	0.00533888								
	Parnu									3.82E-06	2.88E-07	5.75E-06	1.40E-08				
	N-Baltic													2.11E-05	1.51E-06	1.31E-05	1.52E-05
	GoFinland													0.00082922	0.00010509	2.67E-07	4.38E-06
2	Kihnu	0.03699232	0.00573556	0.01663009	0.00116595	0.01787473	6.05E-07	7.48E-07	1.35E-05								
	Ruhnu	4.73E-06	0.00089922	0.04726882	2.25E-05	9.20E-07	4.40E-07	5.52E-08	4.39E-06								
	Vilsandi	0.00101373	9.31E-06	0.00017032	4.09E-06	0.00859631	0.00021778	2.25E-05	2.96E-05								
	Parnu-Sauga	1.09E-05	7.94E-05	0.00037038	2.08E-05	1.51E-06	5.01E-05	7.88E-08	2.18E-06								
	Parnu									1.11E-07	4.91E-08	8.30E-06	2.78E-08				
	N-Baltic													4.97E-05	4.23E-10	2.14E-09	3.07E-06
	GoFinland													9.88E-10	6.90E-09	1.56E-08	1.30E-06
3	Kihnu	0.4227101	0.01328686	0.05160585	0.2914254	9.10E-09	6.50E-06	3.93E-08	8.11E-08								
	Ruhnu	0.00033107	0.1767098	0.01792079	0.6478908	3.05E-09	3.50E-08	2.59E-08	2.50E-08								
	Vilsandi	0.00022345	2.81E-05	0.005827	0.00030449	4.02E-10	1.77E-08	7.71E-09	1.45E-09								
	Paernu-Sauga	0.03706773	0.00729425	0.00600897	5.47E-07	1.41E-05	5.21E-05	6.06E-08	2.83E-08								
4	Tuktoyaktuk	4.11E-06	0.00101718	8.90E-06	1.52E-02	1.28E-08	0.1323993	5.48E-10	0.0001645								

Appendix 4. Event comparison between hindcast and observed data (in rows "(1)"), as well as between hindcast and the RCP scenarios (2a is hindcast vs. RCP4.5, 2b is hindcast vs. RCP8.5 and 2c is RCP4.5 vs. RCP8.5) for Gudrun. Conducted using either the paired-samples t- (if both sets were parametric), or the Wilcoxon signed-rank test (if at least one set was non-parametric).

Parameter	Wind speed				Wind direction				Storm surge				Significant wave height			
Test	(1)	(2)			(1)	(2)			(1)	(2)			(1)	(2)		
		a	b	c		a	b	c		a	b	c		a	b	c
Vilsandi	t = -4.1283; df = 53; p-value =	t = -5.9768; p-value = 1.858e-07	t = -4.1667; p-value = 0.0001123	t = -0.49089; p-value = 0.6255	1.43E-07	0.171	0.08663	0.7895	-	-	-	-	-	-	-	-
Ruhnu	9.95E-13	0.001444	8.07E-07	0.07058	4.16E-05	0.9725	0.2667	0.1212	-	-	-	-	-	-	-	-
Kihnu	1.32E-11	t = -4.1709; p-value = 0.0001107	t = -5.9149; p-value = 2.334e-07	t = -2.0315; p-value = 0.04713	0.03871	0.6236	0.4435	0.5296	-	-	-	-	-	-	-	-
Pärnu-Sauga	0.6968	t = 2.3647; p-value = 0.02167	t = 2.263; p-value = 0.02768	t = -0.21401; p-value = 0.8313	0.03032	0.5816	0.01874	0.07901	-	-	-	-	-	-	-	-
Pärnu	-	-	-	-	-	-	-	-	0.7534	1.38E-13	< 2.2e-16	9.59E-07	-	-	-	-
N. Baltic Proper	-	-	-	-	-	-	-	-	-	-	-	-	0.2571	3.18E-15	3.96E-12	0.8478
Gulf of Finland	-	-	-	-	-	-	-	-	-	-	-	-	0.4433	0.2824	0.1197	0.9584

Appendix 5. Event comparison between hindcast and observed data (in rows "(1)"), as well as between hindcast and the RCP scenarios (2a is hindcast vs. RCP4.5, 2b is hindcast vs. RCP8.5 and 2c is RCP4.5 vs. RCP8.5) for St. Jude. Conducted using either the paired-samples t- (if both sets were parametric), or the Wilcoxon signed-rank test (if at least one set was non-parametric).

Parameter	Wind speed				Wind direction				Storm surge				Significant wave height			
Test	(1)	(2)			(1)	(2)			(1)	(2)			(1)	(2)		
		a	b	c		a	b	c		a	b	c		a	b	c
Vilsandi	t = -6.366, df = 54, p-value = 4.391e-08	t = -2.4216, p-value = 0.01884	t = -2.8151, p-value = 0.006791	t = -0.21744, p-value = 0.8287	t = 7.0674, p-value = 3.202e-09	t = 0.32333, p-value = 0.7477	t = 0.4995, p-value = 0.6195	t = 0.37027, p-value = 0.7126	-	-	-	-	-	-	-	-
Ruhnu	t = -14.559, df = 54, p-value < 2.2e-16	t = 1.5784, p-value = 0.1203	t = -1.3255, p-value = 0.1906	t = -2.575, p-value = 0.0128	t = 1.4021, p-value = 0.1672	t = 1.7052, p-value = 0.0939	t = 3.498, p-value = 0.0009466	t = 3.3288, p-value = 0.001576	-	-	-	-	-	-	-	-
Kihnu	t = -2.3037, df = 29, p-value = 0.0286	t = -0.98304, p-value = 0.33	t = -3.1679, p-value = 0.002527	t = -2.9817, p-value = 0.004293	t = 2.6805, p-value = 0.012	t = 0.64849, p-value = 0.5194	t = 2.0607, p-value = 0.04416	t = 2.9534, p-value = 0.004646	-	-	-	-	-	-	-	-
Pärnu-Sauga	t = 3.4883, df = 54, p-value = 0.0009751	t = -2.2704, p-value = 0.0272	t = -3.674, p-value = 0.0005497	t = -1.136, p-value = 0.261	t = 12.928, p-value < 2.2e-16	t = 0.71166, p-value = 0.4797	t = 2.0834, p-value = 0.04196	t = 2.6479, p-value = 0.0106	-	-	-	-	-	-	-	-
Pärnu	-	-	-	-	-	-	-	-	t = 3.7463, df = 54, p-value = 0.0004379	t = -4.6463, df = 162, p-value = 6.96e-06	t = -11.122, p-value < 2.2e-16	t = -8.2986, p-value = 3.904e-14	-	-	-	-
N. Baltic Proper	-	-	-	-	-	-	-	-	-	-	-	-	t = -3.4802, df = 142, p-value = 0.0006658	t = -8.4151, df = 168, p-value = 1.643e-14	t = -5.3771, p-value = 2.503e-07	t = -0.1486, p-value = 0.882
Gulf of Finland	-	-	-	-	-	-	-	-	-	-	-	-	t = -9.5372, df = 166, p-value < 2.2e-16	t = -4.2, df = 168, p-value = 4.321e-05	t = -2.6167, p-value = 0.009689	t = 0.76246, p-value = 0.4469

Appendix 6. Event comparison between hindcast and observed data (in rows "(1)"), as well as between hindcast and the RCP scenarios (2a is hindcast vs. RCP4.5, 2b is hindcast vs. RCP8.5 and 2c is RCP4.5 vs. RCP8.5) for Xynthia (ID 1) and Tuktoyaktuk (ID 2). Conducted using either the paired-samples t- (if both sets were parametric), or the Wilcoxon signed-rank test (if at least one set was non-parametric).

ID	Parameter	Wind speed				Wind direction			
	Test	(1)	(2)			(1)	(2)		
			a	b	c		a	b	c
1	Vilsandi	t = -1.4834, df = 54, p-value = 0.1438	t = 5.3242, p-value = 2.012e-06	t = -3.1817, p-value = 0.002428	t = -8.2099, p-value = 4.529e-11	t = 3.6384, df = 54, p-value = 0.0006141	t = -0.42086, , p-value = 0.6755	t = -1.3209, p-value = 0.1921	t = -1.3988, p-value = 0.1676
	Ruhnu	9.33E-10	0.9657	0.0001464	5.28E-08	t = 0.59793, df = 54, p-value = 0.5524	t = -3.4477, , p-value = 0.001103	t = -5.9678, p-value = 1.921e-07	t = -4.1972, p-value = 0.0001015
	Kihnu	0.06714	0.5935	0.0008099	1.20E-06	t = 3.6824, df = 54, p-value = 0.0005353	t = -2.909, , p-value = 0.005255	t = -6.4174, p-value = 3.627e-08	t = -5.7145, p-value = 4.873e-07
	Pärnu-Sauga	t = -0.92359, df = 54, p-value = 0.3598	t = 2.2214, p-value = 0.03054	t = -3.068, p-value = 0.003366	t = -6.9727, p-value = 4.563e-09	t = 0.9212, df = 54, p-value = 0.361	t = -2.2324, p-value = 0.02976	t = -3.068, p-value = 0.003366	t = -5.7156, p-value = 4.853e-07
2	Tuktoyaktuk	0.0005984	0.6966	0.03605	0.1331	0.001259	2.04E-05	0.6993	2.85E-05

List of research achievements

(a) Journals

Mäll M., Suursaar Ü., Nakamura R., Shibayama T. Modelling a storm surge under future climate scenarios: case study of extratopical cyclone Gudrun (2005). Natural Hazards. Vol.89(3), pp.1119-1144, 2017.

Nakamura, R., **Mäll, M.**, Shibayama, T. (2019). Street-scale storm surge load impact assessment using fine-resolution numerical modelling: a case study from Nemuro, Japan, Natural Hazards, Vol.99(1), pp.391-422, 2019.

Takabatake, T., **Mäll M.**, Esteban M., Nakamura R., Kyaw T.O., Ishii, H., Valdez, J.J.P., Nishida Y., Noya F., Shibayama T. (2018). Field Survey of 2018 Typhoon Jebi in Japan: Lessons for Disaster Risk Management. Geosciences. Vol.8(11), pp.412-431.

Suursaar Ü., Sepp M., Post P., **Mäll M**. (2018) An Inventory of Historic Storms and Cyclone Tracks That Have Caused Met-Ocean and Coastal Risks in the Eastern Baltic Sea. Journal of Coastal Research. Vol.85(special issue), pp.531-535.

Nakamura R., Iwamoto T., Shibayama T., Mikami T., Matsuba S., **Mäll M.**, Tatekouji A., Tanokura Y. Field survey and mechanism of storm surge generation invoked by the low pressure with rapid development in Nemuro Hokkaido in December 2014. (2015). Transactions of the Japan Society of Civil Engineers (Ocean Development). Vol.71(2), pp.31-36.

(b) Conference articles

Mäll, M., Suursaar, Ü., Nakamura, R., Tasnim, K.M., Shibayama, T. (2019). Modeling parameters and impacts of future cyclones: South-East Asian and Northern European case studies. *2019 IEEE International Geoscience and Remote Sensing Symposium (IGARSS), July 28–August 2, 2019, Yokohama, Japan.* IEEE, 9346−9349.

Mäll, M., Suursaar, Ü., Shibayama, T., Nakamura, R. (2019). Modeling cyclone-related precipitation changes in future climates using WRF model and CMIP5 output data. *2019 IEEE International Geoscience and Remote Sensing Symposium (IGARSS), July 28–August 2, 2019, Yokohama, Japan.* IEEE, 7590−7593.

(c) Conferences

Mäll M., Suursaar Ü., Shibayama T., Nakamura R. Modeling cyclone-related precipitation changes in future climates using WRF model and CMIP5 output data. IEEE International Geoscience and Remote Sensing Symposium (IGARSS). Yokohama, Japan, July-August, 2019. (peer reviewed, presentation type: oral)

Mäll M., Suursaar Ü., Nakamura R., Tasnim K.M., Shibayama T. Modeling parameters and impacts of future cyclones: South-East Asian and Northern European case studies. IEEE International Geoscience and Remote Sensing Symposium (IGARSS). Yokohama, Japan, July-August, 2019. (peer reviewed, presentation type: oral)

Mäll, M., Nakamura R., Shibayama T., Suursaar Ü. Modelling parameters and impacts of four extratropical cyclones under climate scenarios. The 36th International Conference on Coastal Engineering. Baltimore, US, July-August, 2018. (peer reviewed, presentation type: oral)

Mäll, M., Kull A., Nakamura R., Shibayama T., Suursaar Ü. Modelling storm surge conditions under future climate scenarios: A case study of 2005 January storm Gudrun in Pärnu, Estonia. The 35th International Conference on Coastal Engineering. Antalya, Turkey, November, 2016. (peer reviewed, presentation type: oral)

Nakamura R., **Mäll M.**, Shibayama T., Kato S. Inter-comparison of coastal models: case study of storm surge at Nemuro in Japan. The 36th International Conference on Coastal Engineering. Baltimore, US, July-August, 2018. (peer reviewed, presentation type: poster)

Nakamura R., Shibayama T., Mikami T., Esteban M., Takagi H., **Mäll M.**, Iwamoto T. Comparison of two recent storm surge events based on results of field surveys. Proceedings of The International Conference of Global Network for Innovative Technology and AWAM International Conference in Civil Engineering. Penang, Malaysia, August, 2017. (peer reviewed, presentation type: oral)